

# NASA CONTRACTOR REPORT

NASA CR-1922



NASA CR-19  
0.1

0060975

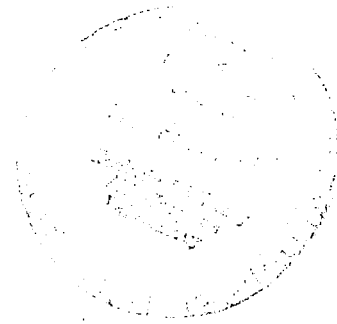


**LOAN COPY: RETURN TO  
AFWL (DOUL)  
KIRTLAND AFB, N. M.**

## INVESTIGATIONS OF HIGH-POWER PROBLEMS IN SPACE-SHUTTLE ANTENNA DESIGNS

*by W. C. Taylor and N. J. Alvares*

*Prepared by*  
STANFORD RESEARCH INSTITUTE  
Menlo Park, Calif.  
*for Langley Research Center*





0060975

1. Report No. NASA CR-1922		2. Government Accession No.		3. Recipient's Catalog No. 750/115-21-01-01	
4. Title and Subtitle INVESTIGATIONS OF HIGH-POWER PROBLEMS IN SPACE-SHUTTLE ANTENNA DESIGNS				5. Report Date February 1972	
				6. Performing Organization Code	
7. Author(s) W. C. Taylor and N. J. Alvares				8. Performing Organization Report No. 8677	
9. Performing Organization Name and Address Stanford Research Institute Menlo Park California				10. Work Unit No.	
				11. Contract or Grant No. NAS1-10068	
12. Sponsoring Agency Name and Address National Aeronautics and Space Administration Washington, D.C. 20546				13. Type of Report and Period Covered Contractor Report	
				14. Sponsoring Agency Code	
15. Supplementary Notes					
16. Abstract This program consisted of two parts: (1) a study program including a survey of industry and Government laboratories, to determine the state of the art in dealing with problems of high power levels in reentry antenna design, and (2) a laboratory program to develop techniques for testing dielectric materials for effects on RF transmission, with emphasis on high-power applications in space and reentry flights.  The study program resulted in a set of guidelines for avoiding breakdown in reentry antenna design. A discussion of temperature effects on dielectric breakdown is also given. From the laboratory program, the report gives a description of techniques for (1) heating with carbon-arc image furnace, (2) temperature measurement (thermocouples and infrared pyrometer), (3) massspectrometric monitoring of outgassing, and (4) testing for RF breakdown in both heated dielectrics and the dielectric/air and dielectric/plasma interface. Also reported are data and observations taken in technique development using candidate shuttle materials falling in three different categories: (1) lightweight refractory foams, (2) dense RF window materials, and (3) ablative materials.					
17. Key Words (Suggested by Author(s)) Antenna breakdown, dielectric breakdown, shock tube measurements, ablation, reentry heating, dielectric losses, antenna window materials, thermocouple, pyrometer.			18. Distribution Statement  Unclassified - Unlimited		
19. Security Classif. (of this report) Unclassified		20. Security Classif. (of this page) Unclassified		21. No. of Pages 93	22. Price* \$3.00

\*For sale by the National Technical Information Service, Springfield, Virginia 22151

1. Antenna -- Design -  
2. Space Shuttle -  
3. Dielectric properties -  
24 Feb 72 mf



## CONTENTS

---

LIST OF ILLUSTRATIONS . . . . .	v
LIST OF TABLES . . . . .	vii
LIST OF SYMBOLS . . . . .	ix
I INTRODUCTION . . . . .	1
II BACKGROUND . . . . .	3
III STUDY PROGRAM RESULTS . . . . .	9
A. Breakdown in Gases--Application to Shuttle . . . . .	9
1. General Discussion . . . . .	9
2. Breakdown Alleviation . . . . .	17
3. Nominal-Shuttle-Trajectory Examples . . . . .	19
B. Electrical Breakdown in Solids--Effects of Thermal Heating . . . . .	21
1. Intrinsic Breakdown . . . . .	22
2. Thermal Breakdown . . . . .	23
IV LABORATORY PROGRAM RESULTS . . . . .	27
A. Description of Techniques . . . . .	27
1. Overall Configuration Considerations . . . . .	27
2. Carbon-Arc Image Furnace . . . . .	31
3. Temperature Measurement . . . . .	36
a. Thermocouples . . . . .	36
b. Infrared Pyrometer . . . . .	38
4. Microwave System and Techniques . . . . .	46
B. Data from Techniques Development . . . . .	49
1. Dense RF Window Materials . . . . .	49
2. Lightweight TPS Materials . . . . .	57
3. Ablative Material . . . . .	61
4. Gas Breakdown Data . . . . .	62
V SUMMARY AND RECOMMENDATIONS . . . . .	65
REFERENCES . . . . .	69
APPENDIX RADIATION PATTERNS . . . . .	71



## ILLUSTRATIONS

---

Figure 1	Field-Strength Thresholds as a Function of Pressure for Various Values of Diffusion Parameter $pD/\Lambda^2$ . . . . .	10
Figure 2	Illustration of Measured Breakdown Threshold Scaling for Three Geometrically Similar Monopole Antennas . . . . .	13
Figure 3	Predicted Thresholds at High Temperature for One Value of Diffusion Parameter . . . . .	15
Figure 4	Effects of Pulse Duration on Breakdown Thresholds, Compared with CW Thresholds . . . . .	16
Figure 5	Effect of Bias in Raising Tip-Breakdown Thresholds of Monopole in Presence of Plasma . . . . .	18
Figure 6(a)	Thresholds for Open-Waveguide Slot Antenna ( $f = 10$ GHz) Predicted on Basis of Transitions in Local Air as Shown . . . . .	20
Figure 6(b)	Thresholds for Hemispherically-Capped, Quarter-Wave Monopole Antenna, One Inch in Diameter . . . . .	20
Figure 7	Qualitative Illustration of Thermal Breakdown in Solids . . . . .	24
Figure 8	Standard Test Configuration . . . . .	29
Figure 9	Mass Spectrometer. (a) Intake Tube; (b) Installation with Shock Tube . . . . .	30
Figure 10	Spectral Irradiance of a Cored Carbon Arc Source . . . . .	32
Figure 11	Schematic Presentation of Apparatus for Measurements in Shock Tube . . . . .	33
Figure 12	Distribution of Radiant Energy at Front of Sample . . . . .	34
Figure 13	Thermocouple Circuitry and Recording System . . . . .	37
Figure 14	IR Pyrometer. (a) Detector; (b) Circuitry and Recording Equipment . . . . .	39
Figure 15	Pyrometer Calibration Scheme Using $CO_2$ Laser . . . . .	40

Figure 16	Spectral Emittance Data for Calibration . . . . .	42
Figure 17	PbS Pyrometer Signal Voltage Against (a) Temperature for Lavite Samples and (b) Arbitrary Irradiance for Foam and Lavite Samples . . . . .	44
Figure 18	PbS Pyrometer Signal as Function of Temperature of Three Surfaces . . . . .	45
Figure 19	Photograph of Heated Sample Using Radiated Light, Taken Through Pyrometer Optical Link . . . . .	46
Figure 20	Block Diagram of Microwave System . . . . .	47
Figure 21(a)	Transmission and Reflection Data from Test Run with AS3DX Sample . . . . .	50
Figure 21(b)	Corresponding Temperature Profiles at Various Times During Test . . . . .	51
Figure 21(c)	Raw Data on Temperature and Microwaves at Beginning of Heating Cycle and Beginning of Cooling Cycle . . . . .	52
Figure 22	Transmission, Reflection, and Temperature Data from a Test Run with Lavite . . . . .	55
Figure 23	Transmission and Reflection Data on Boron Nitride (HBR) . . . . .	56
Figure 24	Mass Spectrum Early in Boron Nitride Heating Run . . . . .	56
Figure 25	Boron Nitride Fiberboard Sample (a) Before and (b) After High-Temperature Exposure to Air . . . . .	58
Figure 26	Boron Nitride Fiberboard (a) Before and (b) After High-Temperature Test in Evacuated Enclosure . . . . .	59
Figure 27	Results of Transmission Test with Aluminum Phosphate Foam Sample During Both Heating and Cooling Cycle . . . . .	60
Figure 28	Transmission Test Data for LI-1500 Sample . . . . .	61
Figure 29	Gas-Breakdown Thresholds . . . . .	62
Figure 30	Shock-Tube Breakdown Data (a) Incident and Reflected Pulses, and (b) Magnetron Pulse Timer and Ion Probe Current . . . . .	64
Figure A-1	E- and H-Plane Radiation Patterns of the Standard Test Configuration as a Function of Frequency . . . . .	74

TABLES

---

Table I	Equivalent Diffusion Lengths for Nonuniform Ionization (Planar Geometry) . . . . .	11
Table II	Equivalent Diffusion Lengths for Nonuniform Ionization (Cylindrical and Spherical Geometry). . . . .	12





## SYMBOLS

D	Diffusion coefficient
$D_f$	Free-diffusion coefficient
E	Electric-field strength
$E_\infty$	Intrinsic breakdown (field) threshold at very high temperature
$\Delta \mathcal{E}$	Energy increment
f	Frequency
$l$	Monopole length
n	Electron density
$n_0$	Initial, or thermal, electron density
p	Pressure
Q	Heat flow
$Q_i$	Heat gain
$Q_0$	Heat loss
r	Radius
t	Time
$t_c$	Time during cooling cycle
T	Temperature
$T_t$	True temperature
$T_\lambda$	Apparent temperature
Z	Distance
$\alpha$	Absorptivity
$\epsilon_\lambda$	Spectral emittance at wavelength $\lambda$
$\lambda$	Wavelength
$\Lambda$	Diffusion length

$\Lambda_e$	Effective diffusion length
$\nu$	RF ionization rate (by electron impact)
$\nu_a$	Electron attachment rate
$\rho$	Air density
$\rho_0$	STP air density

INVESTIGATIONS OF HIGH-POWER PROBLEMS IN  
SPACE-SHUTTLE ANTENNA DESIGNS

By W. C. Taylor\* and N. J. Alvares†  
Stanford Research Institute

I INTRODUCTION

This is the Final Report of a 10-month study of problems anticipated in space-shuttle antenna designs, with special emphasis on use of high RF power levels and upon communications during the reentry phase of the shuttle orbiter. Because of the shuttle's unique reentry and economic constraints, this program arose out of concern for some of the problems expected at the "interface" of the communications and guidance systems with the thermal protection system.

This program was performed largely in the Electromagnetic Sciences Laboratory, but with considerable participation in the area of heating and temperature measurement by personnel from the Fire Research Group of the Materials Laboratory.

This report is divided into four major sections. Following this Introduction, Section II gives the background and reasoning for the type of effort that was undertaken. Section III gives a summary of information, developed and/or assembled during the program, pertaining to space-shuttle high-power antenna considerations, including guidelines for design in order to avoid RF breakdown in gases exposed to high-power RF fields. Section IV is a report of the results of the laboratory program, including a description of the techniques developed and the data gathered.

---

\* Senior Research Engineer, Stanford Research Institute, Menlo Park, California.

† Mechanical Engineer, Stanford Research Institute, Menlo Park, California.

The Appendix was contributed by National Aeronautics and Space Administration's Langley Research Center to demonstrate the antenna pattern changes that can occur with nominal variation of the dielectric constant of sample dielectrics.

The authors wish to acknowledge the assistance of J. B. Chown, G. W. Wagner, R. G. McKee, and D. L. Clarke, in performing most of the measurements.

## II BACKGROUND

The shuttle orbiter reentry presents design problems considerably different from those of most previous reentry vehicles because of (1) the quite long exposure (10 to 20 minutes) to moderate heating rates, (2) the requirement of reusability, and (3) its configuration as both a space/reentry craft and subsonic airplane. The heating rates, which are moderate because of the lift capability of the configuration, make it possible to consider reusable thermal protection systems. Two types of such systems are currently being considered for eventual use--metallic radiative heat-shield and external insulation made of low-density refractory materials. In addition, since both of these systems require considerable technological advancement before they can be used on the shuttle, (nonreusable) ablative materials are now being considered<sup>1\*</sup> as an interim Thermal Protection System (TPS).

The nature of the TPS is important to antenna design since provision must be made for the RF energy to propagate through the covering, the problem being amplified by the diversity of RF systems required for this versatile vehicle. If a metallic shield is used, the antenna systems must use openings such as holes and slots in the shield, covered with high-temperature dielectric materials. In the case of insulative or ablative dielectric coverings, it may be possible to transmit RF through the coatings without the necessity of making external breaks in the shield for separate RF window materials, which would represent a considerable saving in cost and weight. In any case, the dielectric materials used as part of the RF transmission path of a given antenna must be RF-transparent for the periods when that antenna functions, after many cycles (~100) of exposure to the various environments.

---

\* References are listed at the end of the report.

Most dielectric materials absorb RF energy increasingly as temperature is increased. This property (loss factor, or loss tangent, or conductivity) must be measured to determine whether the absorption level over the relevant temperature range can be tolerated. In addition, the permittivity (or dielectric constant) of dielectrics is generally a function of temperature, and too large a variation in permittivity cannot be tolerated in some systems because of pattern and impedance-matching considerations (half-wave slabs, etc.). There is an additional complication when high RF power levels are used, since the material is subjected to heat input from two sources--aerodynamic heating and RF heating. This combination can, under certain circumstances, cause not only a large loss of RF energy but also an instability called breakdown of the material, which results in permanent damage to it. Still another way in which the RF window and TPS materials can participate in high-power limitations is by sublimation of chemicals from the material into the air shock layer. These chemicals could change the RF-power-handling capability of the rarefield, heated air layer during reentry heating.

The high-power considerations are important to the shuttle because of the possibility that high transmitted power levels will be needed for some of the many communications and guidance functions required of a vehicle with relatively little ground support. For example, high pulsed power may be needed for a radar altimeter since the transmission is two-way, depending upon how high it is deployed. Also, because of its large, flat configuration, the shuttle will have a very thick shock layer, and the reentry heating plasma will be quite thick. Even at velocities and altitudes where slender vehicles would not suffer significant attenuation, the thickness of the shuttle plasma might result in a large attenuation. To compensate for this loss, a higher-than-normal transmitter power might be required on any transmitters

operated during these periods. It will be seen that the same reentry-heating-induced phenomena that produce the plasma attenuation also produce lower thresholds for gas breakdown.

The objectives of this program were as follows:

- (1) Determine, by a survey of government laboratories and NASA contractors, the state of the art in dealing with the high-power problems discussed above.
- (2) Develop techniques for testing of (solid) materials as they affect RF transmission, with emphasis on high-power applications. (Precise measurement of low-power dielectric properties of the materials was not a specific objective of the program since this will be done at the NASA-Langley facility.)

In addition, while these techniques were being demonstrated, data on several different candidate materials were gathered, with an emphasis on nonablating materials of both high and low mass density.

Breakdown in the RF transmission path is both more frequent and better understood in gases (air or ablative-contaminated air) than in solids. A comprehensive review of breakdown in air during reentry is given in Ref. 2. Applications of this body of information to the projected shuttle configuration/trajectory form the basis of Section III-A of this report. It was felt that there was no need for a laboratory effort on this aspect of the problem at this time.

It had been expected at the inception of this program that a portion of the effort in the study program would go toward evaluating specific proposed shuttle antennas for high-power problems. However, the Phase B investigations have not progressed rapidly enough for this specific application, resulting instead in the development of guidelines for design as given in Section III-A,



It will be seen in Section III-B below that there are two kinds of breakdown in solids; the field thresholds at room temperature are in the neighborhood of  $10^6$  V/cm for both kinds, but the thresholds of many materials are reduced at higher temperatures. It is also noted that predictions of the thresholds at shuttle temperatures is not possible without additional (but unavailable) data, such as dependence of the loss tangent on temperature. Thus, techniques for testing the materials for breakdown at high temperature were the principal objective of the laboratory study.

RF breakdown in dielectric materials is not often observed outside such applications as capacitors and window materials for evacuated high-power RF generators. One of the reasons is that there is often no source of heat other than the heating from RF energy absorption due to the conductivity. Another reason is that the materials are usually selected so that the absorption is low, to minimize system losses in any case. However, breakdown has been observed in dielectrics with inadequate dissipation of the generated heat. One of the most dramatic instances was the explosive breakdown of an organic foam that was used as a mechanical support for a helix antenna.<sup>3</sup> This installation had no additional heating source, but the foam possessed typically poor thermal conductivity in addition to the required electrical conductivity behavior with temperature (see Section III-B-2).

It will be seen that none of the RF window and TPS candidates tested in the laboratory program could be broken down with the capabilities of the test equipment we used, despite the simulation of aerodynamic heating up to the expected maximum temperatures of 2500°F. Hence, these low-loss refractory materials appear to be satisfactory from a breakdown standpoint. The possibility of the use of ablative materials, including a possible compromise between low-loss

and cooling effectiveness, brings a completely different family of materials into the picture if these materials are to be used in the RF transmission path.

Measurements relating to the outgassing of materials and to breakdown along a plasma/material interface were made, using the shock tube and the quadrupole mass spectrometer. It will be seen that these tests, using the available candidate materials, gave results that could be anticipated on the basis that the materials do not outgas.



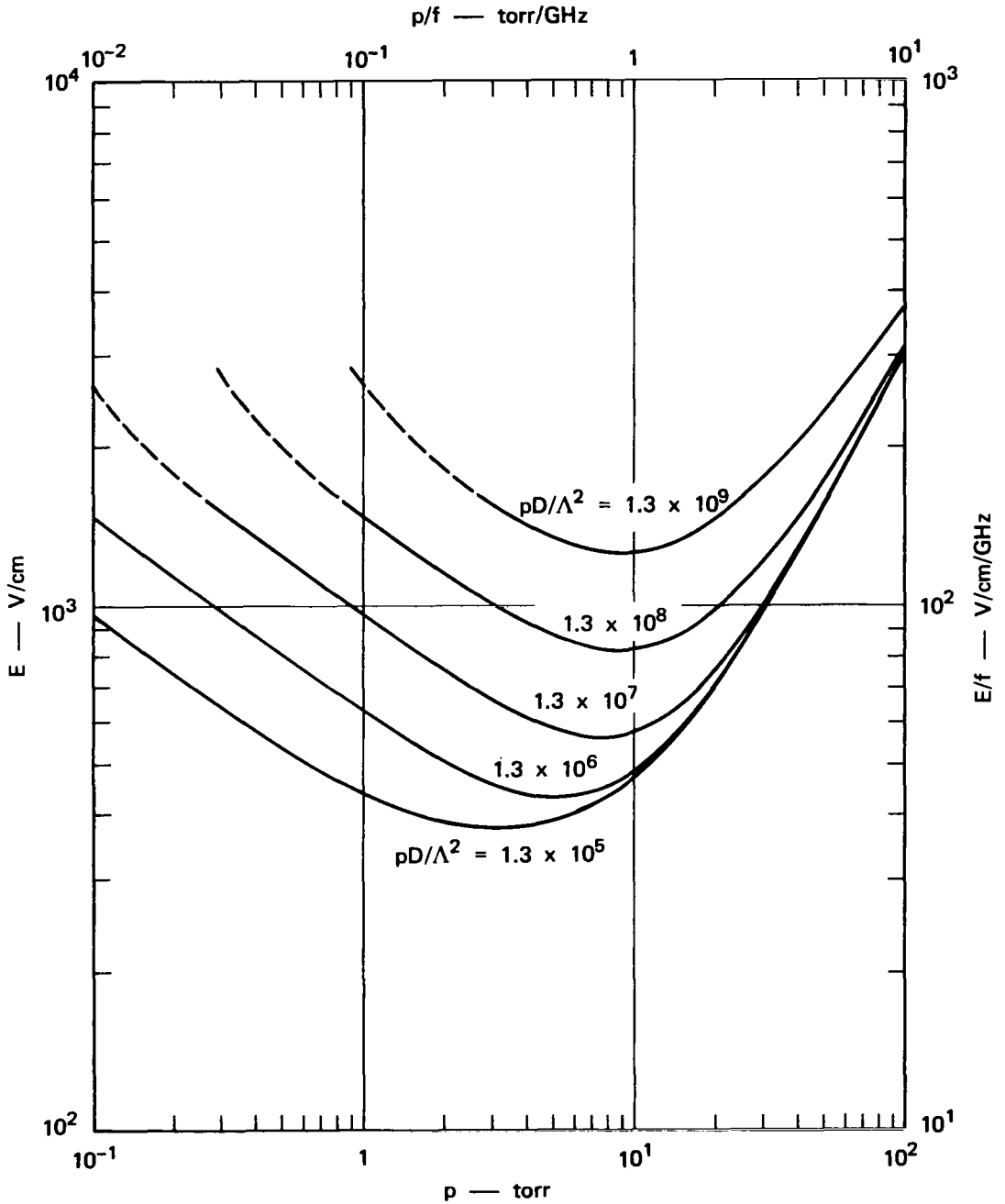
### III STUDY PROGRAM RESULTS

#### A. Breakdown in Gases--Application to Shuttle

This section presents guidelines for shuttle antenna design to avoid breakdown in gases exposed to the antenna RF fields. The background for the information presented here is given in Ref. 2 and will not be repeated here. Instead, the aspects of Ref. 2 that apply to shuttle installations will be adapted to the general shuttle needs.

##### 1. General Discussion

Thresholds for breakdown of air in intense RF fields are dominated by a broad minimum that occurs as the air density is varied through the range found in the atmosphere as a function of elevation. This minimum is found to occur roughly at an ambient pressure in torr equal to the RF frequency in GHz. For example, Figure 1 shows thresholds for a frequency of 10 GHz as a function of pressure, for several different values of the parameter  $pD/\Lambda^2$ . Here, D is called the diffusion coefficient, and  $\Lambda$  is the characteristic diffusion length. Values of D will be discussed subsequently. The diffusion length  $\Lambda$  is a function of the configuration of both the electric fields and the solid structures adjacent to the gas. For example, the diffusion length of a dielectric-plugged open-end waveguide, terminated in a ground plane, is approximately  $b/10$  where  $b$  is the E-plane dimension of the guide. Effective values of  $\Lambda$  for various field configurations and boundary conditions are given in Tables I and II. Figure 1 also has more general coordinates,  $E/f$  and  $p/f$ , indicating the scaling relationships existing between  $p$ ,  $f$ , and length dimensions. (For the general application of Figure 1, using the upper and right-hand coordinates, the parameter  $pD/\Lambda^2$  on the various curves must be replaced by  $10^2 pD/p^2 \Lambda^2$ ). In short, in addition to the usual electrodynamic similarity (wavelength and



Bottom and left-hand scales indicate special-case coordinates for  $f = 10$  GHz.

Top and right-hand scales indicate universal coordinates (see Section III-F).

TB-657522-88R

FIGURE 1 FIELD-STRENGTH THRESHOLDS AS A FUNCTION OF PRESSURE FOR VARIOUS VALUES OF DIFFUSION PARAMETER  $pD/\Lambda^2$

Table I  
EQUIVALENT DIFFUSION LENGTHS FOR NONUNIFORM IONIZATION  
(Planar Geometry)

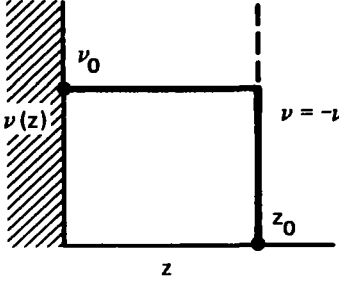
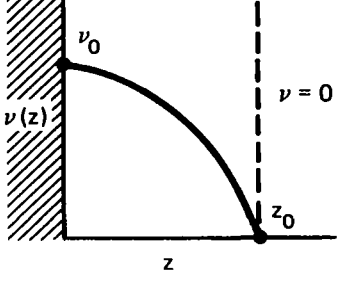
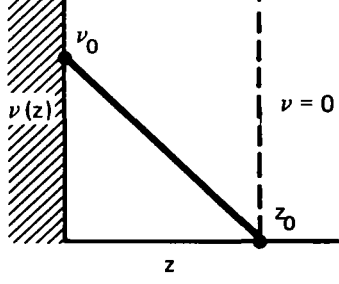
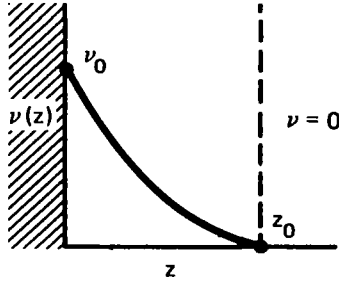
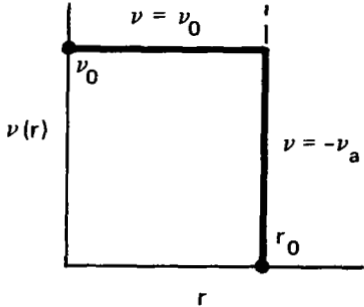
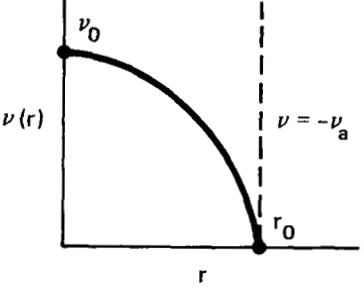
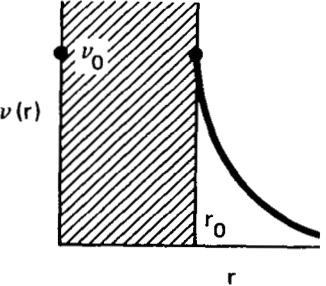
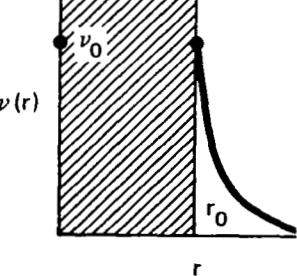
CASE	FORM OF IONIZATION RATE	DEDUCED DIFFUSION LENGTH
<p><b>1 Step Function</b></p> $\nu(z) = \nu_0 \quad 0 \leq z \leq z_0$ $\nu(z) = -\nu_a \quad z > z_0$		$\Lambda_e = \frac{z_0}{\left(\frac{\pi}{2} + \delta\right)}$ <p>with <math>\delta = 0</math> when <math>\nu_a = 0</math> and <math>\delta = \frac{\pi}{4}</math> when <math>\nu_a = \nu_0</math></p>
<p><b>2 Convex Parabolic</b></p> $\nu(z) = \nu_0 \left(1 - z^2/z_0^2\right)$		$\Lambda_e = z_0/3$
<p><b>3 Straight Line</b></p> $\nu(z) = \nu_0 \left(1 - z/z_0\right)$		$\Lambda_e = z_0/3.6$
<p><b>4 Concave Parabolic</b></p> $\nu(z) = \nu_0 \left(1 - z/z_0\right)^2$		$\Lambda_e \cong z_0/5$

Table II

EQUIVALENT DIFFUSION LENGTHS FOR NONUNIFORM IONIZATION  
(Cylindrical and Spherical Geometry)

CASE	FORM OF IONIZATION RATE	DEDUCED DIFFUSION LENGTH
<b>A CYLINDRICAL GEOMETRY</b>		
<p><b>1 Step Function</b></p> $\nu(z) = \nu_0 \quad 0 \leq r \leq r_0$ $\nu(z) = -\nu_a \quad r > r_0$		$\Lambda_e = r_0/1.6 \text{ for } \nu_a = \nu_0$ $\Lambda_e \rightarrow \infty \text{ for } \nu_a \rightarrow 0$
<p><b>2 Convex Parabola</b></p> $\nu(r) = \nu_0 (1 - r^2/r_0^2)$		$\Lambda_e = r_0/2.9 \text{ for } \nu_a = \nu_0$ $\Lambda_e \rightarrow \infty \text{ for } \nu_a \rightarrow 0$
<p><b>3 Coaxial (with outer conductor at infinity)</b></p> $\nu(r) = \nu_0 (r_0/r)^5$		$\Lambda_e = r_0/4.2$
<b>B SPHERICAL GEOMETRY</b>		
$\nu(r) = \nu_0 (r_0/r)^{10}$		$\Lambda_e \cong r_0/10$

dimensions kept proportional),  $p^{-1}$  must also be varied proportionally with wavelength and dimensions. It is noted that in the general case, it is not  $E$  that is invariant in scaling, but  $E/f$ . This means that power thresholds are invariant in scaling, since power varies precisely as  $(E/f)^2$  for geometrically similar antennas scaled for different frequencies. Thus, for example, the power thresholds of an X-band open-end waveguide can be used for a slot antenna at any other frequency, provided the dimensions are scaled with (free-space) wavelength. Figure 2 illustrates this principle.

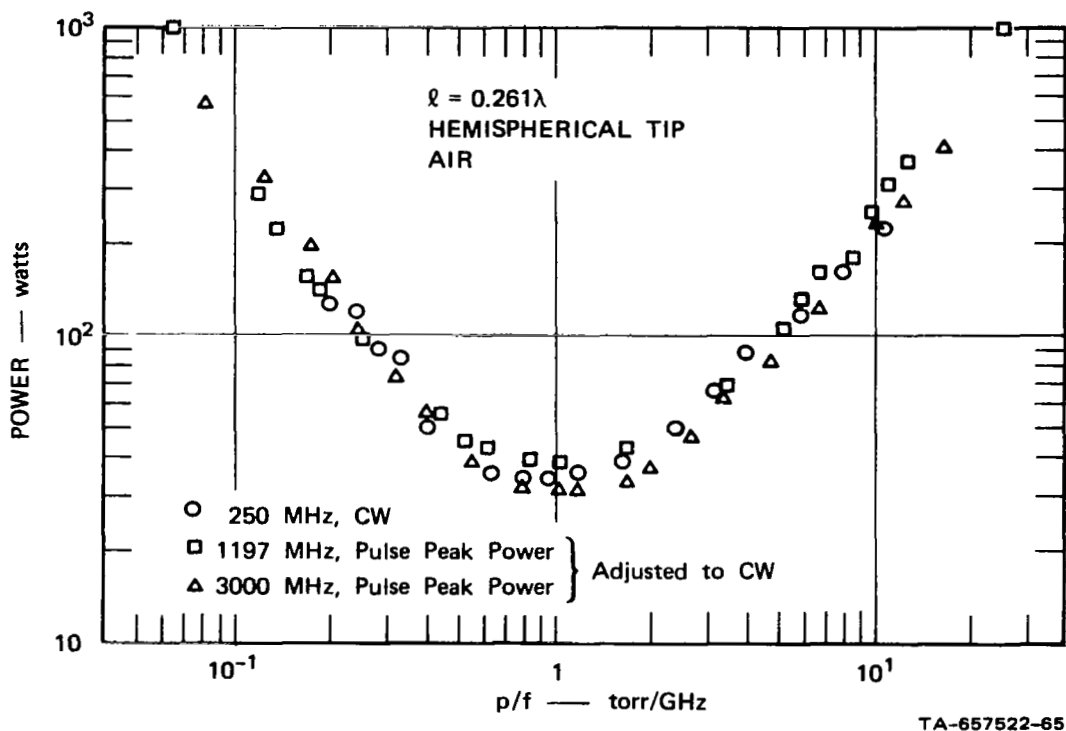


FIGURE 2 ILLUSTRATION OF MEASURED BREAKDOWN THRESHOLD SCALING FOR THREE GEOMETRICALLY SIMILAR MONOPOLE ANTENNAS

Air density in the ambient atmosphere changes approximately an order of magnitude for every 50 kft in altitude. The minimum in the threshold curve for 10 GHz is at approximately 100 kft altitude, for 1 GHz at 150 kft, etc. It should not be overlooked, however, that the ambient atmosphere is severely perturbed by a reentry vehicle, especially in the vicinity of the vehicle. (In general, this means that vehicle flow fields must be specified for accurate breakdown predictions

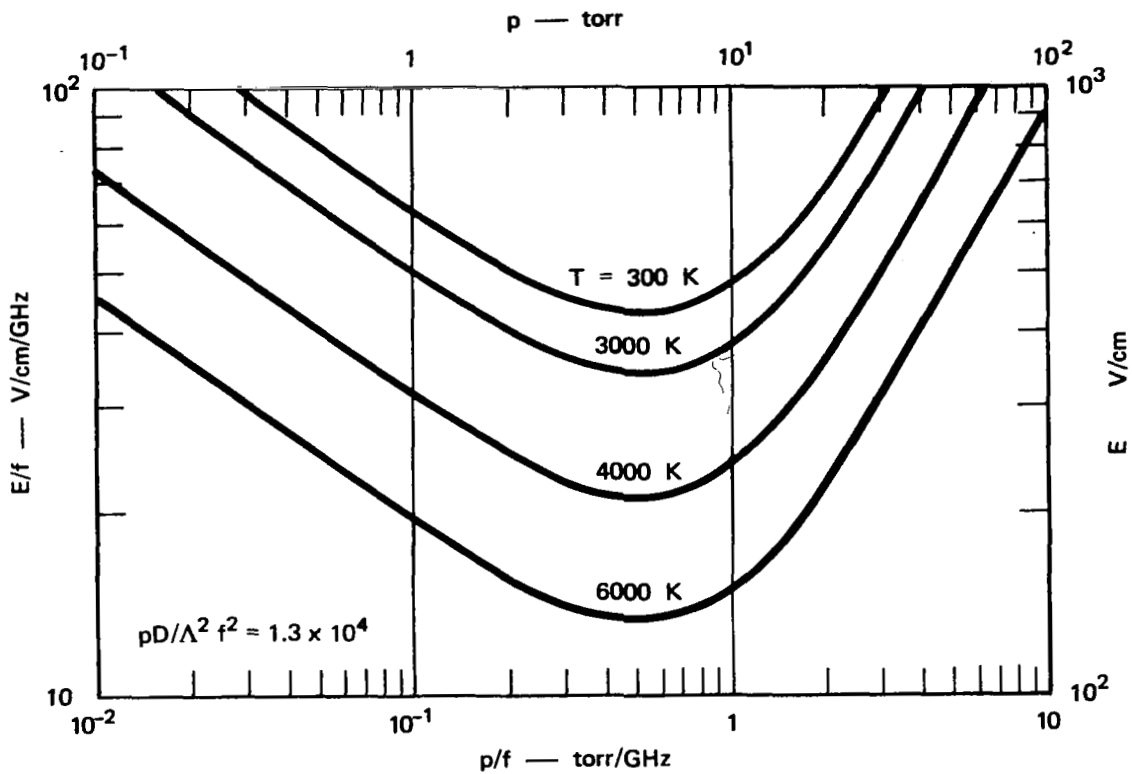


to be made.) Then the density of the air must be used as a proper variable, rather than pressure, since both pressure and temperature within the shock layer are quite different from the ambient atmosphere. (For all cases where  $T \neq 300^\circ\text{K}$ , the definition of "p" used in this section should be  $p = 760 \rho/\rho_0$ , where  $\rho/\rho_0$  is the ratio of air density to STP density.)

There are additional effects of the aerodynamic heating that alter the thresholds. One is the effect of thermal ionization. The diffusion coefficient for low electron density, called free diffusion, is given by  $D_f = 1.6 \times 10^6/p$  in the cgs-torr system. However, beyond a transition regime of electron density, the diffusion mode becomes ambipolar, and the diffusion coefficient reaches an asymptotic value about  $10^{-2}$  times its "free" value. This transition regime of electron density, where  $D$  falls by a factor of  $10^2$ , covers about three orders of magnitude in electron density,  $n$ , and is centered about a value of  $n \sim 3 \times 10^6/\Lambda^2$ . From Figure 1 it can be seen how a reduction in  $pD$  by a factor of 100 affects thresholds, especially on the low- $p$  side of the minimum.

Another effect of aerodynamic heating is that the gas is already excited to some extent, and the RF ionization becomes more efficient in terms of fields required to produce electrons. Figure 3 shows the best available information on this effect by illustrating the (normalized) field thresholds for a given value of the diffusion parameter,  $pD/\Lambda^2 f^2$ . The combined effects of reduced diffusion and more efficient ionization can give about a 10-dB decrease in thresholds on the low- $p$  side of the minimum--for example, when the gas temperature is  $4000^\circ\text{K}$ .

There is an additional effect due to flow of the gas relative to the antenna--to raise the thresholds. However, the effect is small



Top and right-hand scales indicate special-case coordinates for  $f = 10$  GHz.

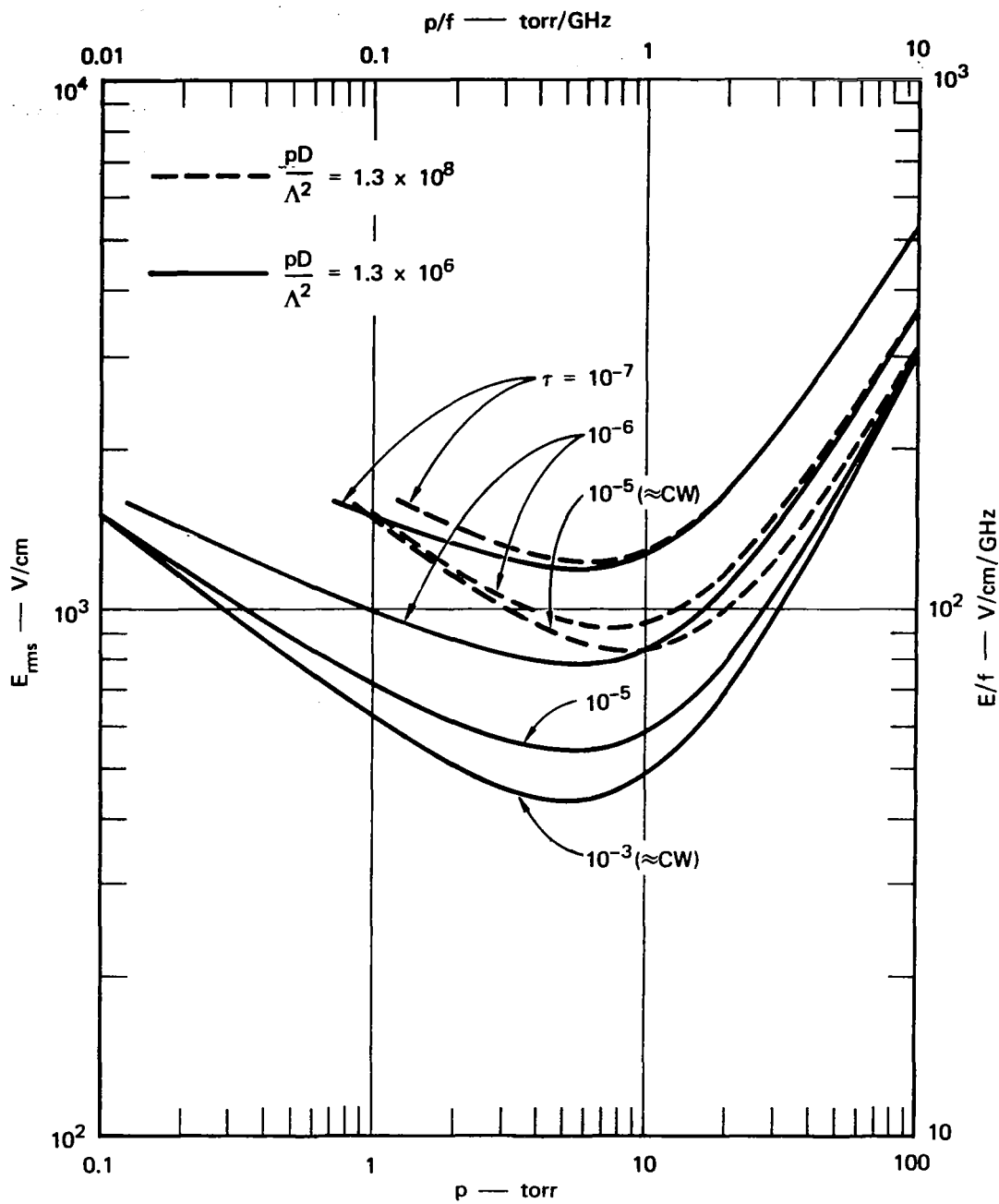
TA-657522-78R

FIGURE 3 PREDICTED THRESHOLDS AT HIGH TEMPERATURE FOR ONE VALUE OF DIFFUSION PARAMETER

enough to be ignored for the present state of projected shuttle antennas.

The above thresholds, for CW applications, can be raised if pulsed RF is used. Figure 4 shows how the thresholds vary for various combinations of pulse duration,  $\tau$ , and the diffusion parameters.

A high-power problem related to breakdown is called multipacting, or secondary-electron-resonance, discharge. It occurs at altitudes higher than ordinary gas discharges, and in fact requires the density to be low enough for electrons to traverse an antenna gap without collision. Although this type of discharge usually does not



Bottom and left-hand scales indicate special-case coordinates for  $f = 10$  GHz.  
 Top and right-hand scales indicate universal coordinates (see Section III-F).

TA-657522-109

FIGURE 4 EFFECTS OF PULSE DURATION ON BREAKDOWN THRESHOLDS, COMPARED WITH CW THRESHOLDS

produce electron density high enough to be deleterious for signal transmission, it has been known to cause outgassing from antenna surfaces sufficiently to then provide an artificial atmosphere in which a signal-attenuating discharge can be triggered.<sup>4</sup>

## 2. Breakdown Alleviation

Several different measures are available for raising breakdown thresholds in air. One is to move RF-generated electrons rapidly out of the intense-field region (faster than the gas flow does). This can be accomplished in some cases by the use of a static electric field. This method has been used effectively in the laboratory, but is not as effective when thermal ionization is present. Figure 5 shows the (experimental and theoretical) reduction in thresholds for various levels of thermal ionization,  $n_0$ .

Another means of raising thresholds is the use of chemical additives to the gas when breakdown is most probable. Measurements,<sup>5,6</sup> showed that electrophilic gases and liquids such as  $SF_6$  attach the RF-produced electrons such as to raise thresholds. However, this effect, too, is reduced by high temperatures and probably requires further investigation to be demonstrated as beneficial in a reentry situation. In addition to intentional addition of chemicals, outgassing from surfaces, especially ablating materials, can also affect breakdown thresholds in air.

Since breakdown occurs in relatively intense near fields of an antenna, gas breakdown can also be suppressed by use of dielectrics as insulative filler to replace the air in the high-field regions. For example, if a dielectric slab is placed over an antenna and if the slab is thick enough to serve as an insulative filler out to a point at which the maximum field in air is reduced by some factor  $F$  compared with the field without the dielectric, the field threshold will be at

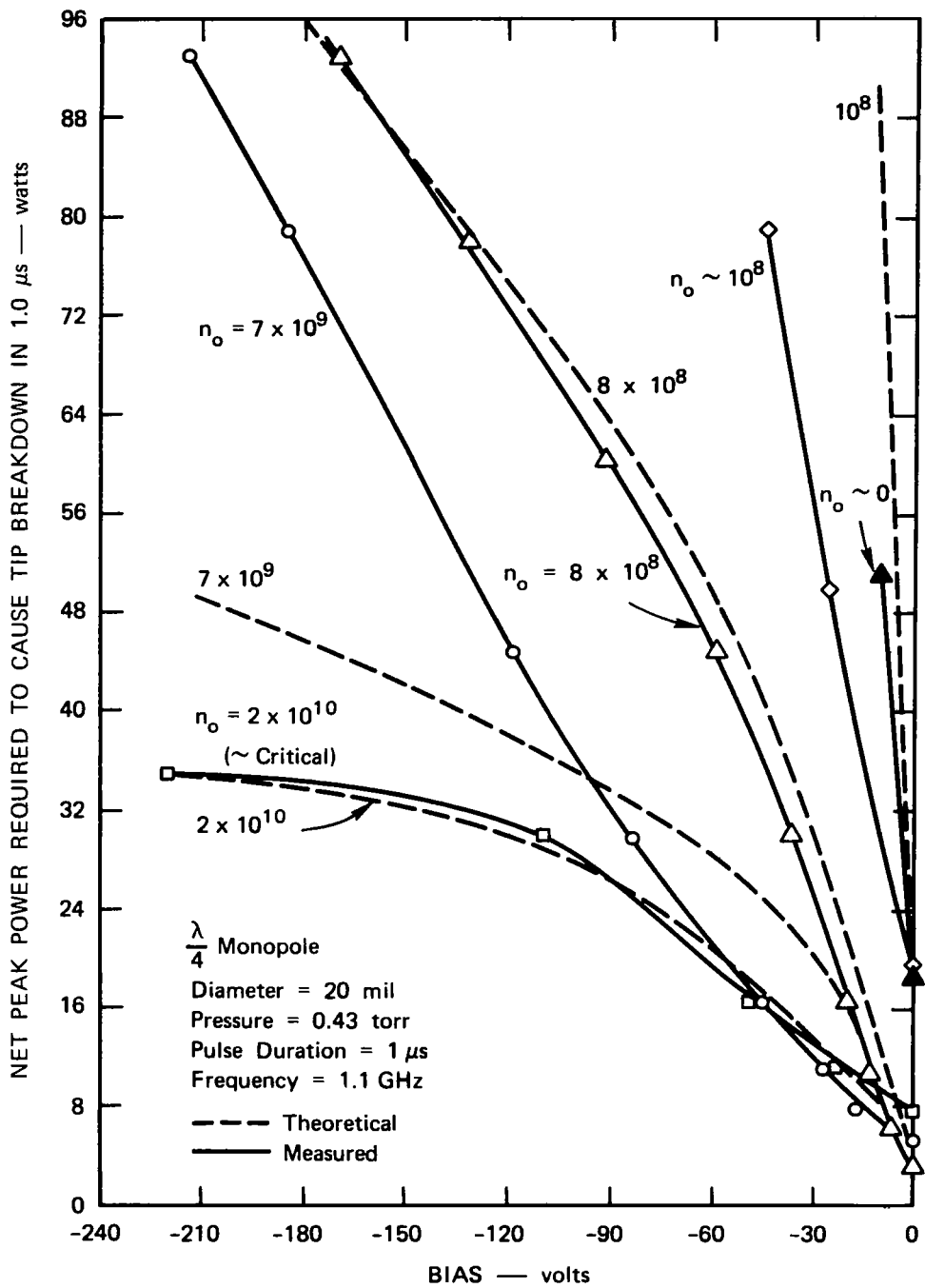


FIGURE 5 EFFECT OF BIAS IN RAISING TIP-BREAKDOWN THRESHOLDS OF MONOPOLE IN PRESENCE OF PLASMA

the same level, but at the new point. However, the power required to produce that high a field at the more remote point will be increased by a factor  $F^2$ .

### 3. Nominal Shuttle-Trajectory Examples

Let us consider an X-band slot antenna as an example for the shuttle. If the frequency is 10 GHz, and the E-plane dimension is 0.4 inches, the nominal minimum in the power threshold (at  $\sim 900$  watts with no dielectric covering) would be expected at an altitude of about 100 kft in the ambient atmosphere. However, before the shuttle gets down to 100 kft, a considerable shock layer is produced, dense enough to cause ambipolar diffusion and hot enough ( $\sim 4000^\circ\text{K}$ ) to further reduce power thresholds about 4 dB. Thus a transition from the cold-air/free-diffusion curve to hot-air/ambipolar-diffusion conditions will occur at perhaps 290 kft, as shown in Figure 6(a). Since the shuttle slows considerably by the time its altitude is 125 kft (down to about 6 kf/s), it is postulated that a re-transition will occur at approximately this altitude, and thresholds will be made higher again. It can be seen from Figure 6 that it is important to define the altitude range in which deployment of a given antenna is necessary. Figure 6(b) shows the similar predictions for a quarter-wave monopole antenna operating at 1.0 GHz, which would have a threshold minimum in the ambient atmosphere at 150 kft and at a power level of 220 watts.

Figures 6(a) and (b) are predicated on the basis of breakdown data extrapolated to a regime (corresponding to the higher altitudes) where the data are very uncertain.

If breakdown occurs on either of the antennas, significant attenuation of the signal occurs. Depending upon the details of the location on the shuttle and the angle of attack, it appears that

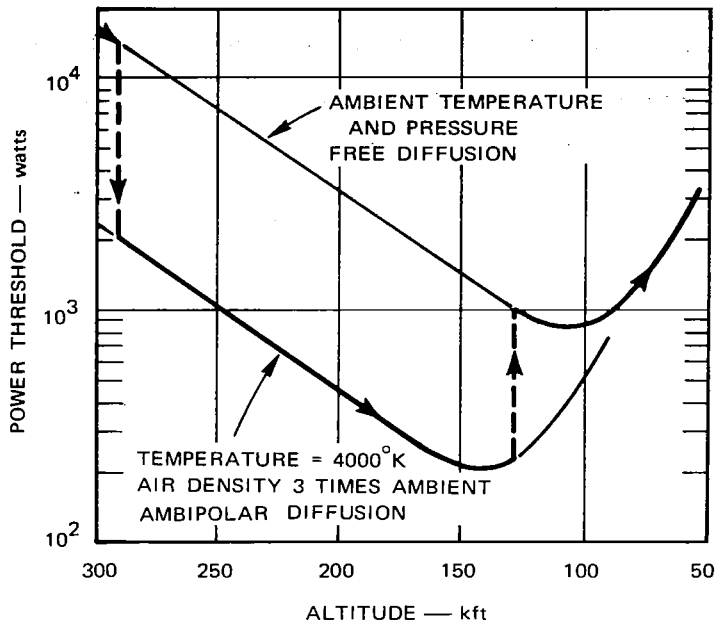
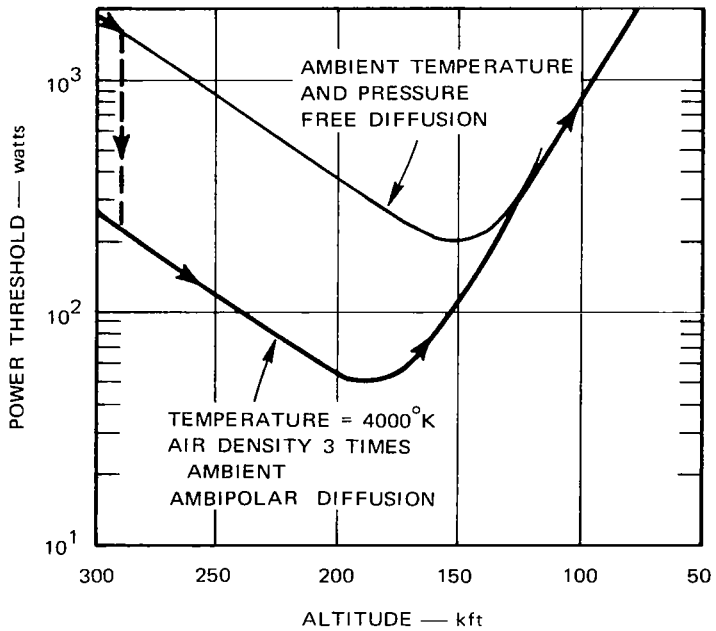


FIGURE 6(a) THRESHOLDS FOR OPEN-WAVEGUIDE SLOT ANTENNA ( $f = 10$  GHz) PREDICTED ON BASIS OF TRANSITIONS IN LOCAL AIR AS SHOWN (Bold line represents composite prediction)



TA-8677-10

FIGURE 6(b) THRESHOLDS FOR HEMISPHERICALLY-CAPPED, QUARTER-WAVE MONOPOLE ANTENNA, ONE INCH IN DIAMETER [same transitions as Figure 6(a)]

microwave frequencies of 5 to 10 GHz (and higher) would have relatively low thermal-plasma attenuation throughout the trajectory. However, the breakdown plasma would cause severe additional attenuation.

B. Electrical Breakdown in Solids--Effects of Thermal Heating

There are two kinds of electrically induced breakdown in solids, either of which usually results in a permanent change in the power-handling capability of the dielectric sample. One is called thermal breakdown, for the simple reason that the precipitating mechanism is RF heating. Although melting or some other change of phase may result from thermal breakdown, the latter differs from simple melting in that a critical RF power threshold exists beyond which an instability in the balance between heat absorbed and heat lost to surroundings produces a quickly rising temperature that has no limit until some change in the material in turn causes a change in the applied field. This material change is usually a permanent one, thus altering the power-handling capability.

A second kind of breakdown in solids is called intrinsic breakdown. This phenomenon is the solid-state analogue to voltage breakdown in gases by impact ionization, because of the following similarities:

- (1) Only electrons, not the principal mass of the material, are heated significantly by the process.
- (2) The thresholds depend on the efficiency of transmitting the electrical energy to electrons rather than to other modes of energy absorption, all of which depends in a very complicated way on the details of the microscopic state of material.
- (3) The characteristic times for it to occur (after initial exposure of the RF electric field) are in the nanosecond-to-microsecond regime.
- (4) Although the phenomenon is not principally a thermal effect, the thresholds are altered when the material surrounding the electrons is heating to temperatures of interest in reentry applications.



The term "electric strength" or "dielectric strength" of insulators usually refers to intrinsic breakdown thresholds. Since intrinsic breakdown is also a result of an instability, the runaway electron production is usually limited by some coupling to the material proper ("lattice") that fractures or punctures it.

In the following paragraphs we discuss mainly the effect of temperature on both kinds of breakdown, especially to determine whether the high room-temperature thresholds could be reduced sufficiently to make either kind a practical consideration in shuttle applications.

#### 1. Intrinsic Breakdown

There are various theories to explain intrinsic breakdown,<sup>7,8</sup> but the state of knowledge still appears primitive enough that none has yet been proved dominant. However, previous measurements show that the general range of field thresholds is around  $10^6$  V/cm. It seems generally agreed that the effect of high temperatures (several times room temperature on absolute scale) is to raise intrinsic thresholds in crystalline solids and to lower them in amorphous solids. Since the room-temperature thresholds are quite above the likely shuttle-produced field levels, the amorphous material thresholds at high temperatures are the only concern for shuttle applications. Unfortunately, there is very little data on these thresholds at shuttle window material temperatures.

A theoretical model for the temperature dependence of intrinsic breakdown thresholds in amorphous solids has the form

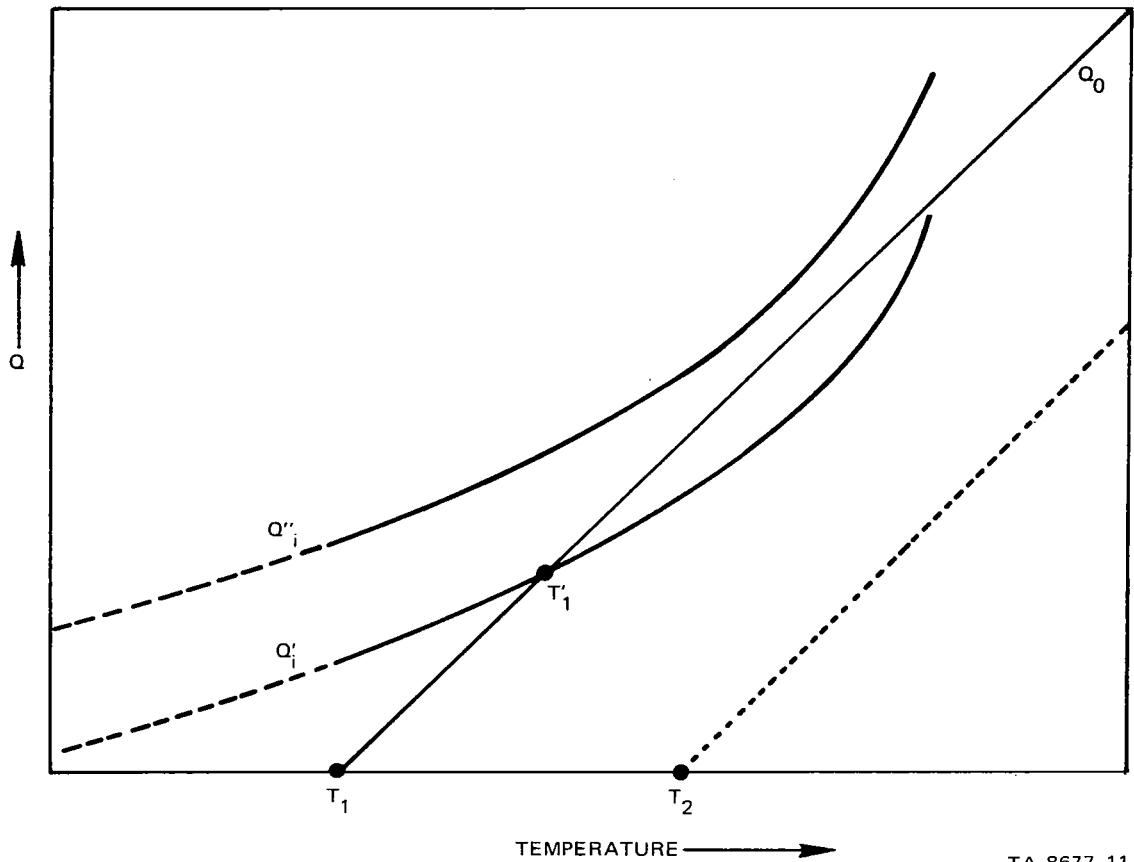
$$E(T) = E_{\infty} \exp (\Delta\mathcal{E}/kT)$$

where  $E_{\infty}$  is the threshold in the limit of high  $T$ ,  $\Delta\mathcal{E}$  is an energy increment that depends on the microscopic details of the material

structure,  $k$  is Boltzmann's constant, and  $T$  is absolute temperature. Typically, it appears, the exponential factor has values of the order of 10 at room temperature,<sup>7</sup> such that the field thresholds are probably reduced only by a factor of about 10 in the limit of high  $T$ . This would bring them down to the regime of  $10^5$  V/cm, which is probably quite above the projected shuttle experiences. For example, the field strength at the aperture of an open-end X-band waveguide is about  $10^3$  V/cm at a power of  $10^4$  W. (It is noted that because of the characteristic times for intrinsic breakdown, the thresholds would apply to peak power in event of pulsed RF. Also, for the sizes of materials for shuttle applications, the intrinsic thresholds are independent of shape and dimensions of the material.) It appears that intrinsic breakdown is unlikely, but should not be ruled out completely as a possibility on the shuttle since theory, data on  $\Delta\epsilon$  for the specific materials, and shuttle power limits are not well known at this time.

## 2. Thermal Breakdown

Thermal breakdown can be understood rather simply in terms of competition between heat flowing into the material (via electrical energy absorption, aerodynamic heating, etc.) and the heat escaping the material, usually through diffusion to cooler surroundings. If the loss tangent increases with temperature too fast to be compensated by heat losses, the RF heat input increases catastrophically to a limit imposed by some other phenomenon, such as intrinsic breakdown or a change in phase of the material--e.g., melting. This competition can be illustrated conceptually by Figure 7. First we consider the temperature of the material without electrical heating to be in equilibrium at  $T_1$ . The heat flow out of the material,  $Q_0$ , will increase approximately linearly with temperature when electrical heating causes an increase in temperature. Figure 7 also shows the heat input,  $Q_1$ , due to



TA-8677-11

FIGURE 7 QUALITATIVE ILLUSTRATION OF THERMAL BREAKDOWN IN SOLIDS

electrical heating at two different levels of applied electrical power. Consider first the lower level,  $Q_i'$ . A sudden application of the electrical power will cause an increase in temperature, causing both  $Q_i'$  and  $Q_0$  to increase from their values at  $T_1$ . This increase will continue until  $Q_0 = Q_i'$ , giving a new equilibrium temperature at  $T_1'$ , where the curves intersect. This then is the temperature that results from the simultaneous application of thermal and electrical heating. There is no breakdown in this case. Now consider some higher level of applied electrical power, giving a higher input  $Q_i''$ . Application of this level causes  $Q_0$  to vary along the same curve as before. However, in this case,  $Q_0$  can never get as large as  $Q_i''$ , and no stable equilibrium temperature is reached in this case. Breakdown

would occur in this case as the temperature increased to the point where either intrinsic thresholds are lowered to the applied field levels, some change of state occurs in the material, or the supply of electrical power becomes limited by some phenomenon not included in the analytical model. The thermal breakdown threshold field level is the level that would give a curve (between  $Q_i'$  and  $Q_i''$ ) just tangent to  $Q_0$ .

Figure 7 also demonstrates that the field thresholds are reduced by an increase in the (nonelectrical) equilibrium temperature of the material. For example, the dotted line represents the  $Q_0$  for some installation with a temperature  $T_2$  in the absence of electrical heating, with  $T_2 > T_1$ . It can be seen that even the lower electrical power level corresponding to  $Q_i'$  is above the threshold since the curves do not intersect.

It is seen from Figure 7 that for a material to break down it is necessary that its loss tangent vary with temperature in such a way that  $Q_0$  and  $Q_i$  do not intersect; this type of variation may not occur in some materials in some applications, regardless of the electrical power level. Quantitatively, when the boundary conditions are given and the electrical properties are known as a function of temperature, the thresholds for breakdown can be evaluated by solving two coupled differential equations<sup>9</sup> (which express continuity of thermal energy and electrical energy). One interesting general result of this theory is that the breakdown field varies inversely as the square root of the electrical conductivity. Thus, for instance, if the threshold is measured at one temperature, and the conductivity is known as a function of temperature, then the threshold at all temperatures can be predicted. It is not unusual for RF materials that are quite transparent at room temperature to increase conductivity by two orders of magnitude at 2500°F. Thus the thermal breakdown threshold is a factor of 10 lower at 2500°F than at room temperature.

Determination of the absolute thresholds would appear to be more easily measured in many cases, by mockup and simulation, than by theoretical prediction. This is especially true for special types of materials such as sandwich construction and forms with large voids. In this case, a loss tangent may be measured on a bulk basis (averaged over the entire volume, including voids), but the RF heat would be absorbed only in relatively thin walls. Unless this heat is well dissipated over the volume, and conducted to surroundings, failure in the wall could result.

## IV LABORATORY PROGRAM RESULTS

### A. Description of Techniques

#### 1. Overall Configuration Considerations

One of the prime objectives of this program was to develop techniques for testing of materials to determine their effect on the power-handling capability of the RF/TPS systems interface. Thus the following somewhat detailed descriptions are given to serve as a guide for NASA and/or its contractors in making similar tests.

It is necessary that some of these techniques be simultaneously applied during a test--for example, the sample must be heated by the carbon-arc image furnace, and the temperature monitored, at the same time that any of several other tests are performed. This requirement posed some problems in configuration design since they must be mutually compatible.

The four primary requirements of the configuration were:

- (1) It must be heated.
- (2) The temperature must be monitored.
- (3) It must make the sample accessible to transmission of an RF wave.
- (4) It must be in a low-pressure vessel, and, for some tests, have an atmosphere on one side and low-pressure on the other side.

It was decided early in the program that heating by a remote optical source would be attempted, for the following reasons:

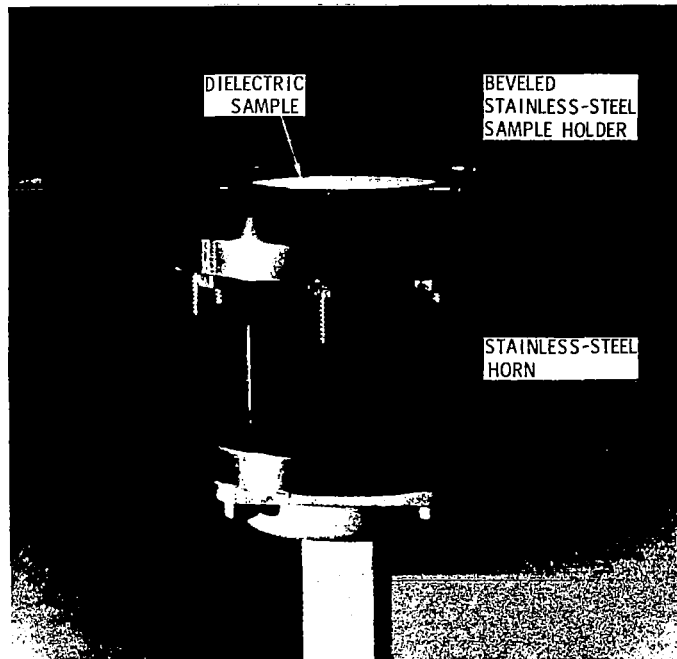
- (1) It is remote enough to be out of the primary radiation region.
- (2) It provides a temperature profile similar to aerodynamic heating.

- (3) Available sources could heat sizable dark samples to temperatures around 2500°F (smaller samples to higher temperatures by added focusing).
- (4) The transmission tests could be made with the heat source on.

The biggest disadvantage is the requirement of a surface optically absorbing enough to reach maximum temperatures of interest, but it was felt that this could be overcome. Section IV-B describes this facility further.

Several configurations were tried, either on paper or in prototype. One that was used for a time employed a relatively large slab of the sample material supported by a collar over an open-end waveguide. It was eventually concluded that this was not an optimum configuration for some of the anticipated tests because of its peculiar radiation pattern and because the foam samples would not be strong enough to withstand one atmosphere of pressure across them. (As it turned out, the smaller samples in eventual test configuration did not withstand the 15 psi either.) A "standard" configuration was eventually reached; it is shown in Figure 8. The stainless-steel horn opens to 0.9 inch in the E-plane to give a square 0.9-by-0.9 inch aperture capped by the stainless-steel sample-holder and the round sample. The sample diameter is 1.4 inch, slightly greater than the aperture diagonal. The pressure seal was accomplished by cementing the sample in the holder using Sauereisen high-temperature ceramic cement, and by the use of silver-plated metal V-seals between the sample holder and the horn flange. High-temperature elastomer seals were used in the cooler joints behind the horn.

The temperature measurements were made either by thermocouples imbedded near the surfaces of the sample or by an infrared pyrometer. The pyrometer was used to monitor only the irradiated



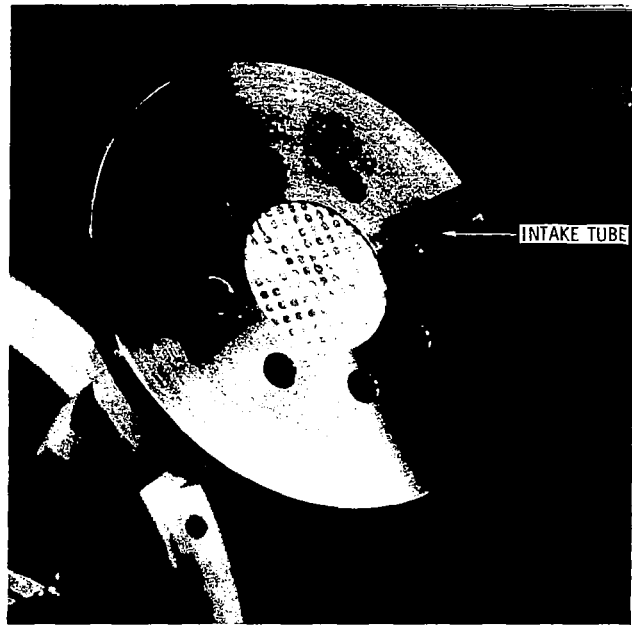
TA-8677-26

FIGURE 8 STANDARD TEST CONFIGURATION

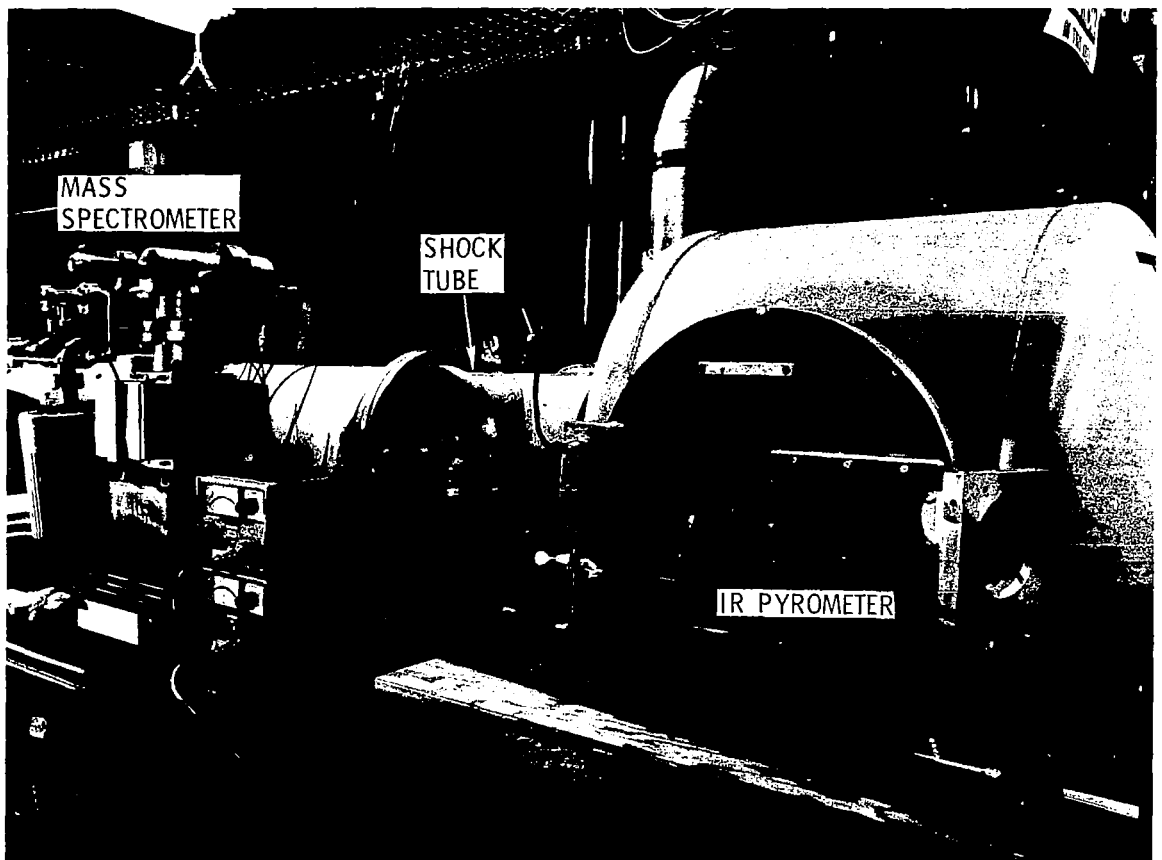
surface (the more difficult problem), although it was feasible to work an optical path from the cooler side through the waveguide system and out an aperture to the IR detector. These techniques are detailed in Section IV-3.

A quadrupole mass spectrometer was used to monitor outgassed products from the heated materials. Its intake was arranged through two different routes. In the earlier arrangement, a quarter-inch stainless-steel tube was used with its intake near the irradiated side of the sample. In the later arrangement, which was an improvement in terms of allowing fewer collisions with walls of the channel, the waveguide itself was used to bring the gas from the back side of the sample to a magic-T junction from where the gas was pumped through the "vertical" arm into the mass spectrometer. The earlier arrangement is shown in Figure 9(a) and (b).





(a) INTAKE TUBE OVER SAMPLE



(b) INSTALLATION WITH SHOCK TUBE

TA-8677-12

FIGURE 9 MASS SPECTROMETER INSTALLATION

Most of the tests were run inside the test section of the SRI 12-inch diameter shock tube. The tube was used both to serve as a pressure vessel and to furnish a plasma over the samples where breakdown at the plasma/sample interface was investigated. The shock tube is described elsewhere.<sup>10</sup>

Microwave pick-up horns were used in both the E-plane and H-plane of the transmitting (sample-covered) horn. They were at a 45° angle with the center line (such as to be out of the focused beam of the carbon arc) and 6½ inches from the sample. Three different X-band signal sources were used. The microwave system and techniques are described in detail in Section IV-4.

## 2. Carbon-Arc Image Furnace

The carbon-arc image furnace used for these measurements was a Strong Model 54007-1 arc lamp using 13.6-mm positive and 12.5-mm negative electrodes. The voltage to the electrodes was 70 Vdc at 150 amps. This gave a positive carbon feed rate of 22 in/hr. The furnace contains an elliptical-mirror imaging system.

Most of the energy used to heat the specimens in these experiments is radiated by an incandescent ball of carbon gas at the tip of the positive carbon. A further small amount of energy comes from the tail flame and from the heated carbon support structures. The tip of the positive carbon is located at the short focal point of the elliptical mirror (15.6 cm from the surface of the mirror), and the specimen is positioned to the long focal point (58.5 cm from the surface of the mirror).

The total amount of energy radiated by the incandescent ball of carbon gas is a function of the size of the ball, its emittance, its temperature, and its stability of position within the primary focus

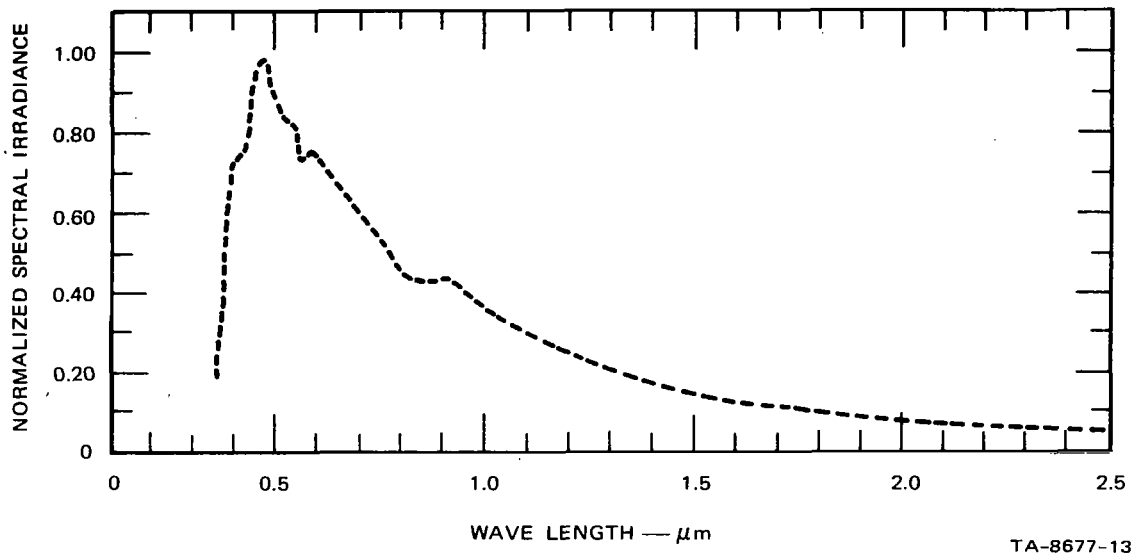


FIGURE 10 SPECTRAL IRRADIANCE OF A CORED CARBON ARC SOURCE

of the mirror. The spectral irradiance of the image furnace is similar to the spectral energy distribution from the sun. Figure 10 shows the carbon arc spectral distribution. Note that the spectrum is terminated at 2.5 microns since most of the emitted energy is contained at shorter wavelengths.<sup>11</sup> The temperature of the incandescent ball of carbon gas has been measured to be about 5800°K. This source produces a blackbody distribution where over 95 percent of the radiative energy is emitted below 2.5 microns. This spectrum does not take into account the emitted energy that comes from hot components of the furnace other than the arc tip.

Figure 11 is a sketch showing the geometry of the thermal imaging system. Position 1 indicates the first focus of the elliptical mirror where the carbon electrodes are located. Position 2 indicates the second focus where the image of the electrodes is directed to the specimen to be heated. The average irradiance (optical radiant intensity) of the source at the image plane was measured to be  $14.3 \text{ cal cm}^{-2} \text{ sec}^{-1}$  at the point of maximum intensity. The radiant intensity across the image plane experiences a cyclic temporal variation because the carbon

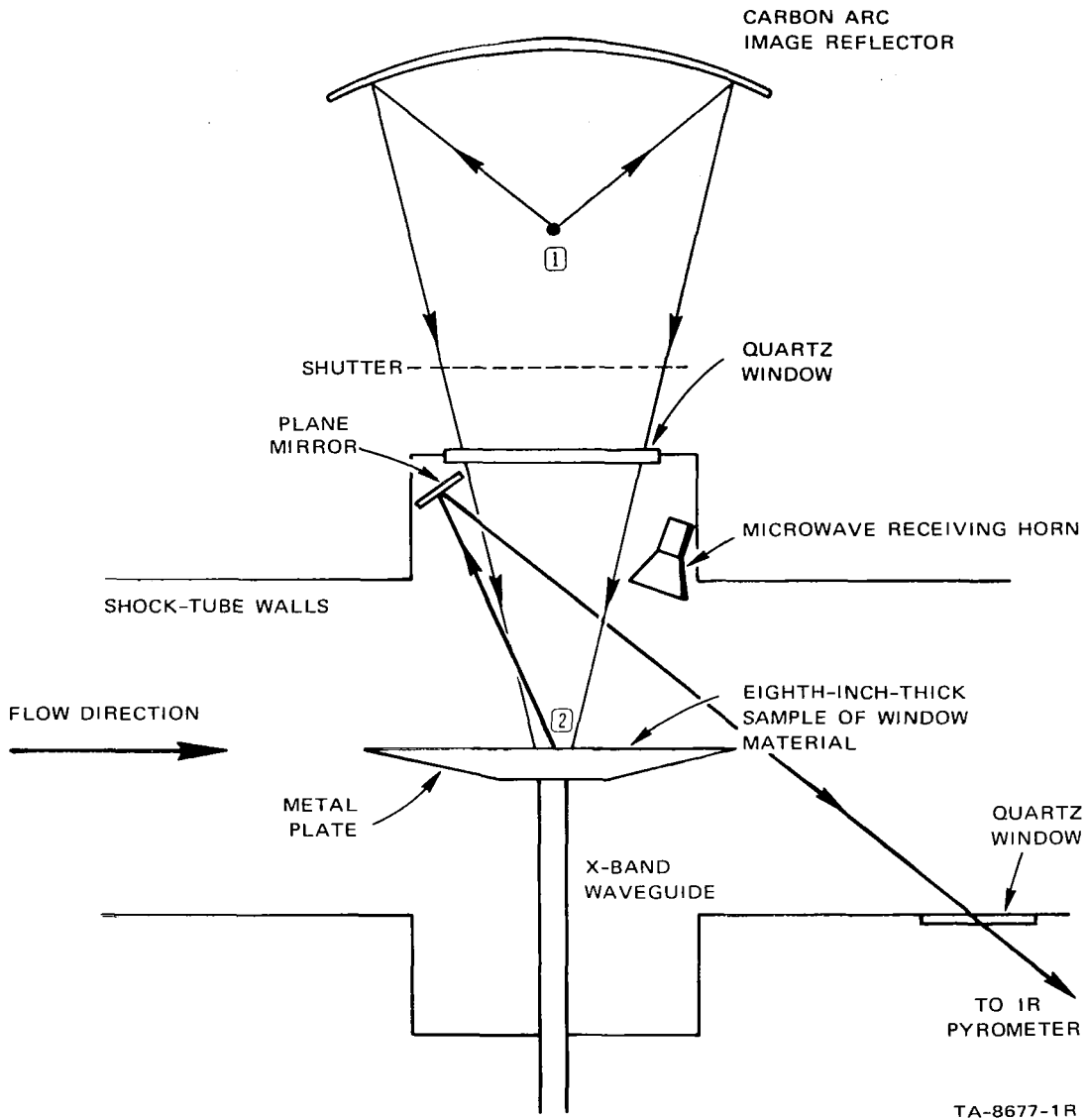


FIGURE 11 SCHEMATIC PRESENTATION OF APPARATUS FOR MEASUREMENTS IN SHOCK TUBE

electrodes feed toward one another as they are consumed during operation; also, the positive electrode rotates so that the cratering action resulting from the arc is uniform. These motions result in a cyclic irradiance level that varies by no more than  $\pm 10$  percent from the average irradiance.<sup>12</sup> The distribution of average irradiance across the specimen's surface is shown in Figure 12. Note that this is

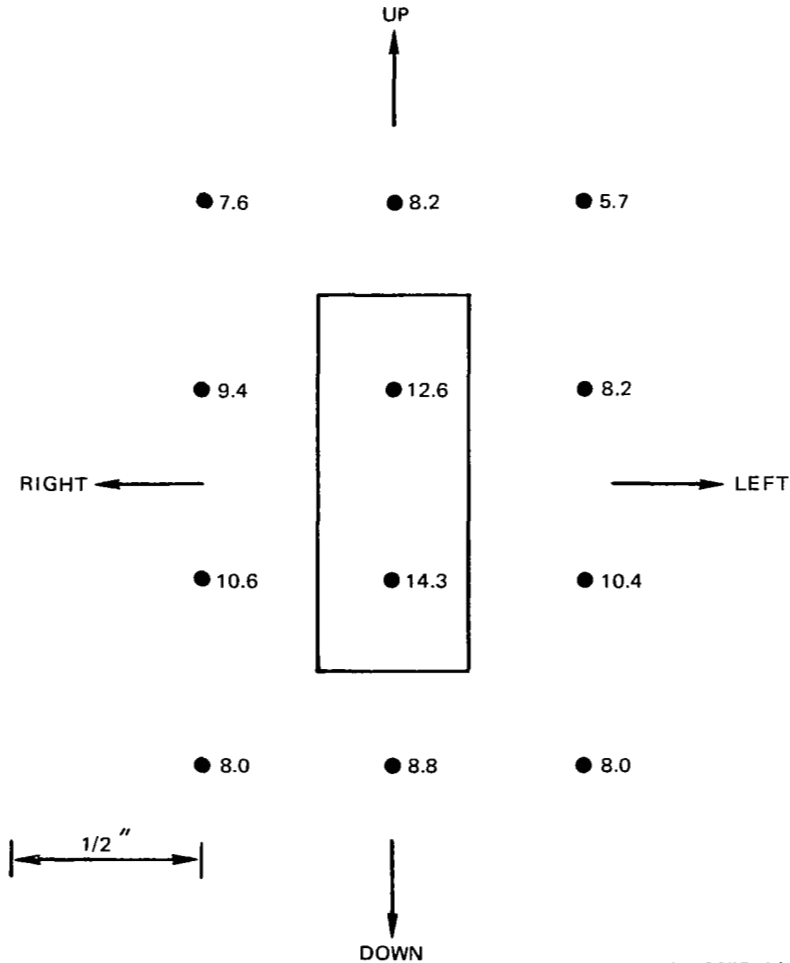


FIGURE 12 DISTRIBUTION OF RADIANT ENERGY AT FRONT OF SAMPLE

the irradiance that was received through the quartz window of the measurement chamber. The dimensions of the waveguide opening of the

specimen holder are superimposed to show the average energy distribution over the area of interest. If the surface of the specimen had an absorptivity of  $\alpha = 1.0$  (i.e., if it absorbed all the thermal energy impinging on the surface), and if there were no conduction or convection losses, the maximum temperature achieved by the specimen would be 2800°F. Any variations in the power to the image furnace would serve to change the attainable temperature of the specimen.

Most of the materials that have been proposed for use as high-temperature microwave antenna window materials and for the TPS are dielectrics, either in the form of low-density ceramic foams or high-density ceramic composites. During the initial phases of the project there were no experimental window materials available to us for testing purposes. Therefore, it was necessary to select an easily obtainable ceramic analog for our high-temperature tests. The material we selected was Lava 1136 (Lavite<sup>\*</sup>). Microwave transmission measurements of "cured" Lavite indicated that it had low losses at room temperatures.

The optical properties of most ceramics are similar in that they generally reflect and transmit visible radiation. Lavite and the proposed antenna window materials have these properties. To efficiently heat them by thermal radiation, it is necessary to provide the material with an optically absorbing surface layer. Several high-temperature paints were tested for this purpose. The testing technique was to apply and cure the paint, according to manufacturers' specifications, on a Lavite specimen and then place the painted specimen in a high-temperature oven at 2000°F. Initially, we found only one paint that survived this treatment. This was the Curtiss-Wright Detectotemp high-

---

\* American Lava Corporation, 3M Company.

temperature-indicator paint. The cured color of the paint was a dark green, which appeared significantly darker than the uncoated Lavite surface. Later, during the course of the project, a different high-temperature paint came to our attention which, upon testing, proved to have optical properties superior to those of the Curtiss-Wright paint. This paint (VHT, Flameproof Coating) appeared to have the properties of a blackbody throughout the spectral region of interest, and was used for all subsequent tests where coatings were employed.

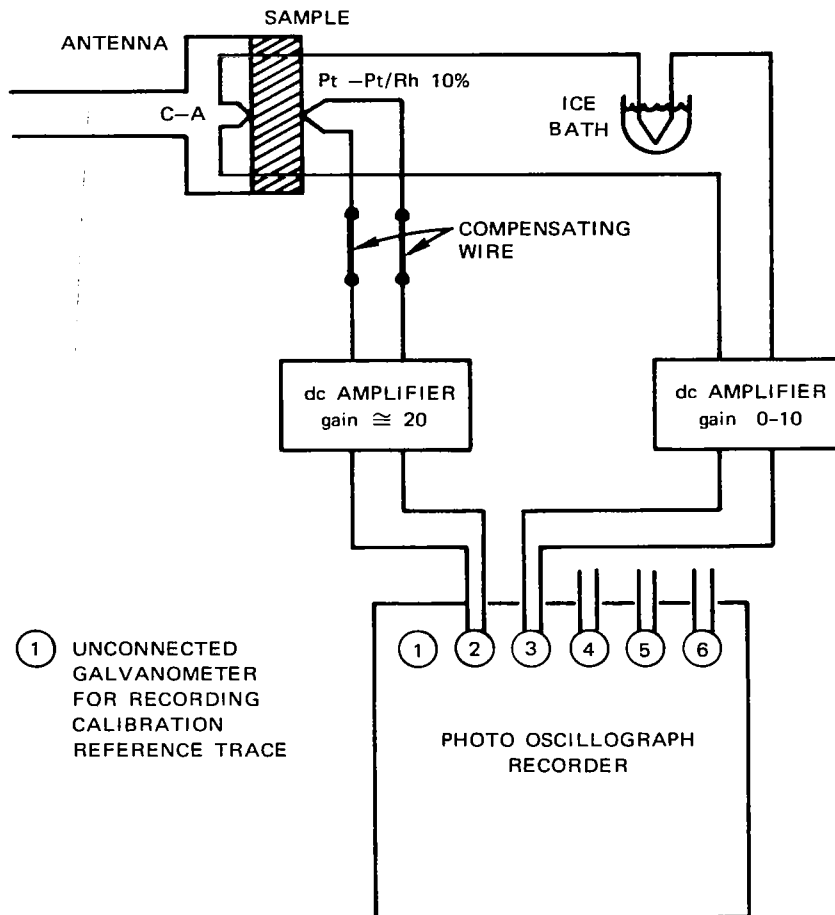
It will be seen below that the maximum front-face temperatures of the coded samples were around 2400°F. Temperatures reached by the various materials without coatings averaged from about 2000°F (boron nitride) to 2300°F (Lavite). (It was also learned that the presence of air at a pressure of 1 atmosphere reduced the maximum temperature by less than 50°F compared with a vacuum.)

### 3. Temperature Measurement

#### a. Thermocouples

The temperature measurements of the high-density specimens were made with thermocouples. The temperature of both front (the surface exposed to radiation from the image furnace) and back (the surface in contact with the waveguide) surfaces were of interest. The thermocouples were installed in the sample by inserting them in shallow slots that had been cut into the surface prior to curing and painting. The thermocouples were secured in the slots by covering them with Sauereisen cement. Due to the difference in temperature through the thickness of the specimen, five-mil-platinum-vs.-platinum-10-percent-rhodium thermocouples were used on the front surface, while 0.010 inch-chromel-vs.-alumel thermocouples were used at the back surface. The latter type was referenced to an ice-bath cold junction.

The thermocouple signals were recorded with a photo-oscillograph recorder, as shown in Figure 13. The thermocouples were calibrated



TA-8677-15

FIGURE 13 THERMOCOUPLE CIRCUITRY AND RECORDING SYSTEM

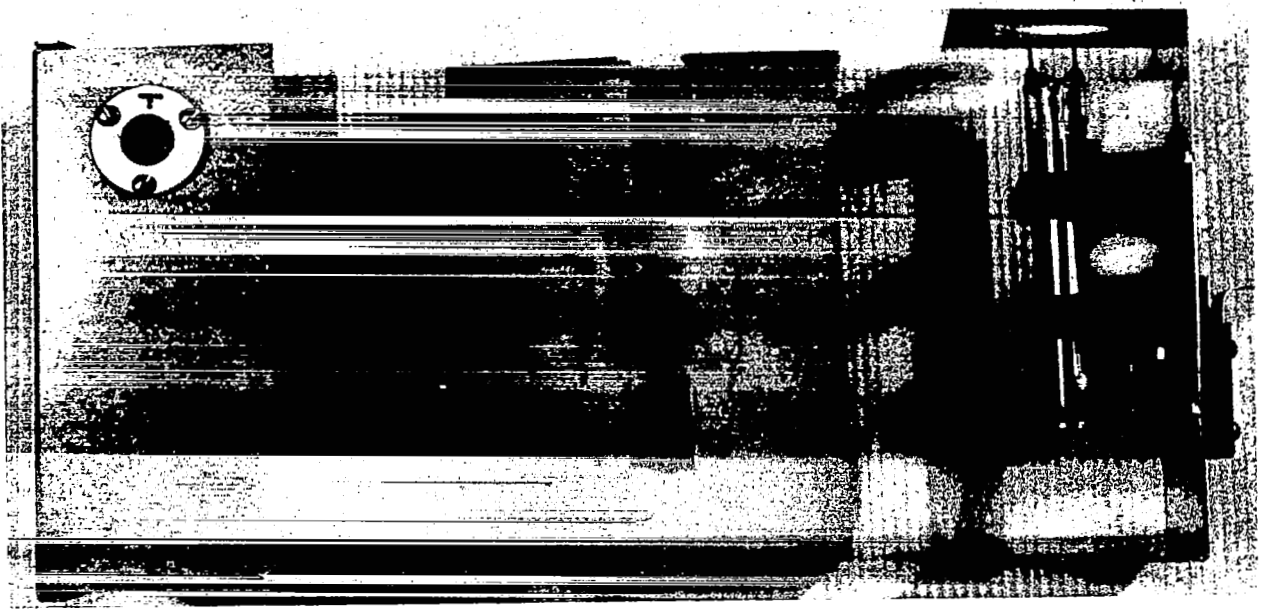
by impressing known step-function millivolt signals in series with the circuit. The highest equilibrium temperatures that the Lavite specimens achieved under image furnace irradiation were  $2400^{\circ}\text{F} \pm 100^{\circ}\text{F}$  at the front surface and  $1000^{\circ}\text{F} \pm 100^{\circ}\text{F}$  at the back surface. The thermocouple leads from the back surface were run through small holes in the sample out the front surface, hence to the external instrumentation. The thermocouple wires were oriented perpendicular to the electric field in order to minimize effects of the wires on the microwaves.



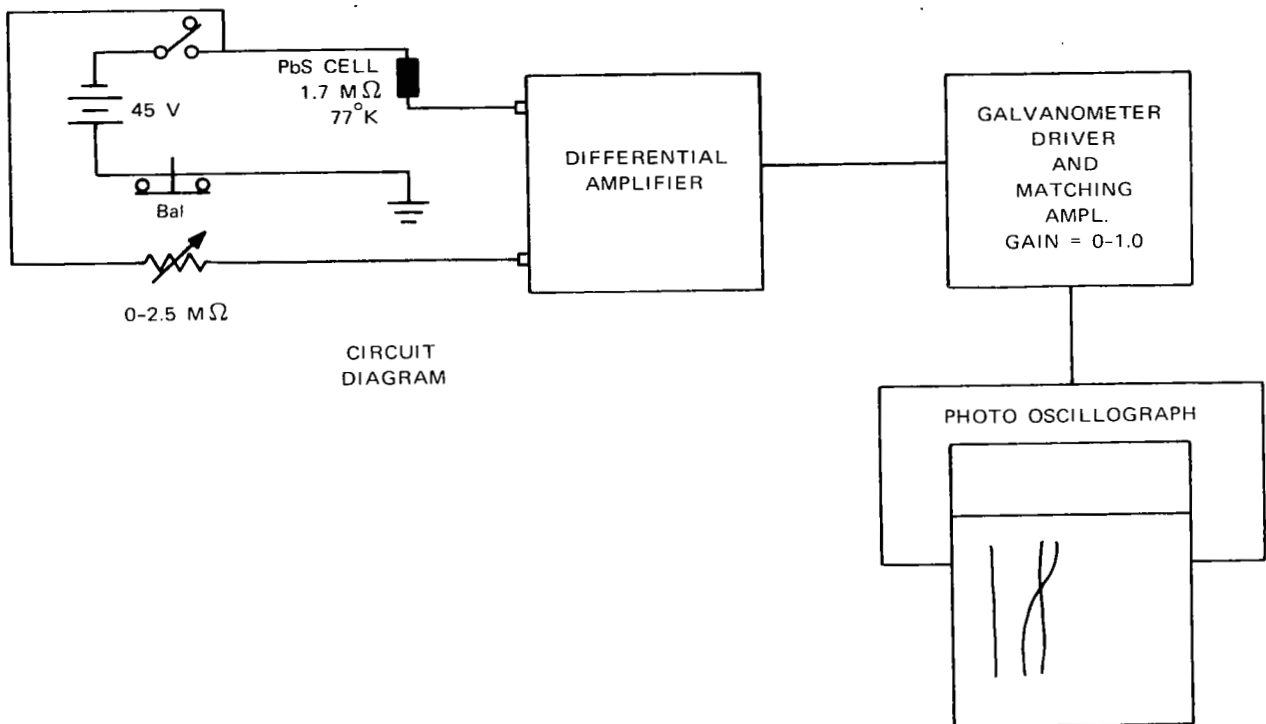
b. Infrared Pyrometer

Thermocouples provide the most efficient and accurate measurements of temperature in opaque, high-density materials. In low-density foams, thermocouple techniques are not feasible due to the difficulty of ensuring intimate thermal contact between the foam and the thermocouple junction. We therefore embarked on a series of experiments to develop a thermal radiation pyrometer that would give us surface temperature during heating with the image furnace. The reason for using this instrument is to select a sampling wavelength for the pyrometer that is remote from the spectral distribution of the irradiance from the image furnace. Ninety-six percent of the irradiated energy from the reacting region between the electrodes of the image furnace falls at wavelengths shorter than 2.5 microns. However, we found that a significant component of thermal energy was emitted at wavelengths longer than 2.5 microns. It is assumed that this energy results from hot carbon support structures within the furnace. By placing a Plexiglas window between the furnace and the quartz window of the measurement chamber, it is possible to filter out all spurious radiant energy longer than 2.8 microns. We can then make surface-temperature measurements of the specimen with the thermal-radiation pyrometer in any wavelength region longer than 2.8 microns. By this technique we avoid detecting any of the image-furnace radiation that would be reflected from the surface of the irradiated specimen to the pyrometer.

Figure 14(a) shows an expanded view of the pyrometer. The detector is a liquid-nitrogen-cooled lead sulfide cell. This cell is encapsulated in an insulated enclosure both to reduce the heat transfer to the cell and to provide a light-tight environment. A 3.41-micron interference filter and an aluminum shutter assembly are located



(a) DETECTOR



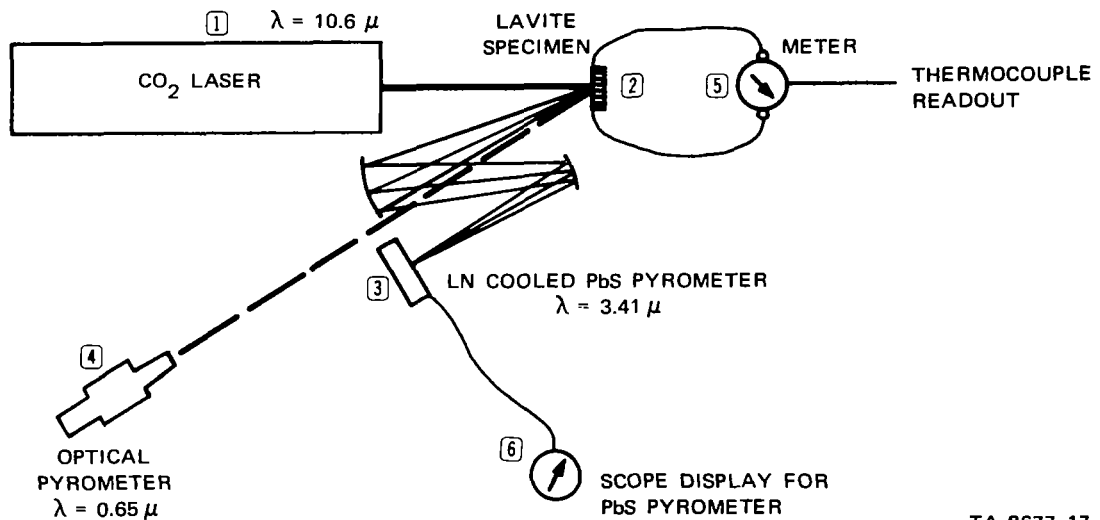
(b) CIRCUITRY AND RECORDING EQUIPMENT

TA-8677-16

FIGURE 14 IR PYROMETER

in front of the sensing element of the cell. A diagram of the detection electronics and recording system is included in Figure 14(b). Calibration and stability checks of the pyrometer were made by focusing the energy from the opening of a high-temperature blackbody furnace onto the sensing element of the detector using a folded optical path that employed a front-surfaced parabolic mirror. Care was taken to always ensure that the sensing element of the lead sulfide cell was covered by the image of the blackbody-furnace orifice.

After the calibration was accomplished, a coated Lavite specimen was located at the position of the blackbody furnace. The beam from a 100 W CO<sub>2</sub> laser was directed to the surface area of the specimen where the thermocouple was imbedded, as shown in Figure 15. Since the



TA-8677-17

FIGURE 15 PYROMETER CALIBRATION SCHEME USING CO<sub>2</sub> LASER

CO<sub>2</sub> laser emits radiation at 10.6 microns only, we can employ the infrared pyrometer to determine the apparent temperature of the surface at 3.41 microns. With a standard hot-wire optical pyrometer, we can also measure the apparent temperature of the surface at 0.65 micron, the standard wavelength for most commercial optical pyrometers. By comparing the thermocouple temperature to the apparent surface temperatures sensed by the pyrometers, we were able to determine the spectral emittance of coated Lavite from 1200°F to 2600°F at  $\lambda = 3.41$  and 0.65 microns, respectively, using the following relation:

$$\epsilon_{\lambda} = \exp \left[ \left( \frac{1}{T_t} - \frac{1}{T_{\lambda}} \right) \frac{C_2}{\lambda} \right]$$

where

$\lambda$  = Measurement wavelength

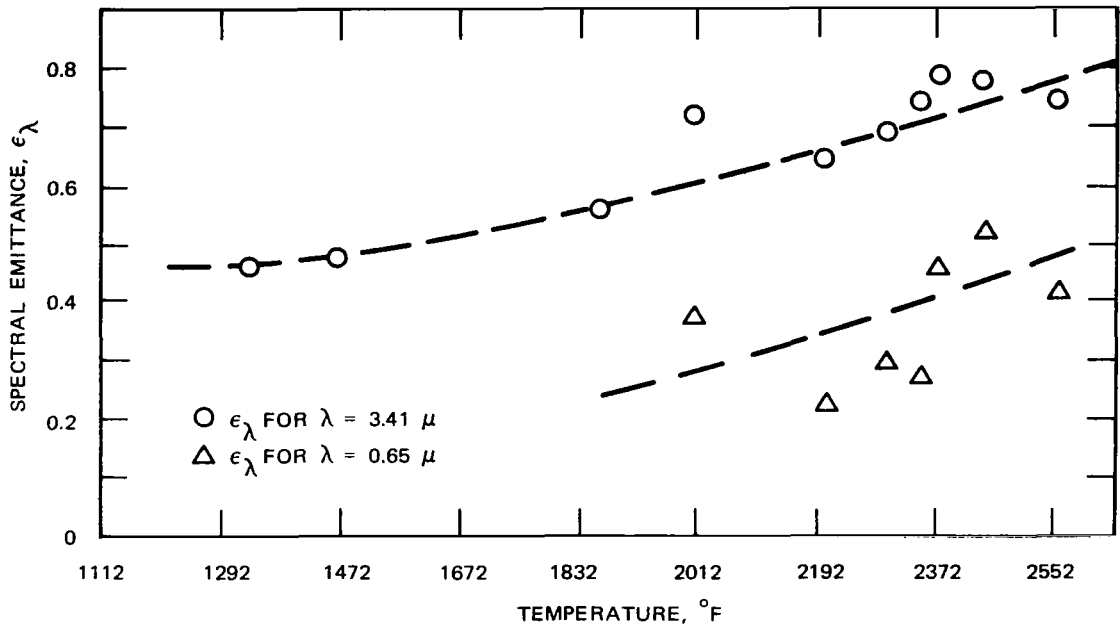
$\epsilon_{\lambda}$  = Spectral emittance at the measurement wavelength

$T_t$  = True surface temperature (thermocouple determination)

$T_{\lambda}$  = Apparent surface temperature (pyrometer determination)

$C_2 = \frac{hc}{k} = \frac{\text{Planck's constant} \times \text{velocity of light}}{\text{Boltzmann's constant}} = 1.44 \text{ cm}^{\circ}\text{K.}$

Figure 16 shows the spectral emittance vs. temperature for coated Lavite. Similar measurements with uncoated Lavite showed that its spectral emittance at 3.41 and 0.65 microns was, within experimental accuracy, the same as that of the coated Lavite. Application of the VHT flameproof coating to a Lavite specimen resulted in optical pyrometer and thermocouple temperature readings that agreed to within  $\pm 50^{\circ}\text{F}$  for exposures to laser radiation. This shows that within the experimental accuracy of the system the VHT coating provides essentially a black surface to the material it coats through the temperature range of interest.



TA-8677-18

FIGURE 16 SPECTRAL EMITTANCE DATA FOR CALIBRATION

The aim of the above calibration procedure was to absolutely calibrate the infrared pyrometer so that it could be used in conjunction with the image furnace during microwave transmission measurements. The parabolic mirror used during the calibration procedures was ideally suited for that purpose. However, after the apparatus was transferred to the microwave facility, we found that the only optical configuration that would allow the pyrometer an unobstructed view of the specimen was incompatible with the imaging properties of the mirror. The commercial availability of parabolas that could be used in place of the existing mirror was tested and found wanting, since it would take roughly three months to purchase a replacement. Therefore, it was decided to make a relative calibration of the pyrometer at the microwave facility over the only feasible optical path. A Lavite specimen instrumented with thermocouples was painted with the VHT flame-proof coating, which provided the specimen with an emittance of near unity. This specimen was mounted in the microwave antenna and was

exposed to selected levels of thermal irradiance until equilibrium conditions were obtained at each level. Both the thermocouple temperature and the signal from the infrared pyrometer were recorded for each equilibrium level. When the surface temperature of the specimen reached about 1800°F, the specimen cracked, terminating the calibration at this point. Previous measurements with an unblackened Lavite specimen showed a near-linear increase in the pyrometer signal with temperature, so it is assumed that the blackened specimen would increase similarly. Next, an aluminum phosphate foam specimen was blackened and installed in place of the blackened Lavite specimen, and was exposed to the same irradiance levels, after which an unblackened foam specimen was exposed to the same irradiance schedule. For both these specimens, the pyrometer signal vs. arbitrary exposure level was recorded.

Figure 17 summarized these data and is comprised of two plots. Figure 17(a) shows the temperature vs. pyrometer signal for blackened and unblackened Lavite. These data show that for the same temperature the radiant output of the blackened surface is about 10 percent more efficient than the unblackened surface. (This is expected, since the emittance of the uncoated Lavite was previously determined to be 0.7). These data also give an indication of what the output of the blackened specimen would have been if it had not cracked. Figure 17 (b) shows the pyrometer signals produced by blackened Lavite, blackened foam, and unblackened foam vs. a selected thermal irradiance level. Here we see that the blackened foam and Lavite specimens have reasonably comparable outputs. The difference in output is probably due to differences in the surface-structure geometry of the two specimens-- i.e., the foam absorbs and emits energy throughout its volume, while the Lavite essentially absorbs and emits energy at its surface.

Figure 18 compares the pyrometer signal from the blackened Lavite and blackened foam at the same energy levels, and the signals

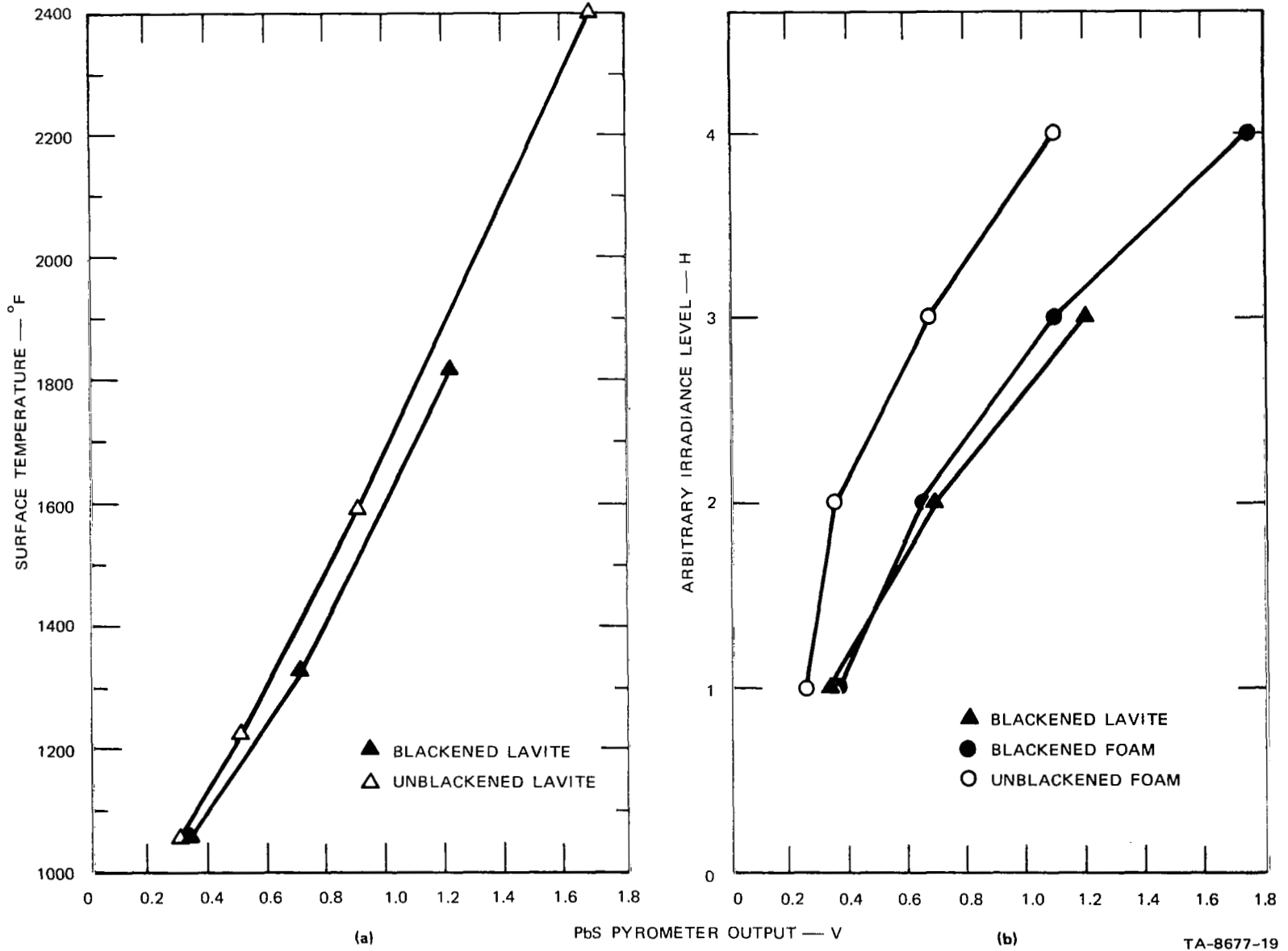
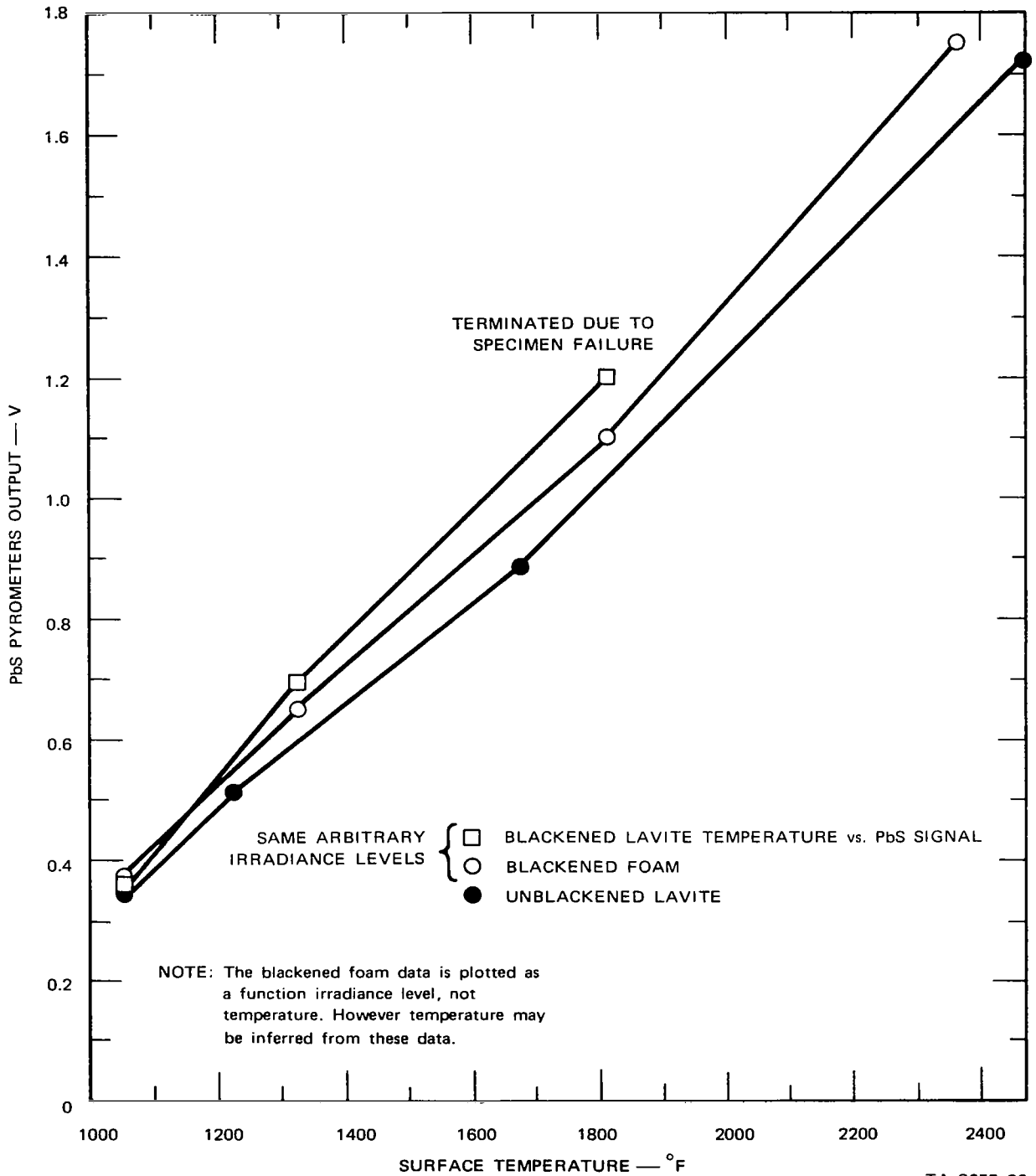


FIGURE 17 PbS PYROMETER SIGNAL VOLTAGE AGAINST (a) TEMPERATURE FOR LAVITE SAMPLES AND (b) ARBITRARY IRRADIANCE FOR FOAM AND LAVITE SAMPLES



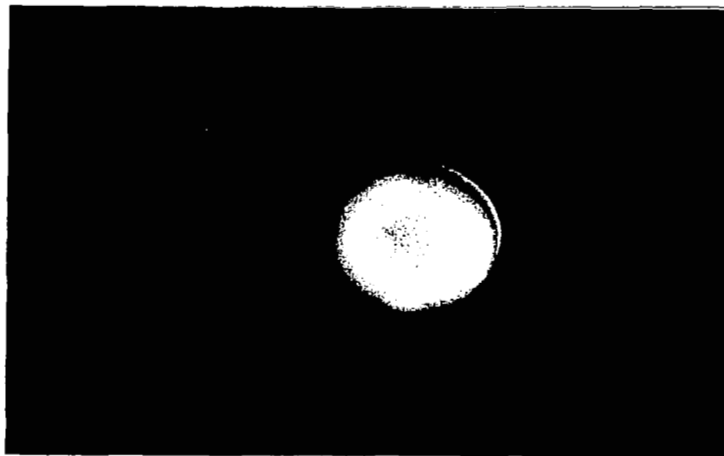
TA-8677-20

FIGURE 18 PbS PYROMETER SIGNAL AS FUNCTION OF TEMPERATURE OF THREE SURFACES



from the unblackened Lavite and blackened Lavite vs. temperature. Here, the pyrometer signal from the blackened foam specimen lies between the output from the blackened and unblackened Lavite specimens. Therefore, we shall assume that the surface temperature of the blackened foam is defined by the pyrometer output curve in Figure 18 within accuracy limits of  $\pm 100^{\circ}\text{F}$ .

Figure 11 shows how the pyrometer signal was optically retrieved from the sample by a plane mirror reflecting an image of the sample through a quartz window in the shock-tube wall, out of the PbS pyrometer. Figure 19 shows a photograph of a heated Lavite sample,



TA-8677-21

FIGURE 19 PHOTOGRAPH OF HEATED SAMPLE USING RADIATED LIGHT, TAKEN THROUGH PYROMETER OPTICAL LINK

using this optical link. The light for the photograph was radiated by the sample.

#### 4. Microwave System and Techniques

The microwave system, shown in block-diagram form in Figure 20, is a standard one for monitoring transmission (two pickups) and reflection of this type. Depending upon the type of measurement, three different sources of X-band power were used during the course of the program: (1) a pulsed magnetron (at a frequency of 9.375 GHz) with

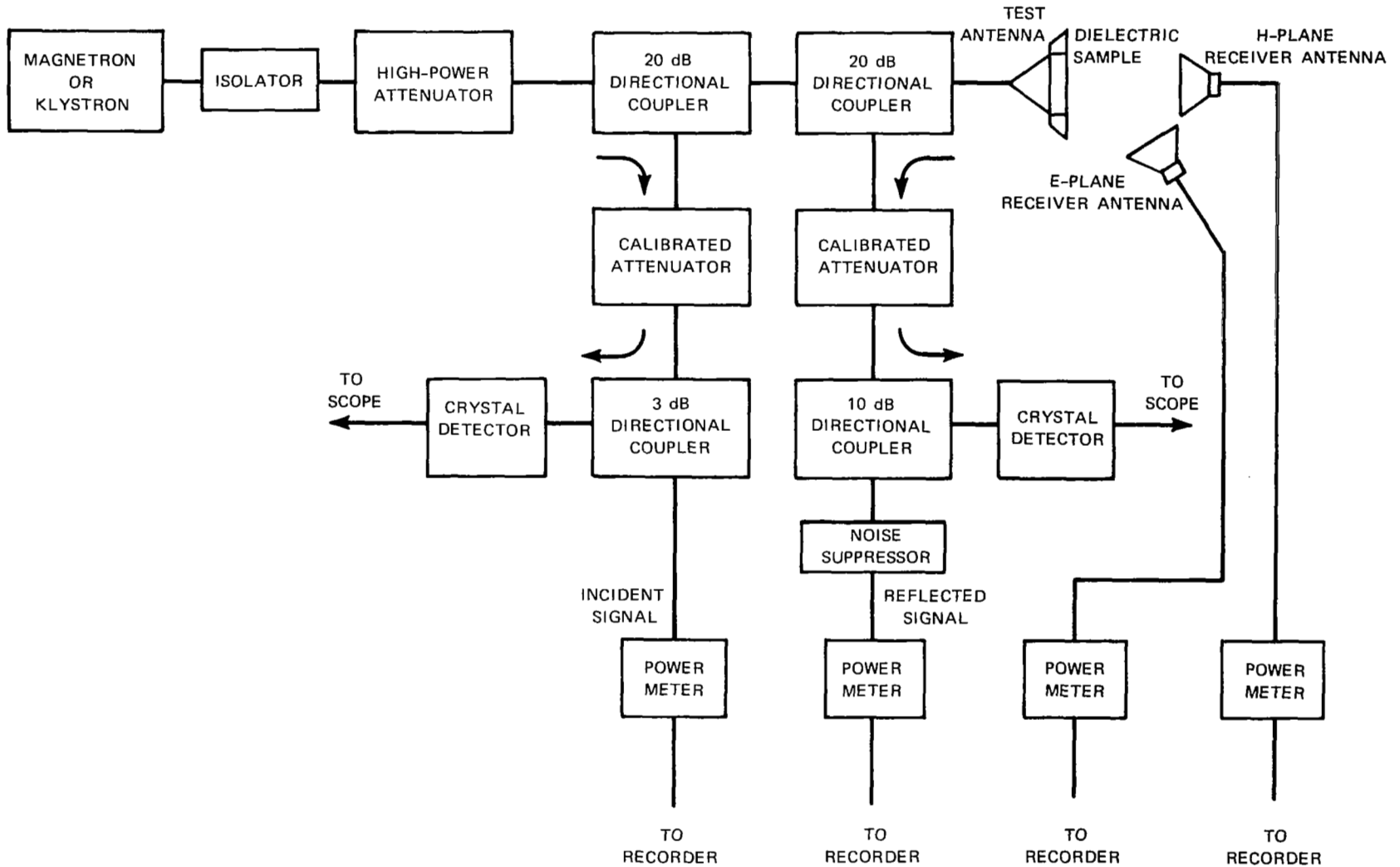


FIGURE 20 BLOCK DIAGRAM OF MICROWAVE SYSTEM

80 kW peak power, for breakdown in gases and (intrinsic) in solids; (2) a CW magnetron with 100 W average power (at 8.9 GHz) for thermal breakdown tests in solids; and (3) an X-13 (low-power) klystron (at 8.9 GHz), for some of the transmission tests when breakdown was not sought.

For breakdown in the solid samples, transmission and reflection measurements were made with the sample in place with a low power level. Then the appropriate breakdown test was run--typically with heating from the carbon arc. Then, in case symptoms of breakdown could not be visually observed in the specimen and could not be detected electrically, the low-power tests were made again to determine if there were any permanent electrical changes in the material.

For breakdown in air outside the dielectric, a high pressure was required inside the horn to prevent breakdown occurring there (where the fields were higher at a given power level). When no plasma was present, a radioactive source was used to provide the "seed" breakdown electron, which is required to get repeatable results.

The technique of firing the magnetron pulse, while the short-lived test plasma of the shock tube is over the aperture, is discussed in Ref. 5. Briefly, ion probes are used to sense the arrival of the shock front, which is followed by a nominally homogeneous slug of ionized air. By using a suitable time delay, the magnetron is fired (for a few microseconds) while the slug of air is flowing over the aperture. The sharp leading edge of the sample holder shown in Figure 8 is for the purpose of minimizing the flow disturbance caused by the holder. This technique is used in the present program for determining breakdown thresholds when the materials are outgassing into a plasma, similar to the reentry situation. The additional procedures for the present program measurements consisted of simultaneously heating the material and monitoring both temperature and outgassed products.

The shock tube enclosure used in these tests is not a very satisfactory pattern range. Indeed, if pattern measurement were a primary objective, it would be better to use no vacuum enclosure, in which case the carbon arc equipment and housing would be the only obstruction in the range. The Appendix of this report consists of patterns measured with the standard configuration at the NASA Langley Research Center.

#### B. Data from Techniques Development

It was not a prime objective of this program to gather data on various materials, which is fortunate since the materials that we acquired arrived quite late during the program. However, it was felt that the techniques could best be developed by the acquisition of worthwhile data, and that any information developed would be useful. Despite the fact that all internal breakdown results with the samples were negative, there were useful observations made on both physical and electrical (low-power) characteristics of the several types of material when exposed to a reentry-like environment.

##### 1. Dense RF Window Materials

The materials tested in this class were Lavite, two makes of boron nitride (HBR and HD-0092), Philco-Ford's silica composites (reinforced with fused quartz) called AS3DX and AS3DW, and slip-cast fused silica (SCFS).\*

Figure 21(a) shows transmission and reflection data for a test run with the AS3DX material, and Figure 21(b) shows corresponding temperature profiles estimated to exist between the thermocouple-

---

\* We are indebted to Mr. Tom Place of Philco-Ford for furnishing the samples of HD-0092 and SCFS in addition to the AS3DX and AS3DW.

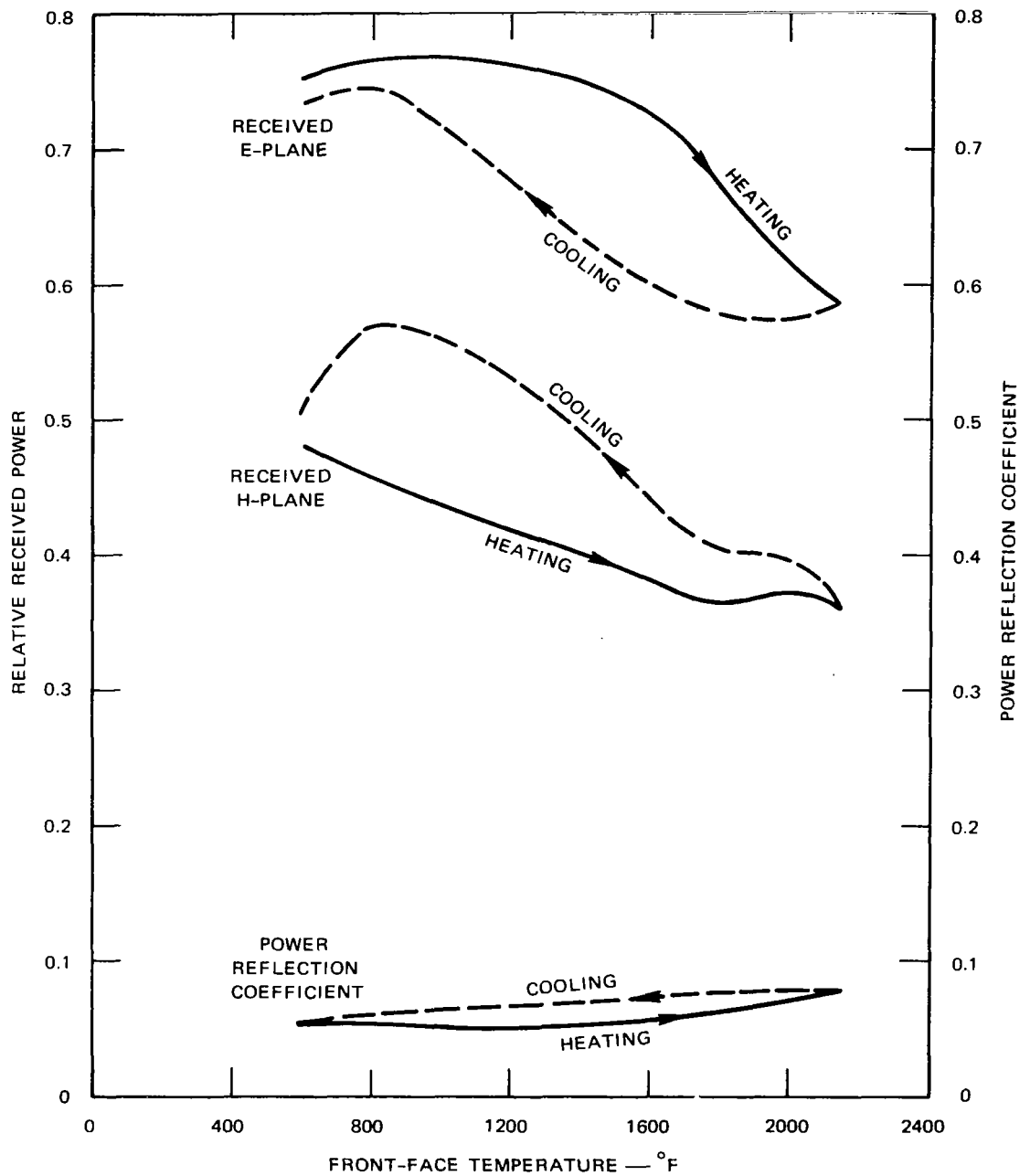


FIGURE 21(a) TRANSMISSION AND REFLECTION DATA FROM TEST RUN WITH AS3DX SAMPLE

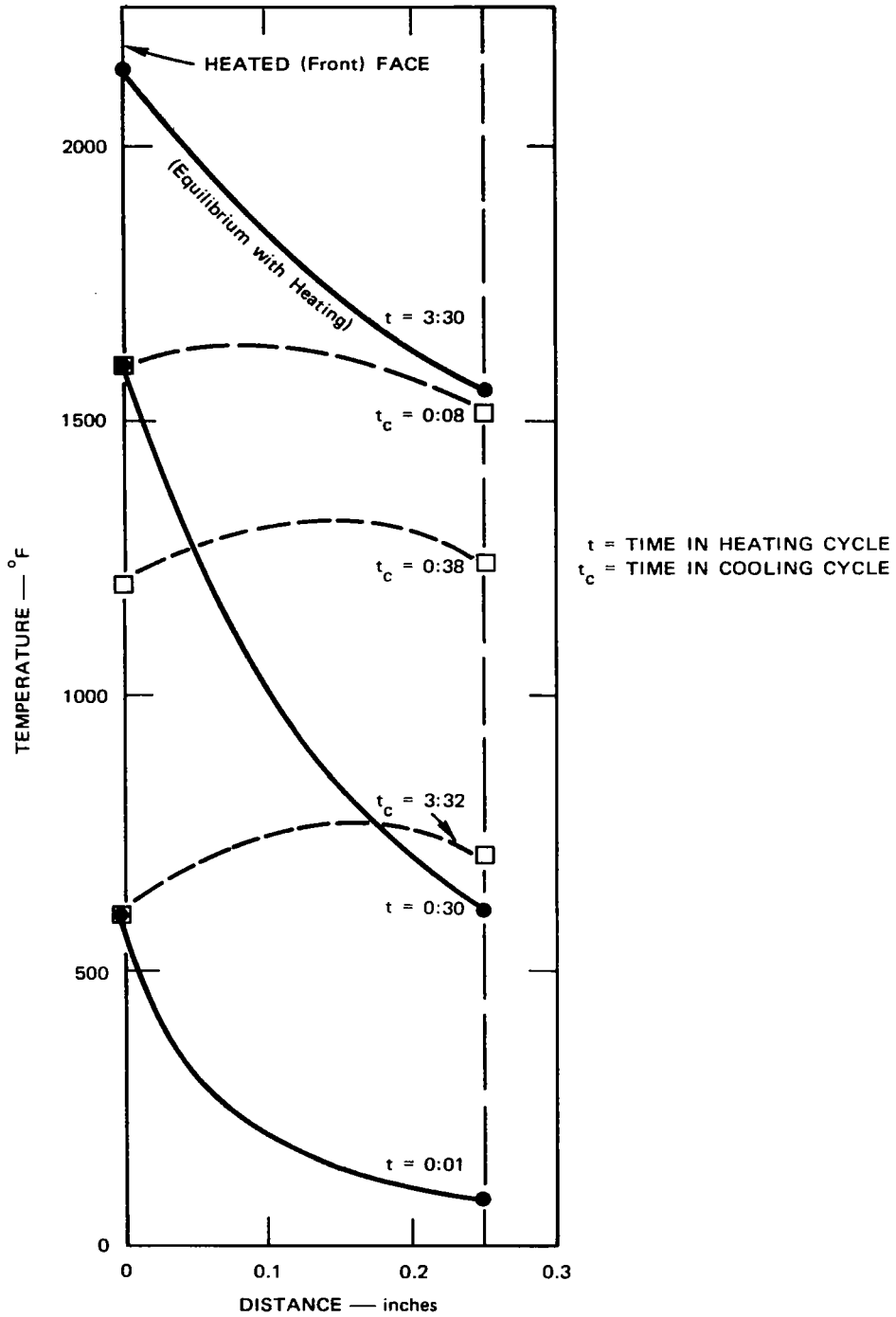


FIGURE 21(b) CORRESPONDING TEMPERATURE PROFILES AT VARIOUS TIMES DURING TEST



FIGURE 21(c) RAW DATA ON TEMPERATURE AND MICROWAVES AT BEGINNING OF HEATING CYCLE AND BEGINNING OF COOLING CYCLE

measured surface points, at various times during both heating ( $t$ ) and cooling phases ( $t_c$ ) of the run. The profiles were estimated on the basis of well known forms of temperature distributions\* for the two different conditions (heating or cooling). The profiles are estimated to be accurate within about  $100^\circ\text{F}$ . It is noted that the heating profiles are similar to flight profiles, whereas the cooling-cycle profiles are flat enough to be comparable with "soaking" methods. The difference in the profiles is responsible for the difference between heating and cooling in the reflected and received signals, since they are plotted against front-face temperature. Since the profiles are quite different, and the RF properties of the material are functions of temperature, the microwave behavior should be different in general at identical front-face temperatures. Since the received power was higher for cooling in one case and lower in the other, and in view of the results shown in

---

\* For example, we know that the slope of the temperature profile at any point in the sample is proportional to the flux of heat across the surface at the point, the proportionality constant being the thermal conductivity. This requirement, together with the measured values of the two end points, is sufficient to give the shape of the curves. The simplest profile to fix is the steady-state one, which would be a straight line were it not for some losses transverse to the primary direction of flow. The transverse flow occurs because the outer portion of the sample holder is not irradiated by the carbon arc, resulting in a transverse temperature gradient. Since the flux therefore decreases slightly all across the sample from left to right, the slope of the curve must decrease from left to right. The slope of the transient curves at the right-hand surface on the heating cycle will be lower than the steady-state profile slope, with the nearly zero slope at  $t = 0:01$  because of the low surface temperature, which precludes significant heat loss across that surface. The cooling-cycle profiles must have a maximum since heat flows in opposite directions at the surfaces. The slopes at the right surface would be expected to be lower than in the steady state since the heat source seen by it on the left is decreasing with time. In the cooling cycle, the left-hand surface apparently "sees" a cooler environment than the right-hand surface, since the temperature there decreases faster with time.



the appendix on pattern effects, it is expected that pattern effects are significant in these measurements. The overall decrease at high temperature ( $\sim 1$  dB) may be due to an increase in absorption (loss tangent); however, similar measurements with AS3DW (quartz fibers in a different pattern from AS3DX) showed essentially no loss with temperature. Note the AS3DX samples details in Figure 9(a), along with the front and back thermocouple leads. Figure 21(c) shows the raw data for the run corresponding to Figures 21(a) and (b).

Figure 22 shows similar data for Lavite, using only an H-plane receiving horn. It is seen that there was a discontinuity in the data starting when the (front) temperature reached  $2340^{\circ}\text{F}$ . Since the sample was found to be forced out away from the horn by about  $1/16$ -inch during the test, it is assumed this was the cause of the discontinuity. It is noted from the low reflection coefficients that the 0.25-inch thickness of both these samples is near a half-wave. (The reflection coefficient of the horn and holder without a sample is negligible.) At a maximum temperature of  $2000^{\circ}\text{F}$ , the SCFS showed a gain of about 2 dB in transmitted signal compared with the room-temperature transmission, with very little change in reflection coefficient.

The greatest loss in signal in both groups of RF materials was with both types of boron nitride. Figure 23 shows that the microwave signals hardly changed until about  $1500^{\circ}\text{F}$  on the front face. (The H-plane power meter drifted during the cooling cycle.) This sort of loss ( $\sim 3$  dB) was representative of both types of BN tested, which has added significance since the maximum temperatures were somewhat lower than for the other materials.

All the dense RF materials except Lavite were physically stable after several repeated runs. The Lavite tended to fracture, especially on the radiated side; cracks of this kind can be visually detected in Figure 19.

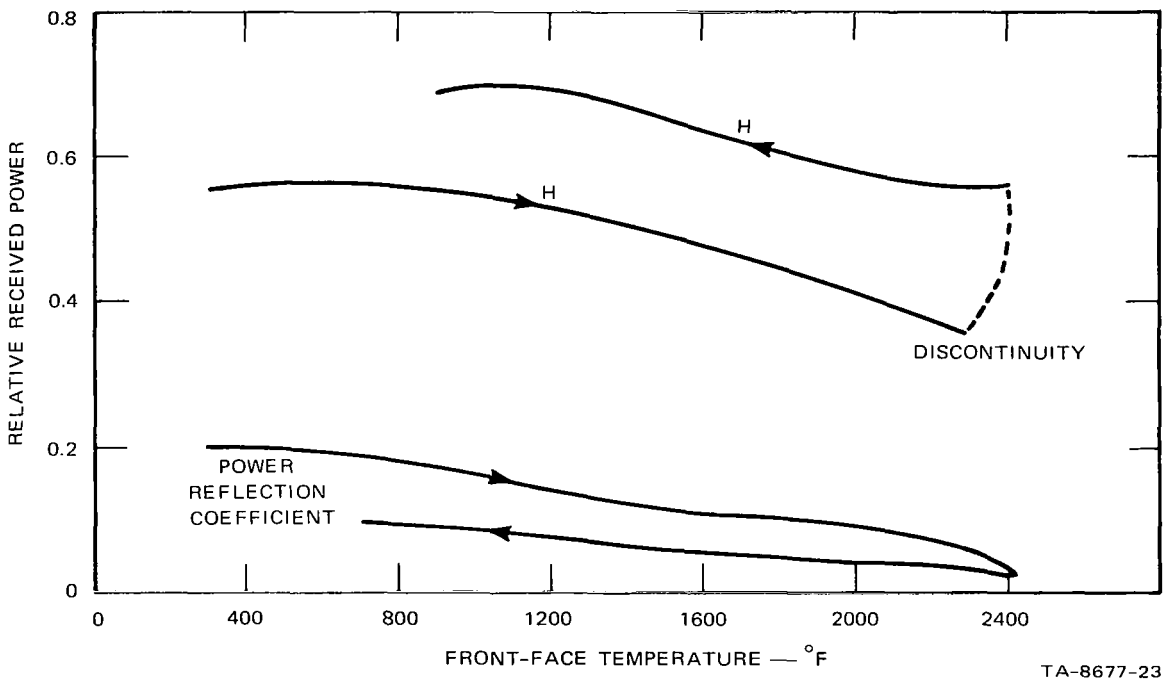
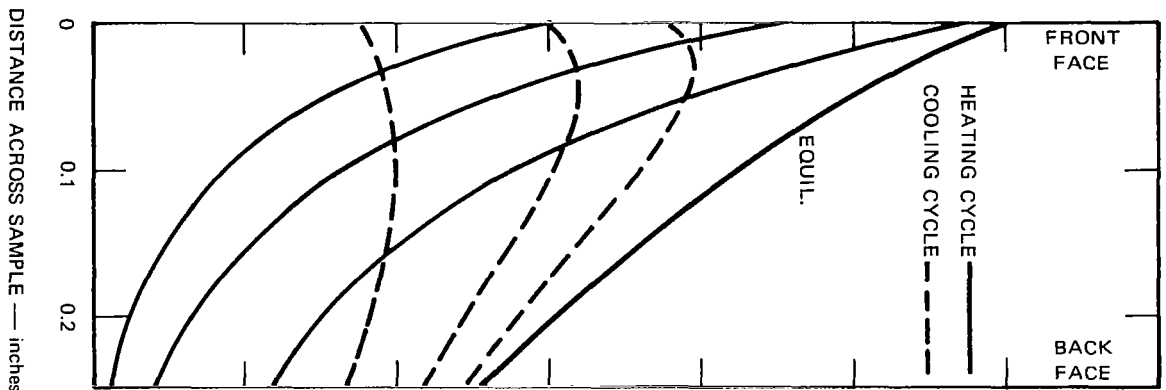


FIGURE 22 TRANSMISSION, REFLECTION, AND TEMPERATURE DATA FROM A TEST RUN WITH LAVITE

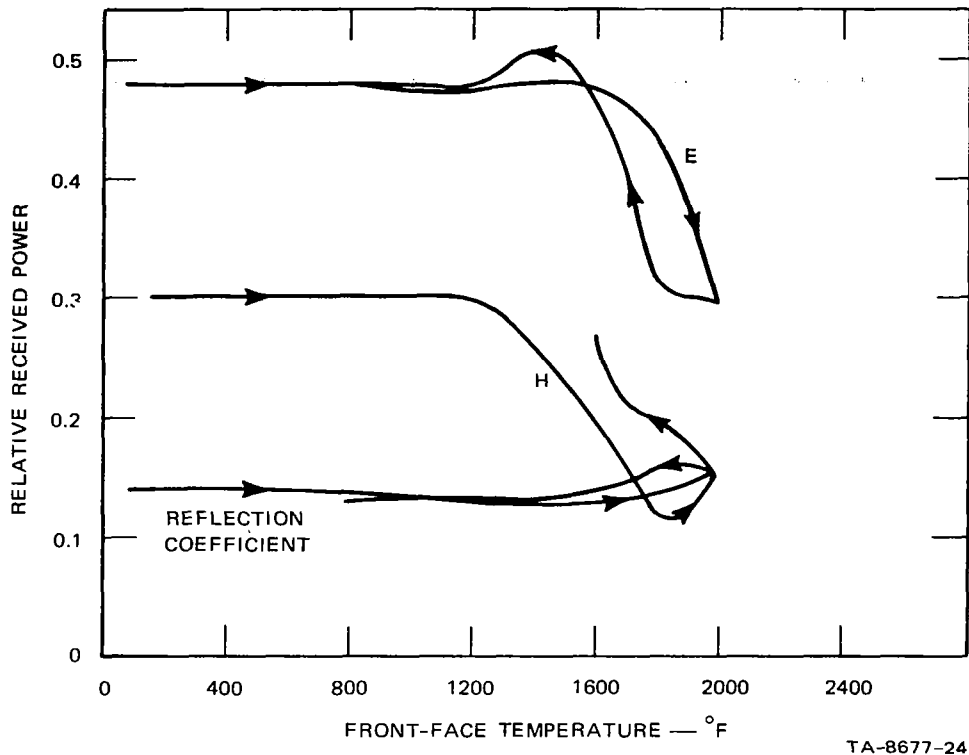


FIGURE 23 TRANSMISSION AND REFLECTION DATA ON BORON NITRIDE (HBR)

The mass spectra taken during the heating of these materials showed no detectable outgassing except for water vapor escaping from the boron nitride. Figure 24 shows a mass spectrum taken early during a heating run with a BN sample. When only air and water are present

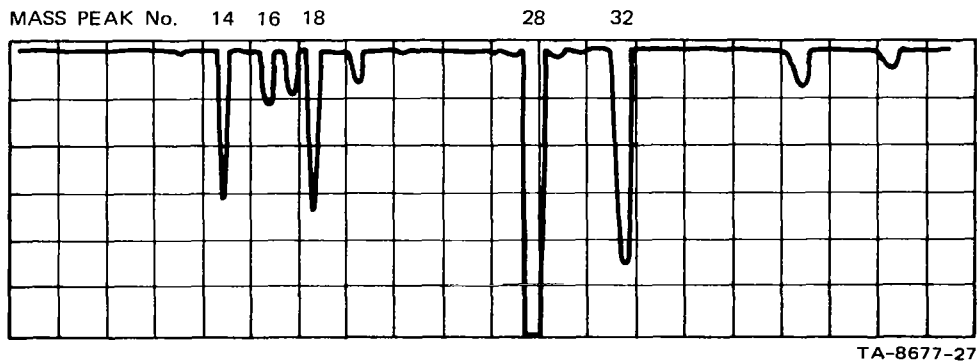


FIGURE 24 MASS SPECTRUM EARLY IN BORON NITRIDE HEATING RUN

(BN would give peaks at Nos. 25, 14, and 11), the volumetric ratio of air to water in the sampled gas goes approximately as the ratio of their main peaks, which are Numbers 28 (for  $N_2^+$ ) and 18 (for  $H_2O^+$ ), respectively. Although the height of Peak 28 is not apparent in Figure 24, we can deduce from the height of Peak 32 (representing  $O_2^+$ ) that it is approximately 5.5 times as great as 18, giving about 15 percent water in the sampled gas. (A typical ambient level for water in the tube at these conditions is no greater than 3 percent.) The total pressure for this test was 1.7 torr, indicating that the partial pressure of water at the tube intake was about 0.25 torr. Spectra taken subsequent to the one in Figure 24 showed rapid decrease in time, however, down to the typical tube ambient level.

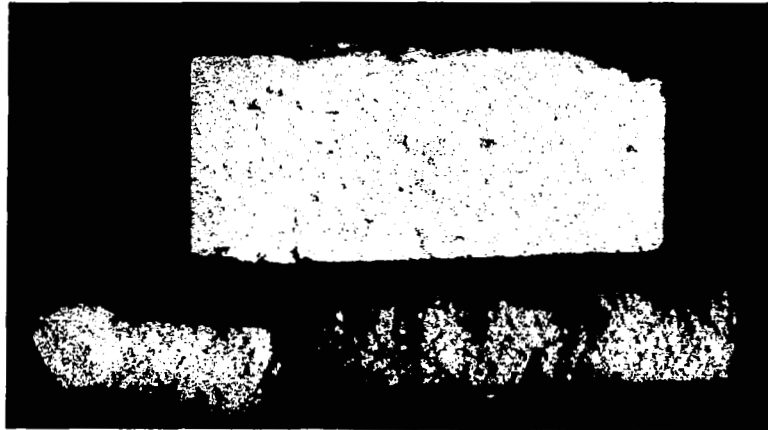
## 2. Lightweight TPS Material

Samples of three lightweight dielectrics that could be considered candidates for the thermal protection system were acquired for testing: (1) aluminum phosphate foam of the Whittaker Corporation,\* (2) Lockheed's LI-1500, and (3) Carborundum's boron nitride fiberboard 89-X. Samples of many other materials were procured, such as Union Carbide's "Zircar" zirconia felt, but none appeared to have the required structural properties. In fact, all three of the above "candidate" materials exhibited structural problems. The two foam materials (of which the Whittaker material is generally stronger) both failed while at room temperature when we evacuated the shock tube with one atmosphere pressure on the antenna side. However, they may still be acceptable since this kind of structural loading will probably not occur on the shuttle. The BN fiberboard decomposed when exposed to air at a temperature

---

\* We wish to acknowledge the assistance of Mr. Vance Chase of Whittaker, who supplied us with the aluminum phosphate foam samples.

of around 1800°F and higher. Figure 25(a) shows a sample of 89-X before, and Figure 25(b), after, a two-hour exposure to air at 1900°F.



(a) BEFORE HIGH-TEMPERATURE EXPOSURE TO AIR



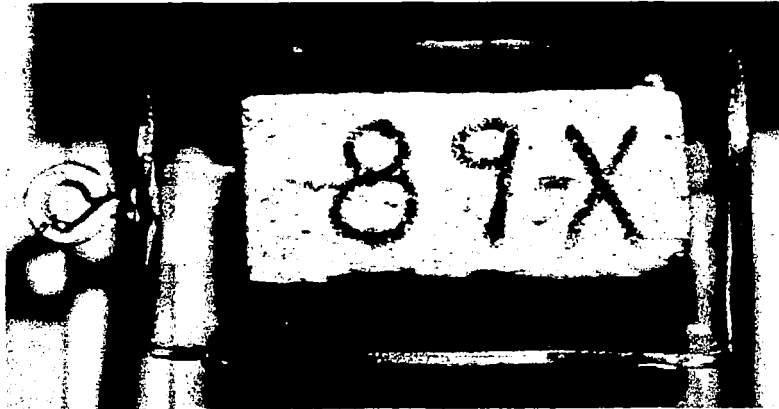
(b) AFTER HIGH-TEMPERATURE EXPOSURE TO AIR

TA-8677-28

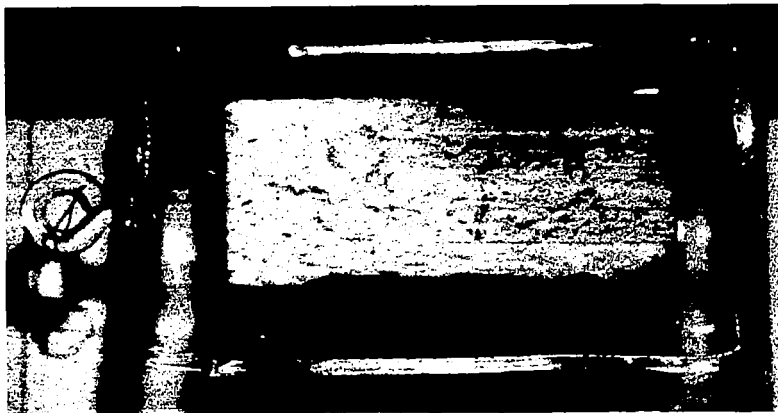
FIGURE 25 BORON NITRIDE FIBERBOARD SAMPLE

This was apparently oxidation of the large-surface-area fibers, as indicated by a test run in a vacuum. Figure 26 shows that only the "89-X" marking faded during a similar test in an evacuated pyrex enclosure. Since it may be possible for the 89-X to be used in an air-tight installation, it probably should not yet be eliminated from shuttle considerations.

The Whittaker foam samples turned somewhat darker in color during prolonged heating, although no products of decomposition were



(a) BEFORE HIGH-TEMPERATURE TEST IN EVACUATED ENCLOSURE



(b) AFTER HIGH-TEMPERATURE TEST IN EVACUATED ENCLOSURE

TA-8677-29

FIGURE 26 BORON NITRIDE FIBERBOARD

detected by the mass spectrometer with this or the other lightweight materials. (Because the mass spectrometer tests were performed in a vacuum, it is likely that any water absorbed by the foams was evaporated during the pump-down, prior to the measurement.) Because one of the Whittaker samples seemed somewhat eroded on the arc-irradiated face, it was weighted before and after extended exposure (9 minutes) to the arc. Indeed, the sample weighed 2 percent less after the test. (Careful

attention was given to differentiating this real sample weight loss from a loss in absorbed water.)

Figures 27 and 28 show the quite similar results of transmission tests performed with samples of the Whittaker and Lockheed

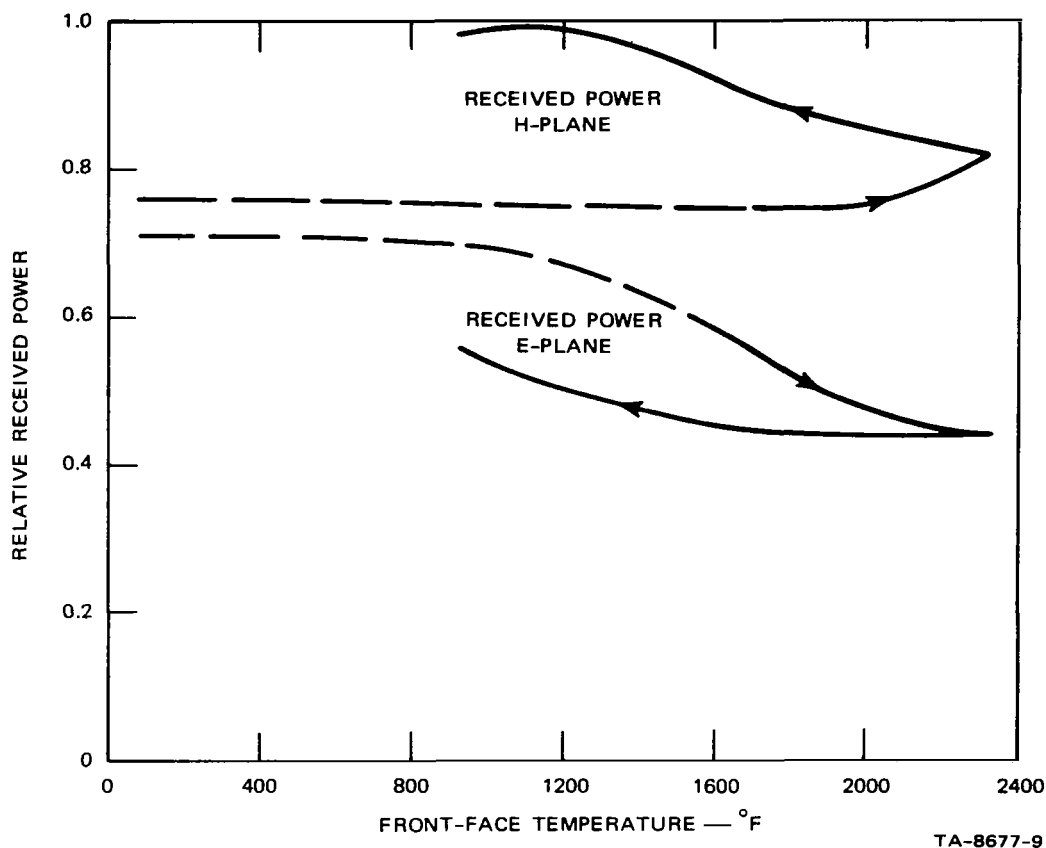


FIGURE 27 RESULTS OF TRANSMISSION TEST WITH ALUMINUM PHOSPHATE FOAM SAMPLE DURING BOTH HEATING AND COOLING CYCLE

foams, respectively. These data, and the fact that neither experienced breakdown in the high-power tests, indicate that both materials are satisfactory from RF considerations. It was noted that the dark green coating on the LI-1500 sample was somewhat bilistered by the 2400°F temperatures. (This dark coating was used on the irradiated side to achieve higher energy absorption than would have been possible with no

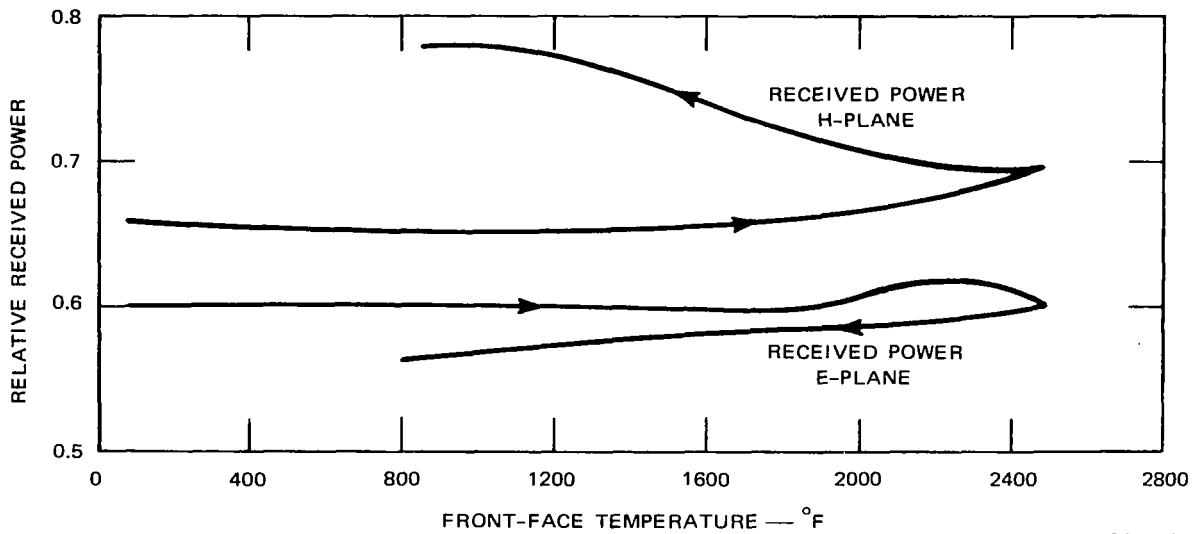


FIGURE 28 TRANSMISSION TEST DATA FOR LI-1500 SAMPLE

coating.) No tests were made with the uncoated sample because of its structural failure in the vacuum test.

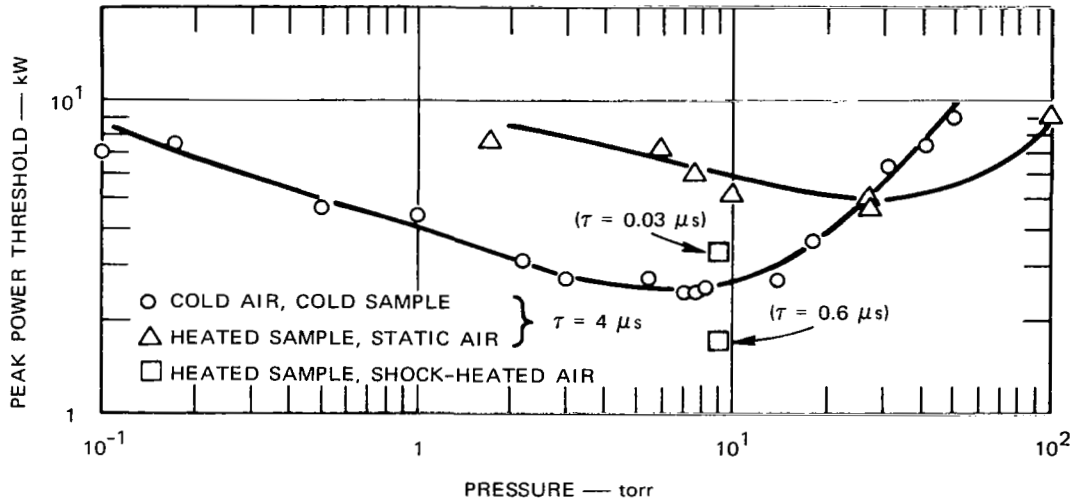
### 3. Ablative Material

A transmission/breakdown test was made with a sample of OTWR (orthogonal-wound Refrasil) after it was learned late in the program that ablative materials were under consideration for the shuttle as an interim measure. With no arc heating, RF heating from the 100-W CW magnetron raised the temperature (at a thermocouple imbedded near the front surface) to 570°F. This temperature did not affect the reflectivity or transmissivity of the sample. Addition of the arc heating, however, giving a maximum temperature of 2250°F, eventually charred the sample badly enough to give 17 dB attenuation and to short out the thermocouple. Since the deterioration occurred over several minutes of time, rather than within a fraction of a second, it is inferred that no catastrophic breakdown occurred in the material.



#### 4. Gas Breakdown Data

Although no subliming products were generally detected by the mass spectrometer during the heating runs, it was decided that tests should be run for other effects of the heated sample on breakdown thresholds of the air to at least demonstrate the feasibility of our technique. Figure 29 shows the results of three different kinds of



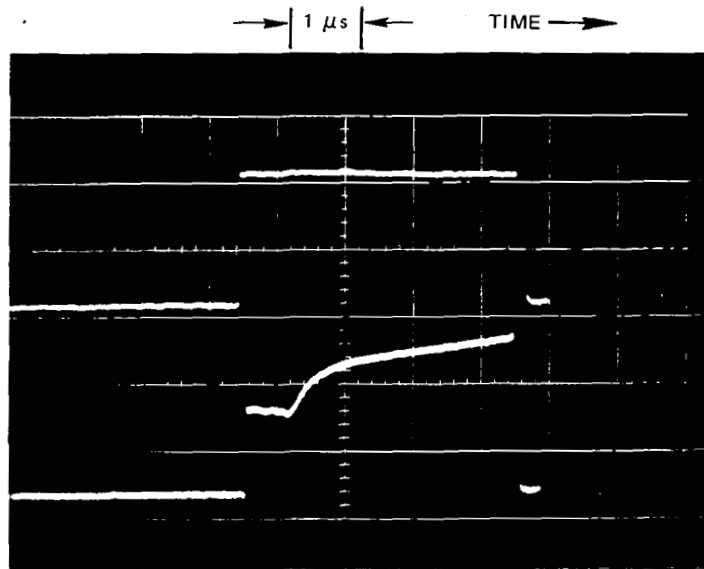
TA-8677-31

FIGURE 29 GAS-BREAKDOWN THRESHOLDS

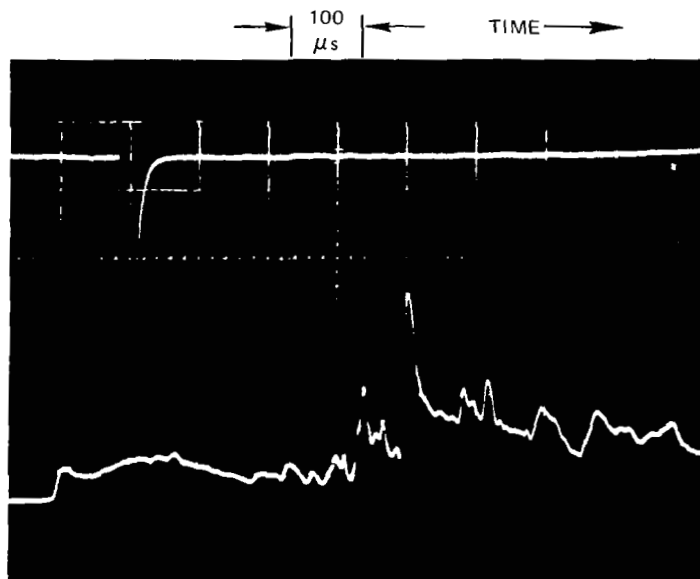
threshold measurements, using a Lavite sample and the pulsed magnetron. First, thresholds were measured in cold air over a range of pressures. Then they were repeated with a hot sample only. It appears from Figure 29 that the difference between these two sets of results can be explained simply by a shift to higher pressure (by a factor of 4) and by a 3-dB shift to higher power. The shift in pressure is quite reasonable since a factor of 4 or so would be the required increase in pressure to compensate for the reduced density in the high air temperature in the layer next to heated sample (at 2400°F). In addition, the higher power requirement is consistent with the apparent losses in the hot Lavite observed on the heating cycle of Figure 22. Some of the runs

were made by starting with a cold sample at a given pressure, and then observing the transition in time to the values shown for the hot sample.

Two data points shown in Figure 29 correspond to shock-heated-air data. The shock tube was fired with a hot sample into air at initial pressure of 1 torr. The resulting plasma has a temperature of 3300°K, an electron density of about  $10^{10}$  (cm<sup>-3</sup>), and an air density equivalent to room-temperature air at 9 torr pressure. Breakdown occurred after effective pulse widths of 0.6 μs (at 1.64 kW peak power) and approximately 0.03 μs (at 3.28 kW peak power). By compensating these thresholds for the shorter times, one can compute equivalent thresholds for a 4-μs pulse (for comparison with the other data in Figure 29). This equivalent for both points is 0.9 kW. Since the sample is hot, this equivalent threshold is compared with the upper curve of Figure 29 to determine the added effect of the plasma, and it is seen that there is approximately 8 dB reduction due to the plasma. This difference is reasonable in view of the combined effects of ambipolar diffusion and high-temperature air. Figure 30(a) shows both incident and reflected pulses for the 1.64-kW shot. Breakdown is said to occur when the electron density reaches approximately critical, thus changing the level of the reflected power. Figure 30(b) shows ion current collected by an ion probe during the shot (lower trace), and the corresponding time during the passing of the plasma when the magnetron fired, as indicated by the discontinuity in the upper trace.



(a) INCIDENT AND REFLECTED PULSES



(b) MAGNETRON PULSE TIMER AND ION PROBE CURRENT

TA-8677-32

FIGURE 30 SHOCK-TUBE BREAKDOWN DATA

## V SUMMARY AND RECOMMENDATIONS

A two-part program was performed and described in this report. A study program was performed in which high-power antenna information was developed and/or assembled from the literature and from a survey of government and industry sources. Two principal contributions resulted from this study effort. One is a set of guidelines for engineering design for avoiding antenna breakdown in air, adapted to the shuttle trajectory. Also included is a discussion of two types of positive measures that can be taken to raise breakdown thresholds--use of static electric fields and electrophilic chemicals. Several conclusions can be reached from these guidelines, as follows:

- (1) A typical slot antenna, approximately  $\frac{1}{2} \times 1$  wavelength, will experience a threshold minimum of about 200 W under nominal shuttle reentry conditions.
- (2) A relatively fat quarter-wave monopole antenna will have a threshold minimum of about 50 W under these conditions.
- (3) Measures for breakdown alleviation in flight are feasible, but difficult, and are limited in extent by the reentry environment.

The second contribution from the study program is a discussion of effects of temperature of dielectrics on breakdown within the dielectric, including both intrinsic and thermal breakdown mechanisms. It is concluded that temperature reduces dielectric breakdown thresholds, for both mechanisms, sufficiently that materials should be tested under the combined intense thermal and RF exposures.

A comprehensive system of laboratory measurements was developed, providing a foundation for high-power RF testing of new materials as

the shuttle program progresses. Some of the notable developments out of this techniques program are the following:

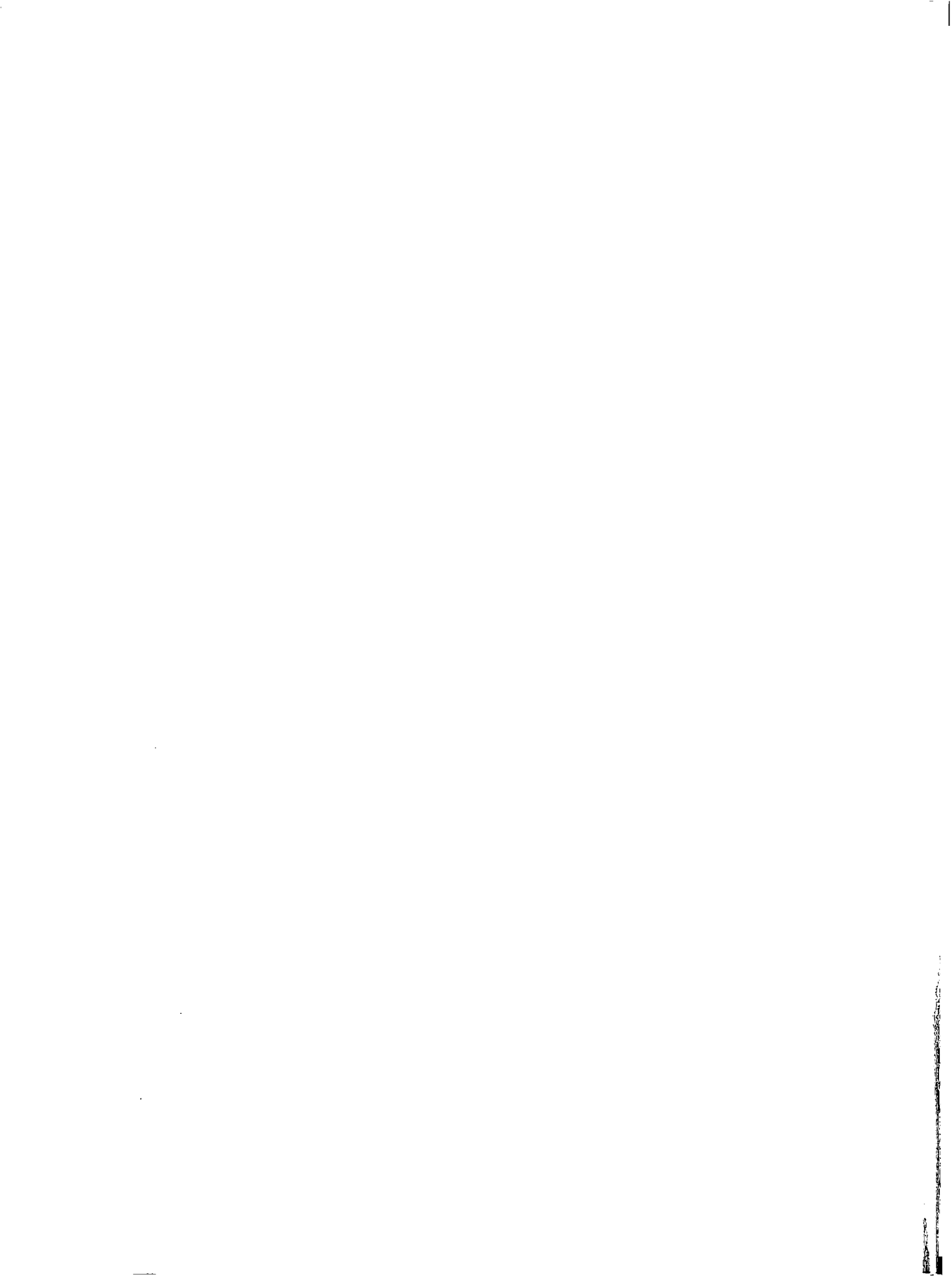
- (1) Heating of samples to reentry temperatures with reentry-type profiles, using a source remote enough to only slightly affect the electrical tests, allowing pattern measurement in addition to impedance and transmission tests.
- (2) Monitoring of temperature of arbitrary materials using an IR pyrometer.
- (3) Monitoring outgassed products through a relatively large mass-spectrometer intake system (waveguide).
- (4) A configuration allowing simultaneous performance of the several different tests.

In the course of the techniques development program, data were gathered from these tests on several candidate materials in both the dense and lightweight RF materials categories. In addition, several valuable observations were made on some of the early shuttle RF-material candidates. It was found that, generally, these materials appear to have less of a problem qualifying electrically than structurally. In addition to having low losses over the temperature range, no breakdown in these materials was produced, and therefore none is expected for any low-loss refractory materials similar to these. However, tests and/or analysis should be performed to confirm this.

The program reported here leads to the following recommendations for future effort regarding use of high power levels with high-temperature materials in the shuttle program:

- (1) New candidate materials, especially including ablative materials, should be tested by using all the techniques described in this report.

- (2) Patterns of specific antenna designs can (and should) be tested using a pattern range into which a remote arc-image heater is incorporated.
- (3) Gas-breakdown thresholds at high field strength and low pressures, corresponding to shuttle applications around 250 to 300 kft, need to be determined. These measurements can be done using standard pulse techniques in the laboratory.



## REFERENCES

1. R. A. Anderson, W. A. Brooks, R. W. Leonard, and J. Maltz, "Shuttle Structure--A Technology Overview," Astronautics and Aeronautics, Vol. 9, No. 2 (February 1971).
2. W. C. Taylor, W. E. Scharfman, and T. Morita, "Voltage Breakdown of Microwave Antennas," in Vol. 7 of Advances in Microwaves, Leo Young, Ed. (Academic Press, New York, N.Y. 1971).
3. Personal Communication from John D. Kelly, Military Aircraft Systems Division, The Boeing Company.
4. G. August and J. B. Chown, "Reduction of Gas Discharge Breakdown Thresholds in the Ionosphere Due to Multipacting," 1970 G-AP International Symposium Program and Digest September 14-16, 1970.
5. W. C. Taylor, "An Experimental Investigation of the Interaction of Plasmas with Antennas," Final Report, Contract NAS 1-8889, SRI Project 7729, Stanford Research Institute, Menlo Park, California (June 1970). (Available as NASA CR-1727, 1970.)
6. C. W. Haldeman and J. McGuirk, "Effects of Some Chemical Alleviants on the Impedance and Breakdown Power of Plasma Covered Microwave Antennas," The Entry Plasma Sheath and Its Effects on Space Vehicle Electromagnetic Systems, Vol. II, NASA SP-253, NASA-Langley, Research Center (October 13-15, 1970).
7. S. Whitehead, Dielectric Breakdown of Solids, Chap. 2 (Oxford, London, 1953).
8. A. Von Hippel, Dielectrics and Waves, pp. 248-252 (G. S. Wiley & Sons, New York, N.Y., 1954).
9. S. Whitehead, Dielectric Breakdown of Solids, Chap. 3 (Oxford, London, 1953).
10. H. R. Bredfeldt, W. E. Scharfman, H. Guthart, and T. Morita, "The Use of Ion Probes in Reentry Physics," Technical Report 26, Contract SD-103 under ARPA Order 281-62 SRI Project 3857, Stanford Research Institute, Menlo Park, California (May 1965).
11. T. S. Laszlo, Interscience Publishers Series: Techniques of Inorganic Chemistry, "Image Furnace Techniques," Vol. V, p. 6 (1965).
12. R. J. Jenkins and C. P. Butler, "The Stability and Reproducibility of a Carbon Arc-Image Furnace," Applied Optics, Vol. 4, No. 3, p. 299 (March 1965).





## Appendix

### RADIATION PATTERNS

This appendix presents the results of radiation-pattern measurements performed at the Langley Research Center with the test configurations and materials used for the breakdown studies.

The radiation patterns of an antenna radiating into a dielectric-loaded cavity, such as that used for the breakdown tests, are greatly influenced by the cavity size and the dielectric properties of the window material. Any changes in these dielectric properties during the thermal test could have produced changes in the radiation patterns. The radiation patterns could not be measured during the breakdown tests; therefore it was necessary to conduct these measurements after the test configuration was removed from the breakdown facility. The thermal environment used in the breakdown evaluation could not be duplicated in the antenna test chamber during the radiation-pattern measurements; therefore a change in frequency was employed to simulate a small change in dielectric constant. The two frequencies used for the transmission and breakdown tests were 8.9 and 9.375 GHz. Radiation-pattern measurements were performed at 8.9, 9.2, 9.4, and 9.6 GHz, where the change from 8.9 to 9.6 GHz represents approximately an 8-percent change in dielectric constant. Such a change is representative of that measured for some of the more dense materials, such as slip-cast fused silica and Union Carbide's boron nitride materials, over a comparable temperature range. The candidate materials evaluated had room-temperature dielectric constants ranging from approximately 1.2 for the low-density thermal-protection-system (TPS) materials up to about 5.3 for the more dense antenna-window materials.

The radiation-pattern measurements were conducted using the standard test configuration shown in Figure 8 of the main text and two other similar configurations having sample holders with straight edges replacing the beveled edge of the standard configuration. This difference produced only small changes in the radiation patterns, with the radiation in the back region being slightly higher for the beveled sample holder due to the increased diffraction from the sharp edge. Since only minor differences were measured among the various configurations, it is assumed that only the standard configuration was used for the pattern measurements. The E- and H-plane radiation patterns measured of the standard configuration with no test material are shown in Figure A-1(a). The transmitted level was adjusted to provide the same pattern level at each test frequency for the no-specimen condition. These transmitted levels were recorded and repeated for the measurements of the various test materials. The amount of change produced in the radiation patterns of the standard configuration when a specific material was used can be determined by a simple comparison with those measured for the no-specimen condition. Radiation patterns were not measured for all materials, due to the structural failure of some test samples during the breakdown evaluation.

The low-density materials (i.e., LI-1500 and aluminum phosphate foam,  $\text{AlPO}_4$ ), having relatively low dielectric constants, produced only small changes in the radiation patterns of the standard configuration from that obtained with no test material. The results of the radiation-pattern measurements for these materials are presented in Figures A-1(b), (c), and (d).

The radiation patterns for the more dense antenna window class of materials are presented in Figures A-1(e) through A-1(i). The discrepancies measured during the breakdown and transmission measurements occurred only for these materials. The radiation patterns exhibit

large differences between the E- and H-plane levels at  $45^\circ$  off axis, where the receiving antennas were located during the breakdown tests. For example, Figure A-1(e) presents the results obtained for a Lavite sample, and at 8.9 GHz there is approximately a 6-dB difference between the E-plane and H-plane levels at  $\theta = 45^\circ$  ( $\phi = 0^\circ$ ) and  $\phi = 45^\circ$  ( $\theta = 90^\circ$ ) or in the directions of the receiving antennas. When the frequency was increased from 8.9 GHz to 9.2 GHz, further changes in the radiation patterns occur that illustrate the type of changes that might be expected for a small change in dielectric constant produced by exposure of the test material to high surface temperatures. Further pattern changes occur as the frequency is increased to 9.4 and 9.6 GHz. Similar results were obtained for the other materials as shown in Figures A-1(f) through A-1(l), with pattern changes being more severe for some materials than for others.

These radiation patterns show that for the more dense materials, having relatively high dielectric constants, a small change in frequency produces large changes in the radiation patterns; therefore, since an increase in dielectric constant could produce similar changes, the discrepancies between the E- and H-plane results obtained during the breakdown evaluation were apparently due to these pattern changes.

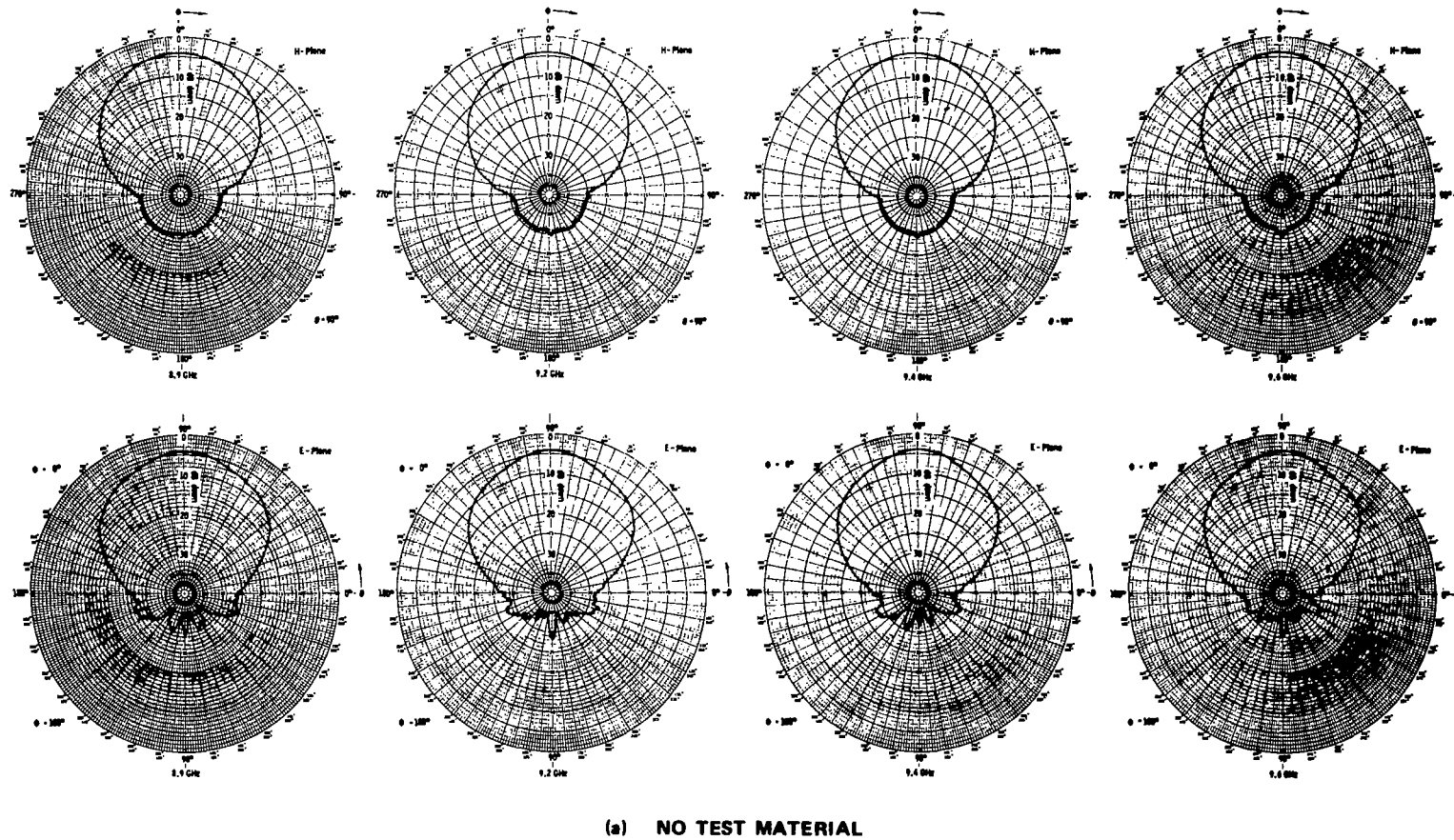
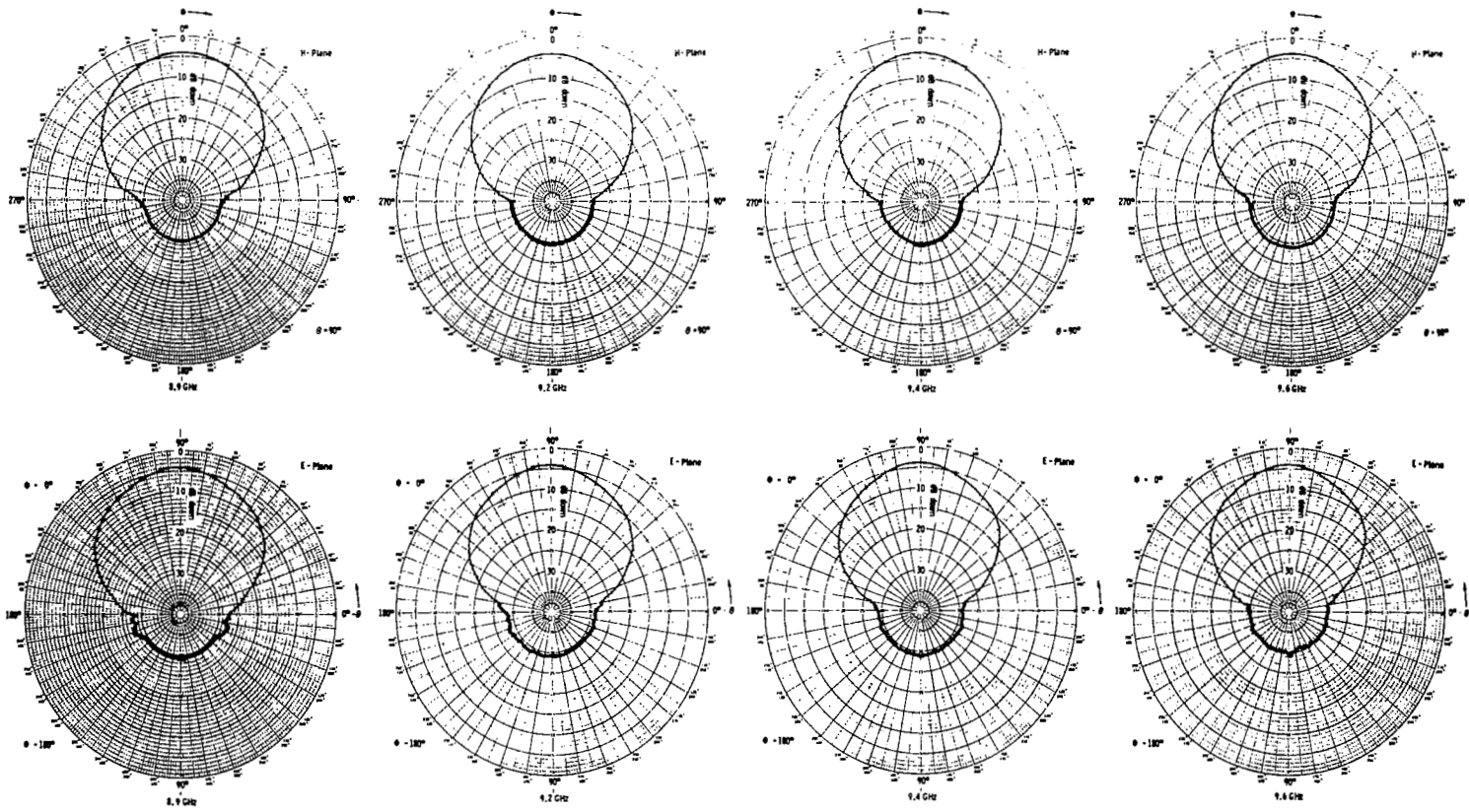
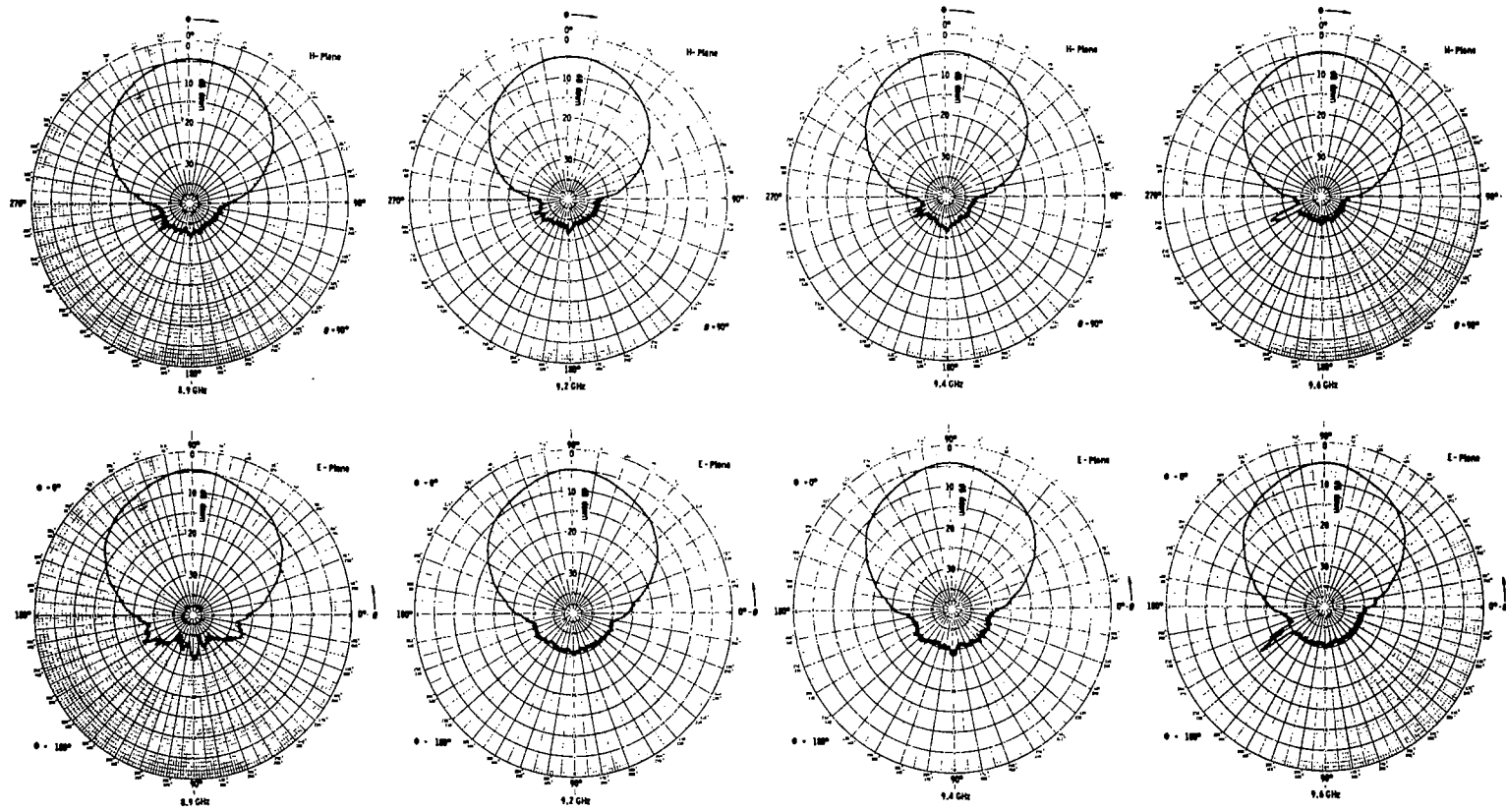


FIGURE A-1 E- AND H-PLANE RADIATION PATTERNS OF THE STANDARD TEST CONFIGURATION AS A FUNCTION OF FREQUENCY



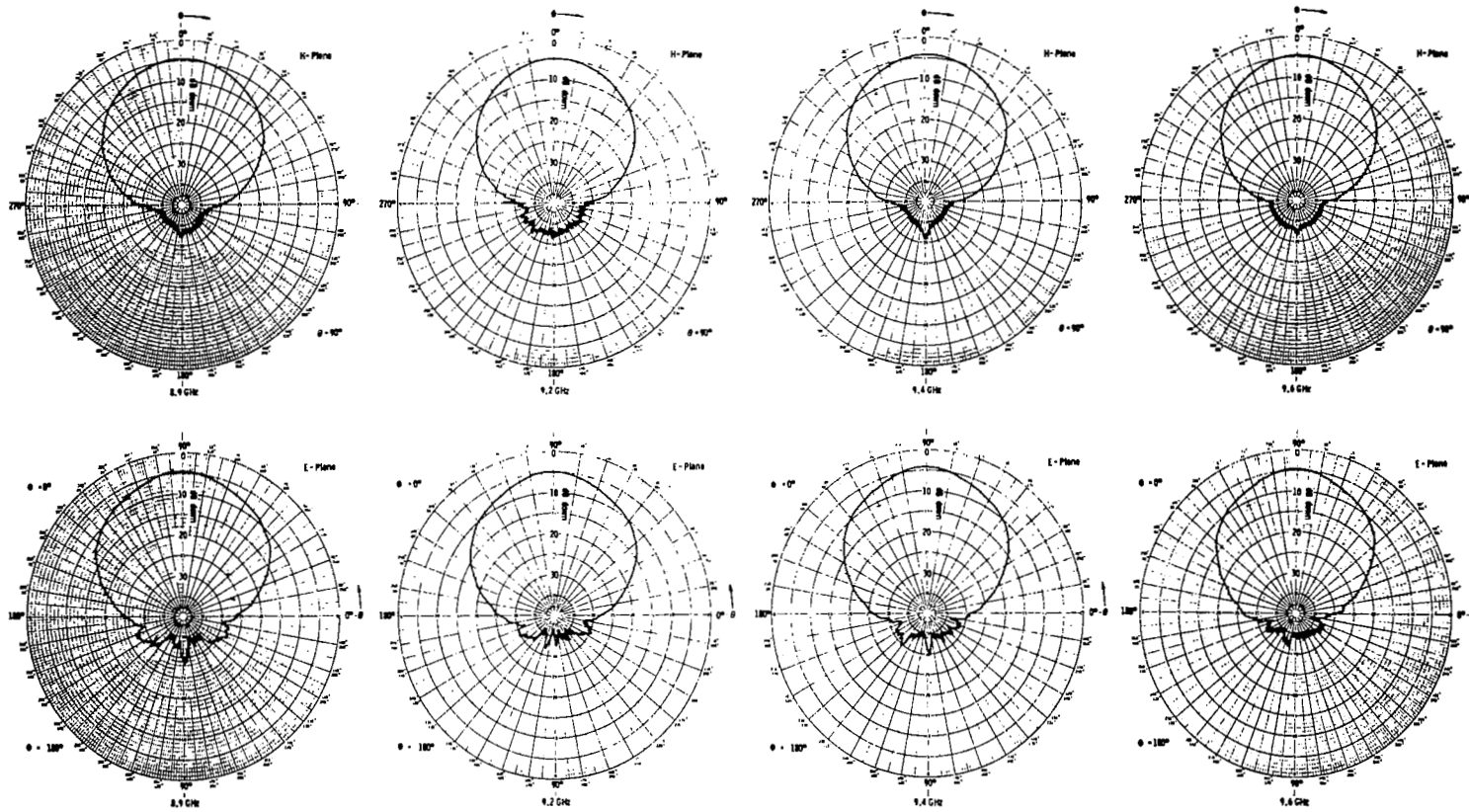
(b) LOCKHEED LI-1500 (with green surface coating)

FIGURE A-1 CONTINUED



(c) WHITTAKER ALUMINUM PHOSPHATE FOAM ( $\text{AlPO}_4$ )

FIGURE A-1 CONTINUED

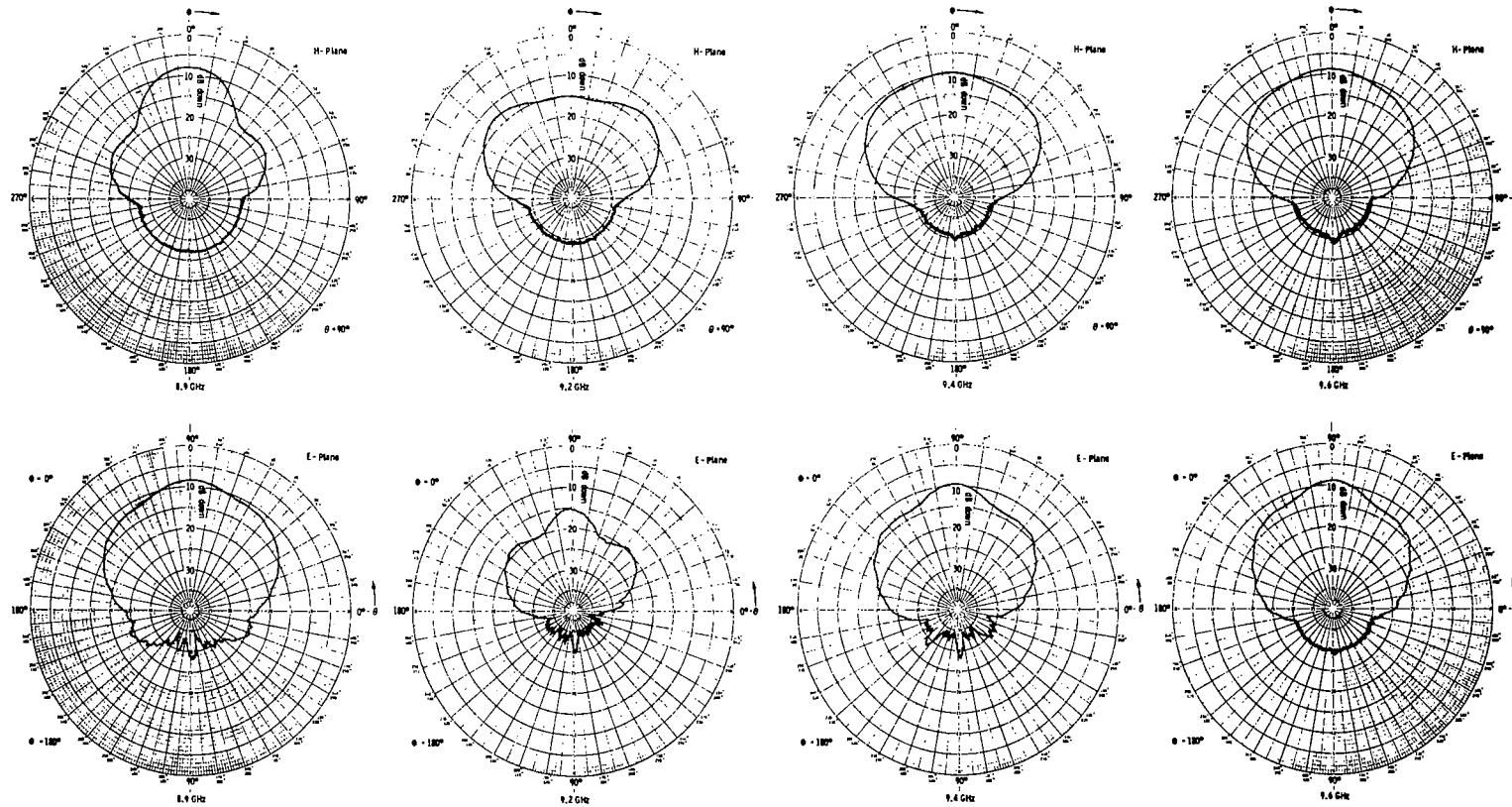


77

(d) WHITTAKER ALUMINUM PHOSPHATE FOAM ( $\text{AlPO}_4$  with VHT flameproof surface coating)

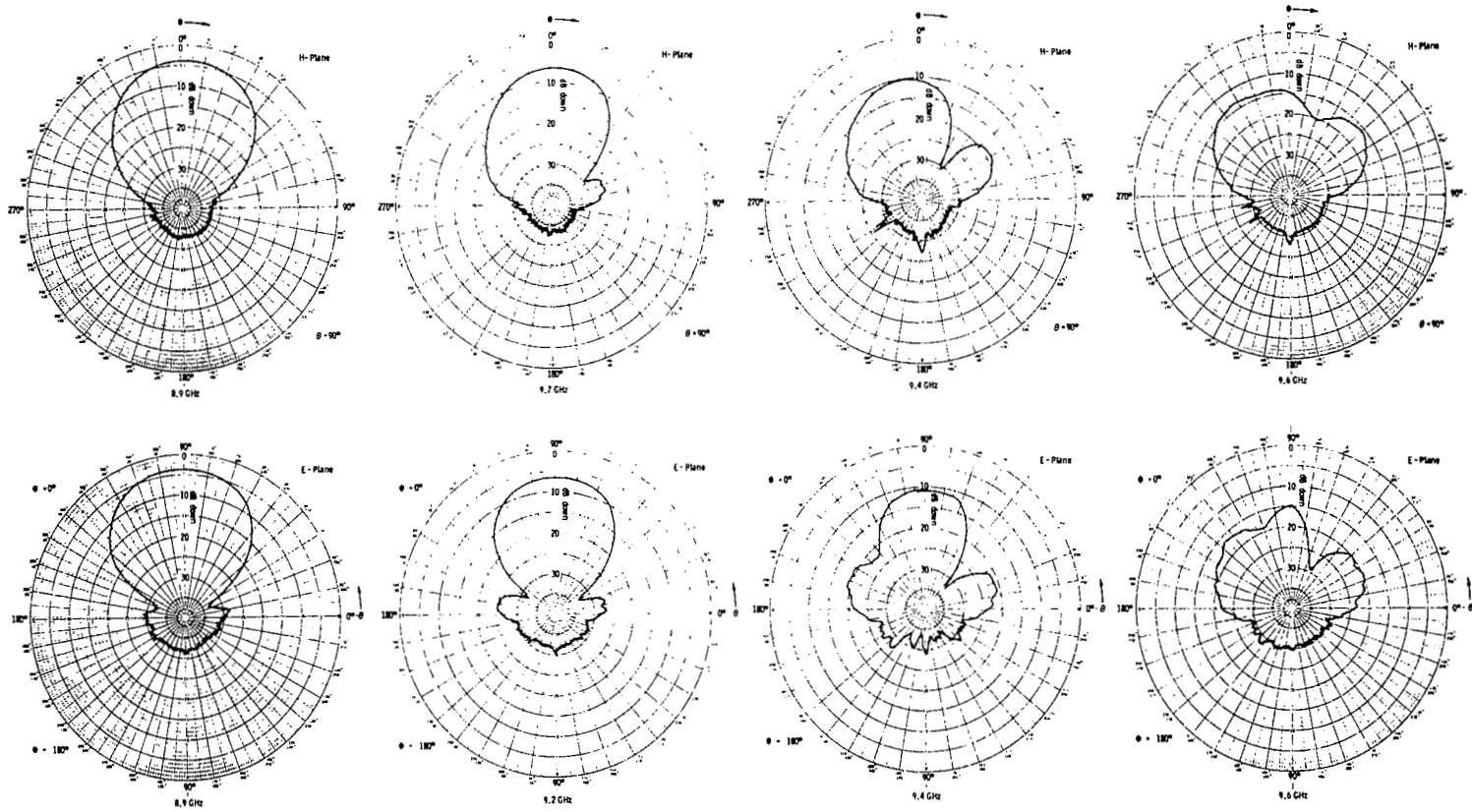
FIGURE A-1 CONTINUED





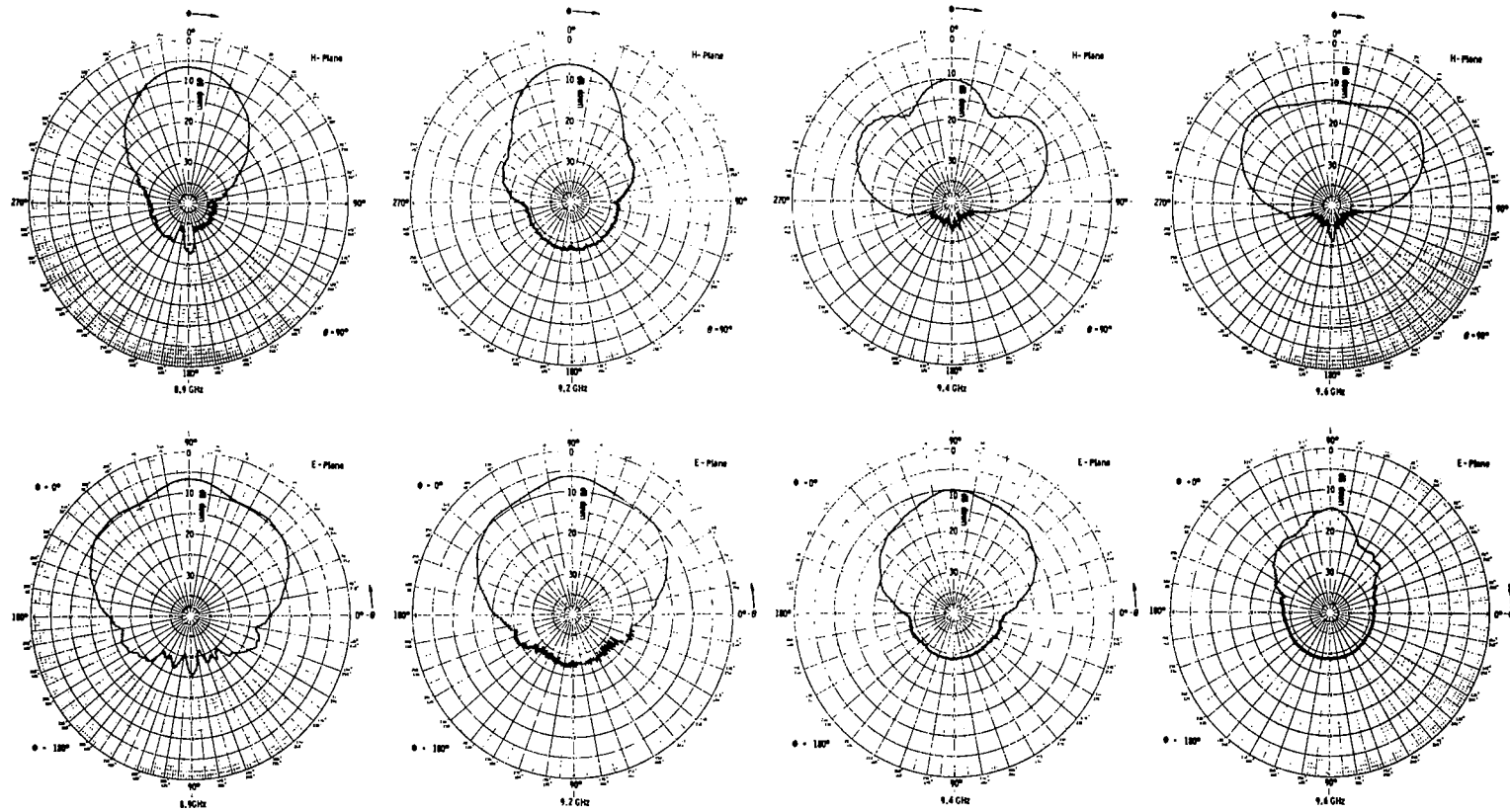
(e) AMERICAN LAVAL CORPORATION'S LAVITE (coated, cured, and unused)

FIGURE A-1 CONTINUED



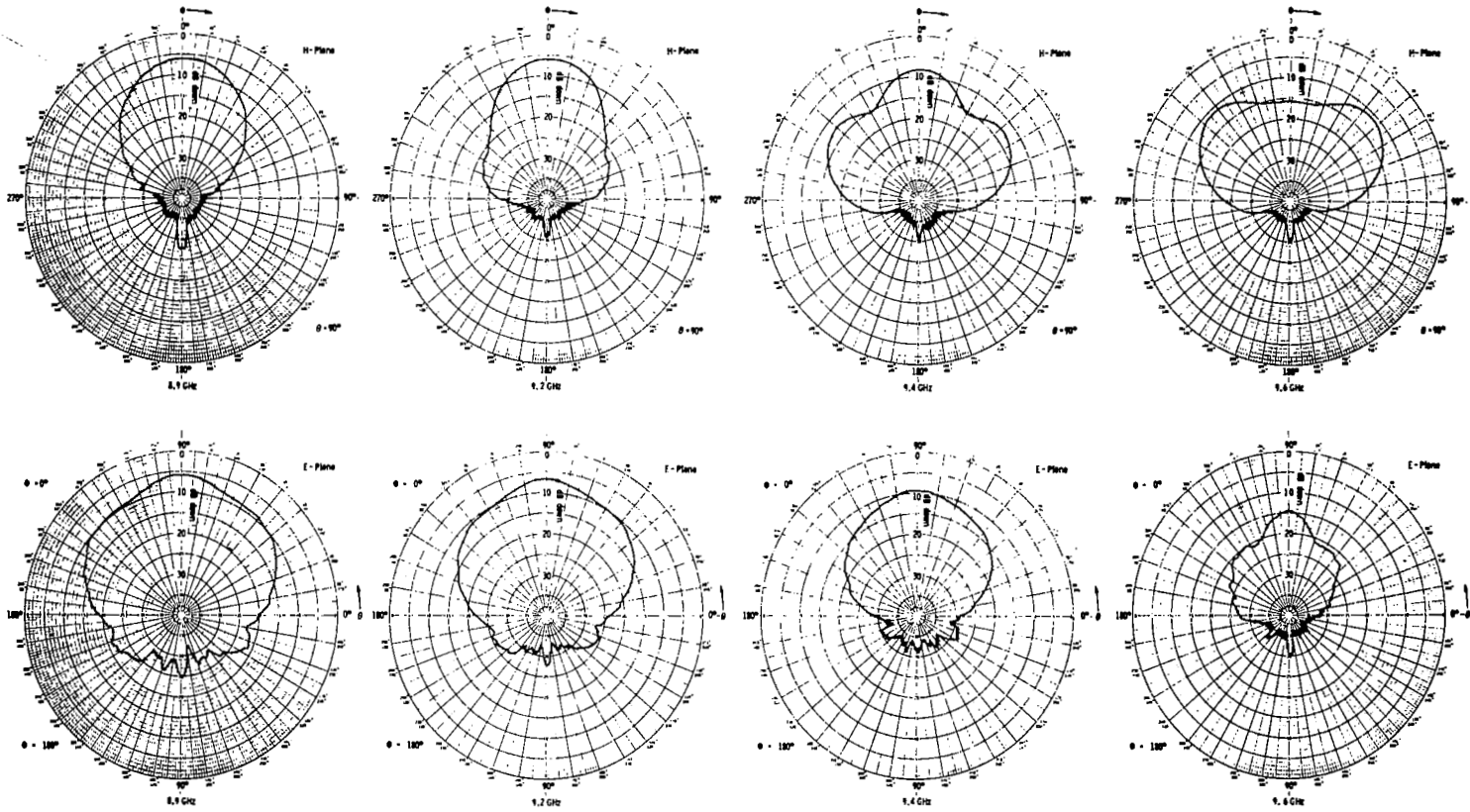
(f) AMERICAN LAVAL CORPORATION'S LAVITE (used)

FIGURE A-1 CONTINUED



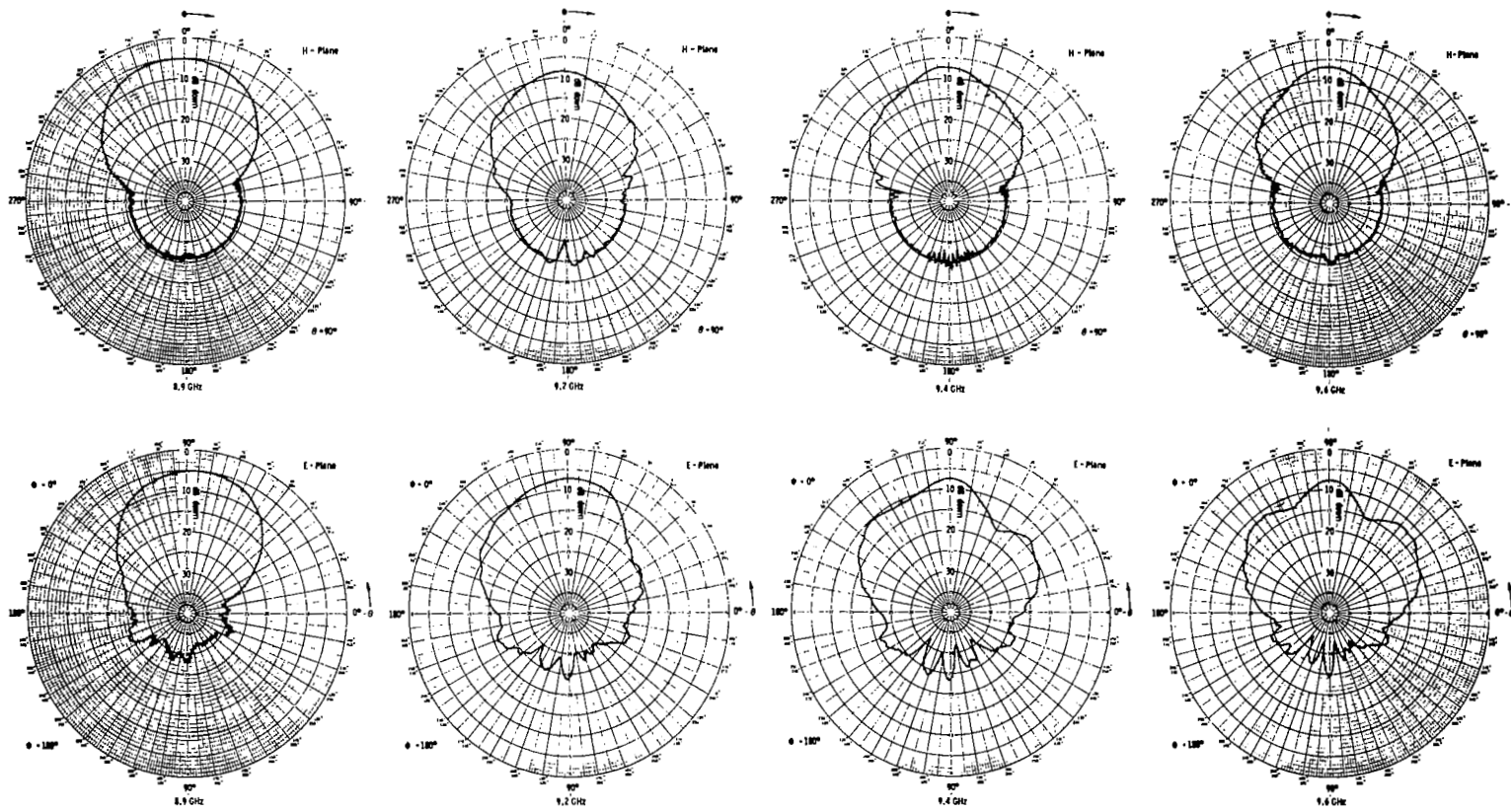
(g) UNION CARBIDE BORON NITRIDE (HBR grade, light color)

FIGURE A-1 CONTINUED



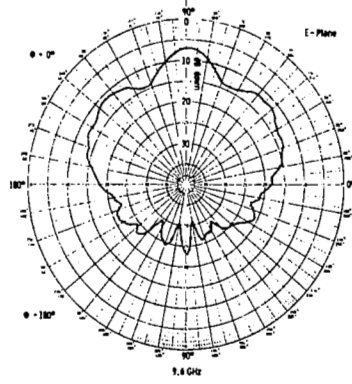
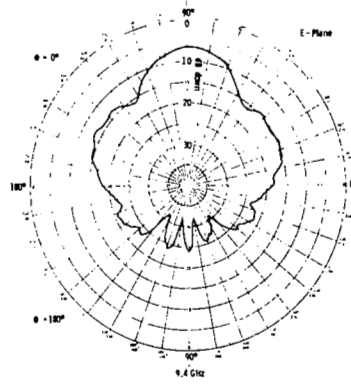
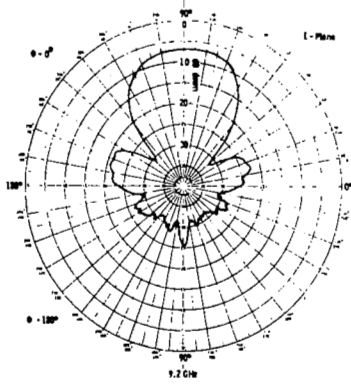
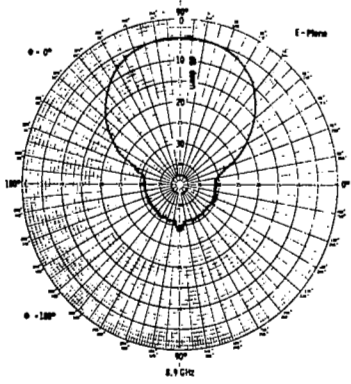
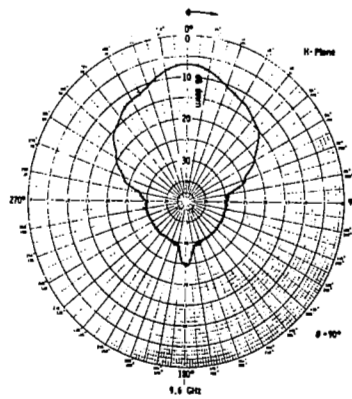
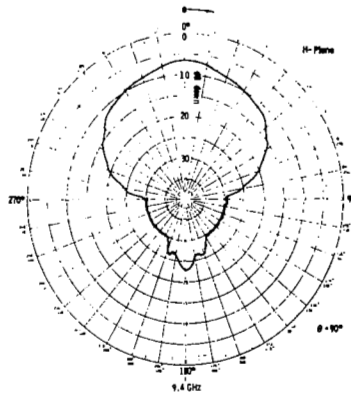
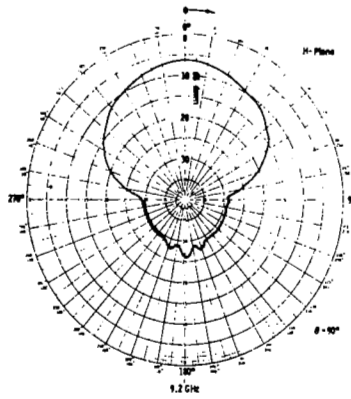
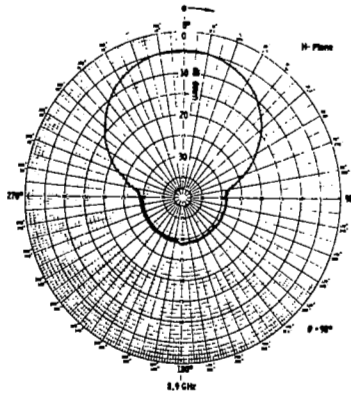
(h) UNION CARBIDE BORON NITRIDE (HBR grade, gray color)

FIGURE A-1 CONTINUED

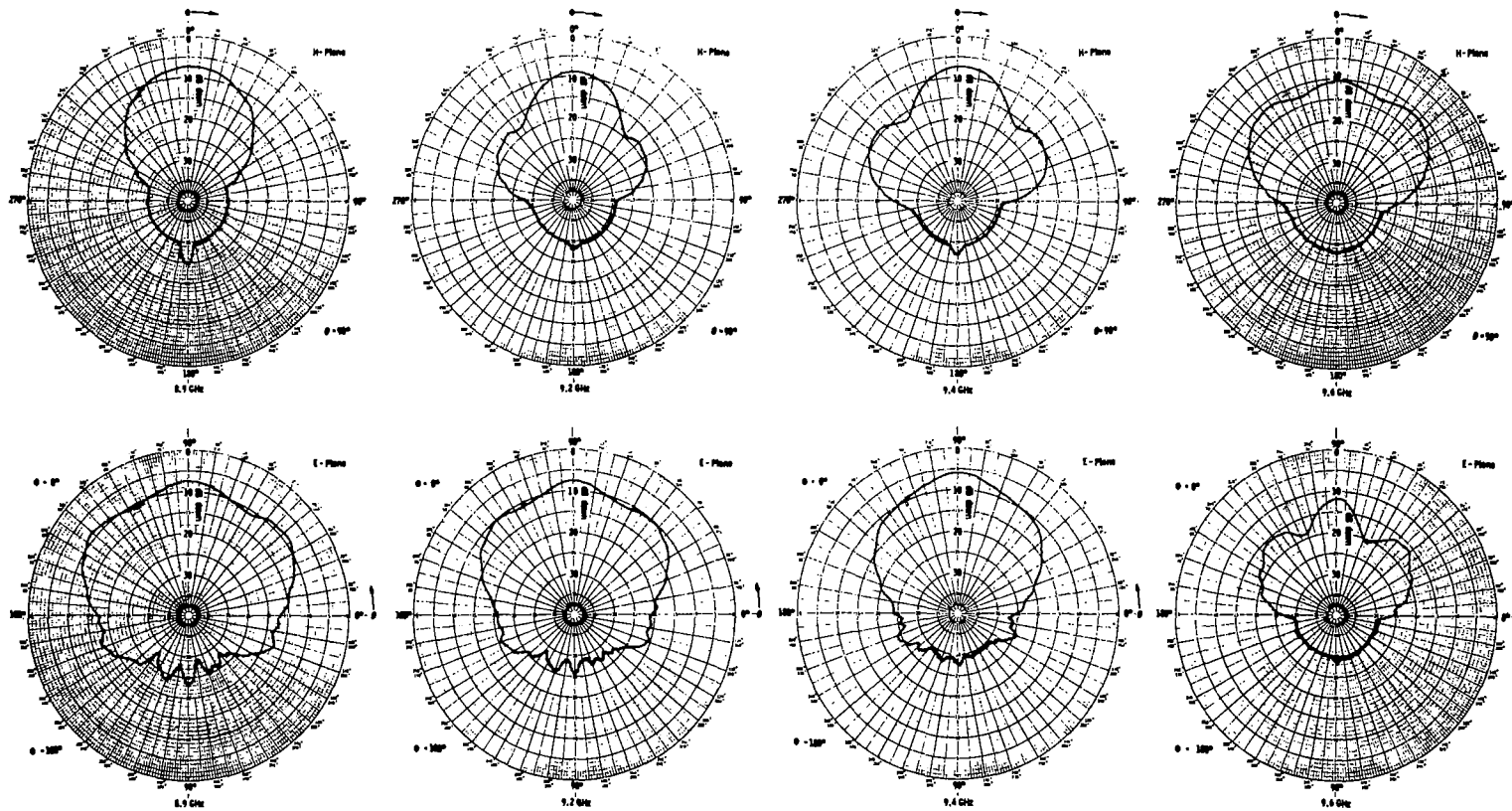


(i) PHILCO-FORD AS3DX (with back-surface thermocouples)

FIGURE A-1 CONTINUED

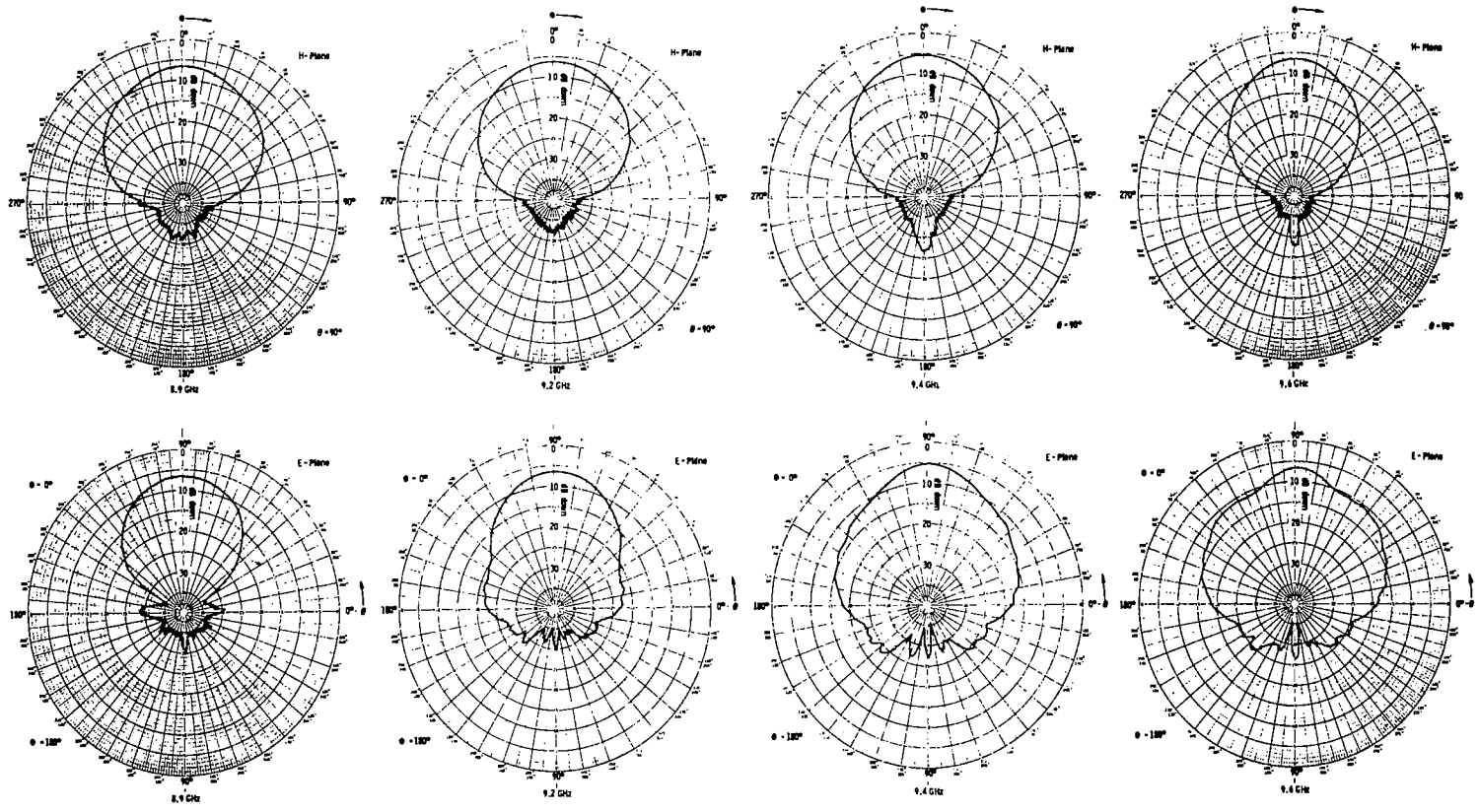


(j) PHILCO-FORD AS3DW  
FIGURE A-1 CONTINUED



(k) UNION CARBIDE BORON NITRIDE (HD-0092)

FIGURE A-1 CONTINUED



(I) SLIP-CAST FUSED SILICA (7941)

FIGURE A-1 CONCLUDED